

Protein cage clustering:
towards functional biohybrid
materials

Martijn Verwegen

Title: Protein cage clustering: towards functional biohybrid materials

Author: Martijn Verwegen

Composition of the graduation committee:

Chairman: Prof. dr. ir. J. W. M. Hilgenkamp University of Twente

Supervisor: Prof. dr. J. J. L. M. Cornelissen University of Twente

Referee: Dr. C. Blum University of Twente

Members: Prof. dr. ir. J. Huskens University of Twente

Prof. dr. ir. J. E. ten Elshof University of Twente

Prof. dr. W. K. Kegel Utrecht University

Dr. ir. N. E. Benes University of Twente

Prof. M. Kostianen Aalto University

The research described in this thesis was performed at the department of Biomolecular Nanotechnology (BNT) at the MESA+ Institute for Nanotechnology and the Faculty of Science and Technology at the University of Twente.

Cover art: Johannes van Staveren

Printed by: Ipskamp Drukkers B.V.

ISBN: 978-90-365-3731-5

DOI: 10.3990/1.9789036537315

Copyright © by Martijn Verwegen. All rights reserved.

**PROTEIN CAGE CLUSTERING:
TOWARDS FUNCTIONAL BIOHYBRID MATERIALS**

PROEFSCHRIFT

ter verkrijging van
de graad van doctor aan de Universiteit Twente,
op gezag van de rector magnificus,
prof. dr. H. Brinksma,
volgens besluit van het College voor Promoties
in het openbaar te verdedigen
op vrijdag 5 september 2014 om 16.45 uur

door

Martijn Verwegen
geboren op 7 maart 1984
te Dordrecht

Dit proefschrift is goedgekeurd door:

Promotor: Prof. dr. J. J. L. M. Cornelissen

Dedicated to my parents

Table of Contents

Chapter 1: Aim and Outline	1
Chapter 2: Literature overview	5
Spherical viruses	6
Synthesis and modifications.....	12
Biohybrid structures of virus-like particles.....	21
Organisation of viruses.....	32
Concluding remarks.....	38
Chapter 3: Encapsulation of nanoparticles	47
Introduction.....	48
Results and Discussion.....	49
Conclusions.....	60
Experimental.....	61
Chapter 4: Clustering with soft macromolecules	65
Introduction.....	66
Results and Discussion.....	67
Conclusion	83
Experimental.....	83
Chapter 5: Clustering with hard nanoparticles	87
Introduction.....	88
Results and Discussion.....	90
Conclusion	108
Experimental.....	109

Chapter 6: Functional virus-like particle based materials	115
Introduction.....	116
Results and Discussion.....	117
Conclusion	130
Experimental.....	131
Appendix A: Coupling data AuNP VLPS	136
Appendix B: Fluorescence lifetime data.....	137
Appendix C: TEM of VLP-Ore488 clusters.....	138
Summary	139
Samenvatting	143
Acknowledgements/Dankwoord	147
List of Publications	153
About the Author	155

Chapter 1: Aim and Outline

Nanotechnology

The goal of nanotechnology is to be able to structure, control and even program materials at the nano-meter scale to enable a wide range of new physical properties and designed functionalities. The materials made by nanotechnology could very well permeate all areas of life and science, its earliest success, microchip fabrication, already doing so. Now, new materials are emerging for such diverse purposes as energy conservation, data manipulation and medical applications. There are two main ways to work towards this goal, known as the top-down and bottom-up approach.

The top-down approach

The top-down approach relies on designing nanoscale structures to be created from bulk material by a variety of lithography and imprinting techniques. In photolithography, for example, a pattern on a mask is transferred to a surface through a series of etching steps, using first light to irradiate away a protective photoresist layer followed by chemical etching to create structures in the substrate. This creates limitations for such techniques upon how small the final nanoscale components can be based on, for example, the wavelength of light, the material and the chemical etching techniques used.

The bottom-up approach

The bottom-up approach instead relies on creating the individual parts first and then growing a larger structure from that through a variety of self-assembly techniques. Using, for example, synthetic chemistry the individual molecular components can be created by design, purified as required and analysed in detail. By integrating supramolecular, covalent or other intermolecular binding sites in the design of these molecules their interaction can be controlled. This control is however limited by the interplay between a wide range of forces that govern the interaction of molecules, whether intended by design or not. Therefore, whilst components can be controlled using synthetic chemistry, the final structure is limited in the degree of macro scale organisation and size that can be achieved.

Learning from nature

Nature, however, excels at self-assembly. It is unrivalled in controlling, organising and exploiting materials, reactions and structures at the nanometre scale and scaling this up all the way to living organisms. Furthermore, biological building blocks like RNA, DNA and proteins are diverse, easily modified and generally well characterised. In the field of bionanotechnology we therefore seek to emulate, learn and improve upon nature by using, modifying and manipulating the building

blocks of nature. After all, nature could very well be the tool towards well structured, controlled and programmable materials that hold properties well beyond the boundaries of biology.

On the boundary between chemistry and biology

Defining where mere chemistry ends and biology, or life, begins is subject to ever greater debate as new discoveries are made. Viruses seem to thrive on this boundary, fitting many of the criteria for life, yet behaving mostly as complex and hierarchically assembled nanostructures. The most basic virus structure, shared by all viruses, consists of a core of RNA or DNA materials surrounded by a protective protein cage, generally forming either a spherical nanoparticle or rod-like nanotube. Furthermore, though most viruses share many other similarities, they are manifold and diverse in shape, morphology and functioning.[1] Indeed protein cage structures similar to viruses, like encapsulins, have recently been found to be of use in many biological functions.[4] Collectively, this makes for an exhaustive library of different particles that could each be uniquely used.

Virus protein cages

In nature, a virus uses this protein cage to protect the genomic cargo, direct it to a host cell and finally release it, which allows for the genomic material to hijacking the cells organelles and promote virus replication. The underlying natural properties that allow this to be efficient: a symmetrical architecture, monodispersity and a chemically varied surface; turn these protein cages into useful tools for nanotechnology. As such, they can be considered as nanoparticles or nanoshells that follow a discrete and symmetrically assembled structure.[5] Even when restructuring these shells around artificial templates to form a virus like particle (VLP), this still results in a limited set of symmetrical and well defined morphologies.[6, 7] The resulting monodispersity is generally greater than anything that can be artificially made at this scale. Beyond this, virus protein cages also allow for a wide variety of modifications to be made either at the interface between the proteins, on the interior surface or on the exterior surface.[8, 9] Effectively, this makes virus like particles into programmable components that share many essential traits and thus could form the basic uniform building block for larger nanostructures.

Protein cage based nanostructures

The central theme to this thesis is governed by the formation of larger nanostructures from these protein building blocks. In recent years, both a large number of synthetic techniques for forming and modifying VLPs as well as for making structured systems out of viruses have been developed. Still, the properties

of these structures, especially when not made out of native viruses, but rather VLPs, are poorly understood. This naturally leads to the question that this thesis is based upon: “What are the properties of protein cage based nanostructures?”

Cowpea Chlorotic Mottle Virus

To address this question Cowpea Chlorotic Mottle Virus (CCMV) and a number of different VLPs formed from its capsid proteins are used. This virus is well studied, versatile and builds upon the previous experience of our group. An important quality is the ability to disassemble its protein cage into component protein subunits and reassemble this either as a hollow shell or around an anionic template. This templated reassembly allows formation of different sized, but still symmetrical and monodisperse VLPs, allowing a study of different morphologies consisting of the same proteins.

Outline

The central theme that permeates through the various chapters is formed by the desire to create a functional system from CCMV based VLPs. Starting from understanding the field, the thesis further explores the synthesis of relevant VLPs, the formation of VLP based structures with both hard and soft linkers, and finally demonstrates a design for a functional system based on the insights gained.

Chapter 2 further introduces the field of virus based systems for functional materials and aims to give both a basic understanding of the background to this work and an overview of the state of the art systems that are currently in place. Experimentally, the starting aim is to synthesize a reliable, functional, virus-based building block for these studies. This is done in **chapter 3** and describes the easy, efficient and size selective encapsulation of gold nanoparticles inside the CCMV capsid. Next comes an investigation into the effects of VLP size, structure and cargo upon the electrostatic clustering of VLPs in **chapter 4**, using soft cationic macromolecules. Further investigation of this topic is done in **chapter 5**, where small cationic gold nanoparticles are used as a functional, hard linker between the VLPs. Ultimately this culminates in **chapter 6**, where the insights from the previous chapters are combined and used to study a functional system designed to promote metal enhanced fluorescence.

Bibliography

1. Lee, K.K. and J.E. Johnson, *Complementary approaches to structure determination of icosahedral viruses*. Current Opinion in Structural Biology, 2003. **13**(5): p. 558-569.
2. Crick, F.H.C. and J.D. Watson, *Structure of Small Viruses*. Nature, 1956. **177**(4506): p. 473-475.
3. Douglas, T. and M. Young, *Viruses: Making Friends with Old Foes*. Science, 2006. **312**(5775): p. 873-875.
4. Tanaka, S., M.R. Sawaya, and T.O. Yeates, *Structure and Mechanisms of a Protein-Based Organelle in Escherichia coli*. Science, 2010. **327**(5961): p. 81-84.
5. Caspar, D.L.D. and A. Klug, *Physical principles in the construction of regular viruses*. Cold Spring Harbor Symp. Quant. Biol, 1962: p. 27,1-24.
6. Sun, J., et al., *Core-controlled polymorphism in virus-like particles*. Proceedings of the National Academy of Sciences, 2007. **104**(4): p. 1354-1359.
7. Cadena-Nava, R.D., et al., *Exploiting Fluorescent Polymers To Probe the Self-Assembly of Virus-like Particles*. Journal of Physical Chemistry B, 2011. **115**(10): p. 2386-2391.
8. Lee, L.A., H.G. Nguyen, and Q. Wang, *Altering the landscape of viruses and bionanoparticles*. Organic & Biomolecular Chemistry, 2011. **9**(18): p. 6189-6195.
9. de la Escosura, A., R.J.M. Nolte, and J.J.L.M. Cornelissen, *Viruses and protein cages as nanocontainers and nanoreactors*. Journal of Materials Chemistry, 2009. **19**(16): p. 2274-2278.

Chapter 2: Literature overview

Virus based systems for functional materials

Virus based bionanotechnology holds the promise of control over the structure, properties and functionality of materials at the nanometre scale. After all, viruses, and by extension virus-like particles (VLPs), represent some of the largest hierarchical protein constructs found in nature. Their symmetrical architecture as well as their high degree of monodispersity, compared to other nanoparticles, makes them unique as nano-building blocks. Furthermore, many of these particles seem to have specific and tuneable physical properties that can be utilized for their further function and manipulation.

Viruses and VLPs are thus highly desirable nano-building blocks that could find applications ranging from nano-containers, for studying reactions in confinement or drug delivery, to modular structural components, that allow for the creation of complex nano-architectures, and eventually functional materials. This review chapter aims to generate an understanding of how the structure, modification and organisation of viruses enable them to be the key component in these potential, functional materials, a field recently introduced as chemical virology. Ultimately these functional virus-based materials could enable the construction of novel optical, electronic, catalytic, imaging and other nano-scale precision based applications.

Spherical viruses

Basic structure

Viruses come in many different shapes and morphologies, but for most chemical virology purposes it can be subdivided into rod-like and spherical viruses. In both cases a virus nanoparticle consists of an RNA or DNA core protected by a protein coat or capsid, which is held together by non-covalent interactions. Depending on the pH and ionic strength of the solution these virus particles display a variety of swelling, maturation or other structural transformations. For example, the Cowpea Chlorotic Mottle Virus (CCMV), a typical icosahedral virus, is known to have pores that can be opened or closed based on pH and ionic strength, allowing for the influx of materials. Such structural changes are often associated with release mechanisms for the genome cargo carried by viruses.[1]

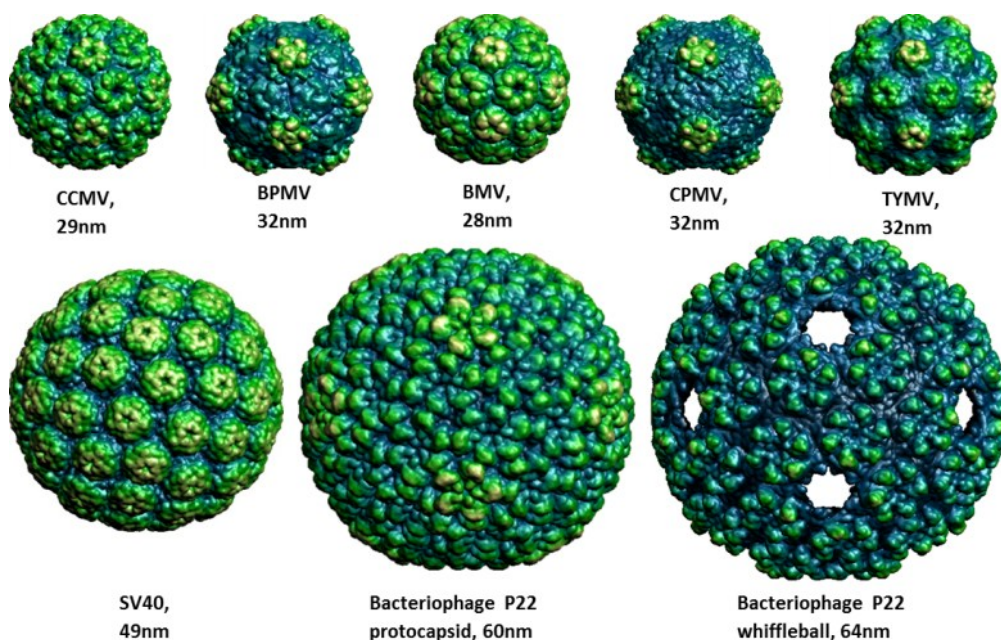


Figure 1: VIPER database reconstructed images of several spherical viruses used in the functional materials that are discussed in this review.¹[2]

Key to understanding these natural nanoparticles is knowing their structure, see figure 1. Common techniques to study this involve X-ray diffraction (XRD) for a crystallographic structure and Small Angle X-ray Scattering (SAXS) as well as (cryo) electron microscopy (EM) to check dynamic structural changes during the various stages of maturation and assembly, see figure 2. More recently, the structural

¹ Images copyright of VIPERdb.[2]

parameters have been studied using atomic force microscopy (AFM), revealing not only the surface topology, but also physical properties, such as the Shear and Young modulus. Additional insights gained by nano-indentation have also revealed the importance and strength of structural components such as the individual subunits and the genetic material inside the capsid. [3, 4]

Such techniques can also be used to probe the nature of the interaction between the RNA and coat protein, especially under conditions where pH and ionic strength are varied. For instance, Makino et al. used X-ray data to reveal several unknown protein segments and their interaction with the RNA strand inside the virus.[5] Small angle neutron scattering (SANS) data by Comellas-Aragons et al. shows the morphology of CCMV and CCMV capsids and confirms the pH and ionic strength based swelling behaviour that had been observed by Speir et al. using cryo TEM, but also reveals that the RNA is bound close to the protein coat.[6, 7]

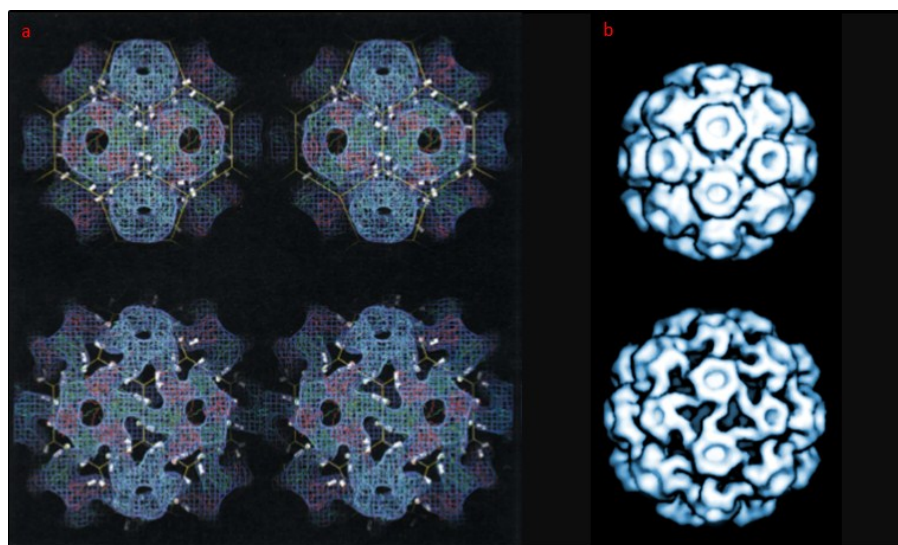


Figure 2: CCMV structures have been solved by both (a) X-ray crystallography² and (b) Cryo-TEM reconstruction³ revealing a closed (top, pH<6.5) and swollen (bottom, pH>6.5) morphology. The symmetrical structure containing pentamers and hexamers is also clearly visible. [1, 7]

Virus symmetry

Spherical virus protein capsids generally adopt an icosahedral symmetry, which were described by the Caspar and Klug triangulation number and corresponds to

² Reprinted (adapted) from Structure, 3(1), Speir et al., Structures of the native and swollen forms of cowpea Chlorotic mottle virus determined by X-ray crystallography and cryo-electron microscopy, p63-78, Copyright 1995, with permission from Elsevier.

³ © IOP Publishing. Reproduced by permission of IOP Publishing and T. Baker. All rights reserved.

the number of subunits that the next symmetrical morphology will take. In essence each set of three subunits is modelled as a triangle on a sphere. This forms a grid of triangles that is arranged in pentamers and hexamers around the spherical form. Symmetrical spheres occur at regular intervals in the number of triangles, which conform to integer values called triangulation numbers and follow $T=[h^2+hk+k^2]$, where h and k represent the distances between pentamers on the spherical grid. The smallest symmetrical assembly ($T=1$) consist of 20 triangles or 60 proteins. For every symmetric assembly beyond this more proteins are needed, thus the number of proteins is $60 \cdot T$ per capsid. [8, 9]

The formation of an icosahedral symmetry cannot be inferred from free energy minimization, and is therefore not necessarily a thermodynamic process. To overcome this Bruinsma et al. suggested additional structural parameters based on the interaction of the sides of capsomers (hexamers and pentamers) that make up the capsid shell.[10] Such interactions allow for the formation of stable icosahedral forms, but also octahedral and cubic capsid morphologies. Zandi et al. speculated that as icosahedral forms grow, ruptures appear in the structure and thus other stable morphologies might aid in the release of genomic cargo.[11]

Further molecular dynamics simulations as well as experiments have found that additional stable capsid shells can be formed, which do not obey the laws of symmetry. This structural polymorphism is described in simulations by Nguyen and Brooks. As a basis of protein folding they took the hexameric and pentameric subunits found in nature to be the first steps towards capsid assembly and applied elementary kinetics to them. This reveals that a large number of non-icosahedral, yet still symmetrical assemblies can be formed, see figure 3. [12] Additional simulations show this polymorphism generally results from hexameric dislocations. These dislocations increase the number of proteins in the coat by $6 \cdot D \cdot T$, where D is the number of dislocations. [13]


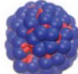
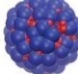
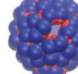
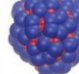
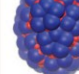
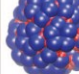
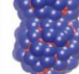
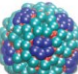
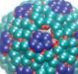
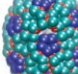
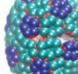
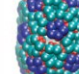
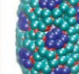
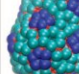
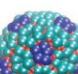
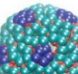
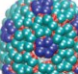
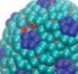
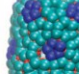
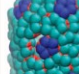
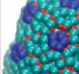
	70%	30%						
T=1	 C=12	 14	 15	 16	 17	 18	 19	 22
T=3	 C=32	 38	 41	 44	 47	 50	 53	
T=4	 C=42	 50	 54	 58	 62	 66	 70	
	D=0	2	3	4	5	6	7	0

Figure 3: Molecular dynamics predicts the formation of nonicosahedral assemblies under non optimal conditions (43.5 μ M of protein and 290 K). Still, around 70% of the proteins yield icosahedral T=1,3 or 4 capsids, the remainder forming nonicosahedral assemblies, with the relative yield decreasing as the number of capsomers (C) increases.⁴ [12]

Although Caspar Klug symmetry and molecular dynamics reveal a great deal about the symmetry of viruses and what stable intermediates may form, the actual assembly process cannot be easily derived from this structure. Whilst some virus structures seem to assemble from single proteins or from dimers of proteins into trimetric or pentameric units, others need an origin of assembly (OAS) for the initial specific binding of the viral genome or form proto capsids not fully adhering to Caspar Klug symmetry before settling down into a final virus form.[14, 15]

Virus assembly

Electrostatic interactions between the protein coat and the RNA or DNA are one of the key mechanisms by which virus protein cages assemble and kept intact, a property that can be exploited for the encapsulation of polyelectrolytes and charged nanoparticles. In fact, there is a 1.6 to 1 charge balance for nearly all native viruses between coat protein charge and genome charge. Calculations by Belyi and Muthukumar have shown that the virus genome is contained in a spherical shell within the cavity with a small gap between it and the protein shell, which is in good

⁴ Reprinted (adapted) with permission from (Nguyen et al., 2008) [12] Copyright 2008 American Chemical Society.

agreement with neutron scattering data.[6] More importantly, however, is the realisation that the confirmation adapted by a native virus is the one that results in the lowest free electrostatic energy.[16]

Still, electrostatic forces are not the only important contributor to viral assembly. Experimental results data indicates that the native RNA of virus is taken up far more efficiently than random cellular RNA fragments due to specific interactions induced by the packing sequence.[17] Castelnovo et al. presented theoretical models that explain these findings by entropy, showing that it likely plays an important role in virus assembly. Qualitatively, this can be described by two processes. The first process, which preferentially selects viral RNA over cellular RNA, simply relies on the fact that viral RNA is larger than cellular RNA. Therefore, a given capsid morphology needs less viral RNA strands per particle compared to cellular RNA, thereby enhancing the entropy of the system. The second process, in which monodisperse polyanions can form stable small capsids at charge ratio's that are not electrostatically favoured, is an entropic effect that favours multiple small capsids at the same protein concentration rather than a reduced number of larger capsids. [18]

Probing the role of the virus sequence thus might provide insights into the process of assembly, provided that such analysis is done uniquely for each virus. For example, in CCMV the deletion of several N-terminal residues does not affect capsid assembly, though it did prevent encapsulation of the RNA. On the other hand deletion of several C-terminal residues completely prevented any assembly from taking place. [19, 20]

Capsid assembly

Disassembly of a virus protein shell allows for the extraction of the coat proteins. This can be done for most viruses by changing the pH and ionic strength to trigger a structural change to open the capsid, followed by extraction and precipitation of the genetic material, for instance by precipitation with Ca^{2+} . For some viruses, these empty capsids can then be reassembled by changing the pH and ionic strength or by adding an anionic template, usually a polyelectrolyte or nanoparticle, to the coat proteins. [21]

A detailed experimental study by Bancroft and later Lavelle et al. on the pH and ionic strength dependent assembly of the CCMV capsid reveals a large amount of variety in the assembly.[22] Depending on the conditions the protein can fold itself into icosahedral capsids, multi-walled capsids, rods, or even dumbbell structures, see figure 4. Similar viruses, such as Brome Mosaic Virus (BMV) and Brown Bean Mottle Virus (BBMV), only show spherical structures (BMV) or no aggregation

without an RNA template (BBMV). [22, 23] These observations can be readily explained by the electrostatic nature of the interaction. Furthermore, TEM images reveal many irregularly shaped capsids. Likely such structures, along with the dumbbell morphology, are an example of non-icosahedral assemblies as described by Nguyen et al. in their simulations.[12]

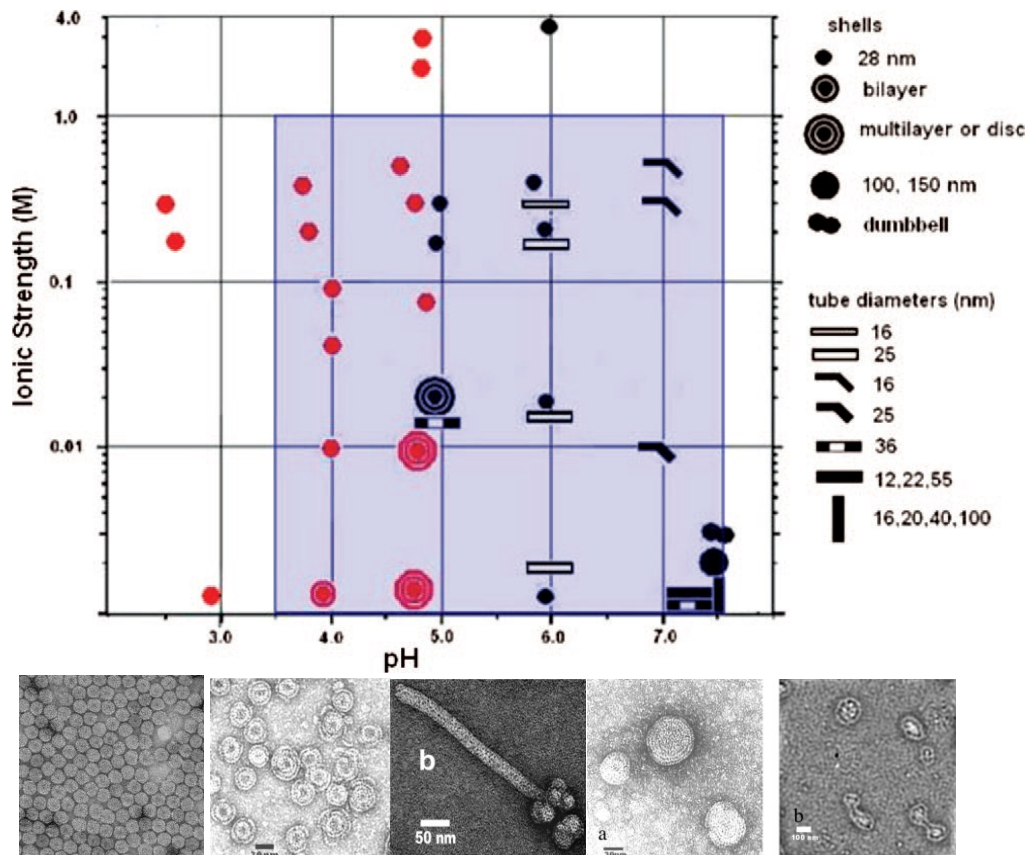


Figure 4: (Top) The phase diagram of the CCMV protein assembly reveals a great variety of shapes and morphologies depending on the buffer conditions used. (Bottom) TEM images of (left to right) single walled, bi-layered, tubular, multi-walled or disk, and dumbbell morphologies.⁵ [23]

Metal binding sites, such as for Ca^{2+} , can also play a role in this capsid assembly. The addition of small amounts of divalent ions can electrostatically crosslink carboxylic acid groups and thus keep a capsid morphology intact or close pores. In Red Clover Necrotic Mosaic Virus (RCNMV) divalent ions (Ca^{2+}) can be used to

⁵ Lower left image own work, other images: Reprinted (adapted) with permission from (Lavelle et al., 2009) [23] Copyright 2009 American Chemical Society.

control the opening of its surface pores. This has been used by Loo et al. to facilitate the controlled uptake and release of dye molecules. Using EDTA to remove Ca^{2+} the pores can be opened, allowing dye molecules to be taken up, subsequent addition of fresh Ca^{2+} trapped them inside. The release could be triggered by addition of EDTA or alternatively by disassembling the capsid shell by raising the pH to 10. [24]

These metal binding sites can, however, also be used for other things. For instance, the metal binding capacity in CCMV was investigated by Basu et al., showing that the metal binding sites in the protein structure are as predicted by its crystallographic structure. The binding of metal was not dependent on the RNA or the positively charged N-terminus. In addition, Tb^{3+} was found to bind much stronger than naturally occurring Ca^{2+} , showing that these capsids have the potential to bind potentially useful ions, for e.g. imaging. This was confirmed by Allen et.al. who used this to bind Gd^{3+} and confirmed that these capsids function as high-relaxivity magnetic resonance contrast agents.[25, 26]

Synthesis and modifications

Due to the icosahedral structure, virus protein cages are symmetrical in the chemical functionalities they display on their surface. In fact, virus proteins have been compared to dendrimers, but with far greater monodispersity and easier synthesis. Moreover, their electrostatic and manifold chemical properties available from amino acid side groups and potential substitution procedures enables a highly versatile chemical surface. This surface can be easily modified using surface chemistry targeting specific groups, or by genetic modifications to introduce additional functionality.[27] This topic is extensively reviewed in the past, [27-29] but as this is an important field within virus based nanotechnology, we present several examples that we found most relevant in relation to our own research.

Chemical modifications

Chemical modifications allow the protein to be equipped with a wide variety of functional groups. Amongst other things, this has enabled the formation of redox active nanoparticles, templates for biomineralisation, ligand attachment sites for high contrast MRI-agents, and charge inversed VLPs. [30-32] The most common groups that are targeted are external amines from lysine residues and carboxylic acids, see figure 5, although by using naturally occurring pores or disassembled coat proteins interior modification is also possible. Though thiol groups from cysteine residues are also a good target for chemical modification, this is generally after such a group has been genetically engineered into the coat protein, as they are usually not found on a native virus surface.

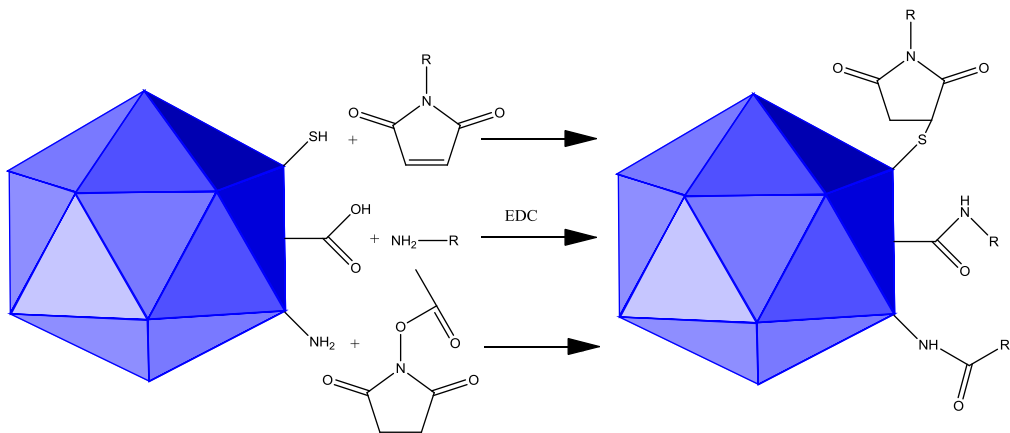


Figure 5: Cysteine thiol groups, lysine amine groups and carboxylic acid groups are common targets for chemical modification using maleimide, EDC coupling or NHS esters.

Addressing the amount of available chemical groups on a protein cage surface provides important information on the virus capacity to act as a chemical scaffold. An effective way to study this is reported by Barnhill et al. who studied the addressability and reactivity of lysine and carboxylic acid groups on Turnip Yellow Mosaic Virus (TYMV). [33] To do this they used dye's with flexible linkers that contained reactive NHS-esters for the lysine groups or could be coupled through EDC-coupling in the case of carboxylic acids. The study shows 60 reactive lysines (one per monomeric subunit) and 180 carboxylic acids (3 per subunit). More importantly, no self-quenching was observed, indicating the reactive groups were evenly spaced with good distance on the capsid. The reactivity of these groups is not always similar. For instance, CPMV has one easily addressable lysine that can be targeted using chemical modifications, see figure 6. Wang et al. explored this using acylation, protein digestion, and mass spectrometry to determine the reactivity of the K38 reactive residue. In addition, they explored the possibility of attaching dye labels and biotinylation. They showed that in addition to K38 up to 4 residues can be forced to react if a large excess of fluorescent dye (4000 equivalents per CP) is presented.[34] Similar work on other viruses also reveals that reactivity follows symmetry with a discrete amount of addressable groups being found on each capsid subunit. [33]

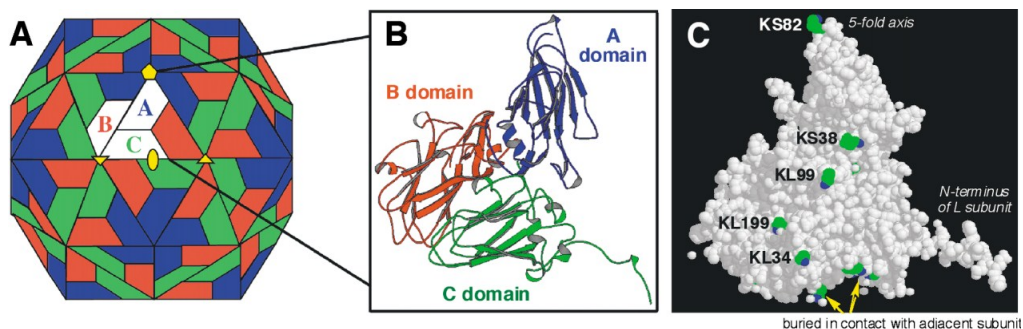


Figure 6: Exploring the capsid structure is key to understanding which residues might be available for chemical modification. In the CPMV structure presented the amines of lysines in the small subunit (KS82, KS38) as well as of the three of the large subunit lysines (KL38, KL199 and KL199) seem solvent accessible, whereas the remaining lysine residues are buried in the structure.⁶ [34]

Chemically available amine groups occur on virtually all viral protein cages. The regular spacing of these groups essentially makes the virus ideal for applications that make use of such regularity and as such it makes a good substitute for dendrimeric structures, which after a certain degree of branching become increasingly difficult to synthesize.[35] Steinmetz et al. used this to create a redox active VLP by decorating CPMV with ferrocene. To achieve this, an NHS ester was coupled to ferrocene and subsequently reacted to the CPMV coat. $240 \pm 10\%$ redox active groups were found on the capsid, indicating that all available amines had reacted and therefore a good spacing of the redox centres had been achieved.[30]

The dendrimer principle also enables the virus to be used as a scaffold for other species. For instance, the key to developing MRI contrast agents seems to be to load as many paramagnetic ions on a single carrier as possible. Virus nanoparticles offer an excellent scaffold for such materials as their symmetry, size and uniformity exceeds those achievable with other attempted species, such as dendrimers. Additionally, they are by nature biocompatible. High relaxivity times have been achieved, for example, for MS2 by chemically attaching empty ligands capable of binding Gd^{3+} to lysine groups.[36]

The above mentioned modifications are not only used to link functional groups, but can also affect the properties of the capsid. For instance, altering the charge on the exterior virus coat protein will change the interaction it has with its environment. Aljabali et al. demonstrated this in their modification of CPMV by succinamate,

⁶ Reprinted from Chem Bio, 9(7), Q. Wang et al., Natural Supramolecular Building Blocks: Wild-Type Cowpea Mosaic Virus, 805-911, Copyright (2002), with permission from Elsevier.

converting amine groups into carboxylic acids, see figure 7. This charge inversion enabled the protein coat to act as an efficient scaffold for the mineralisation of iron oxide and cobalt nanoshells. Furthermore, these surfaces could be further modified with thiolated oligosaccharides.[37]

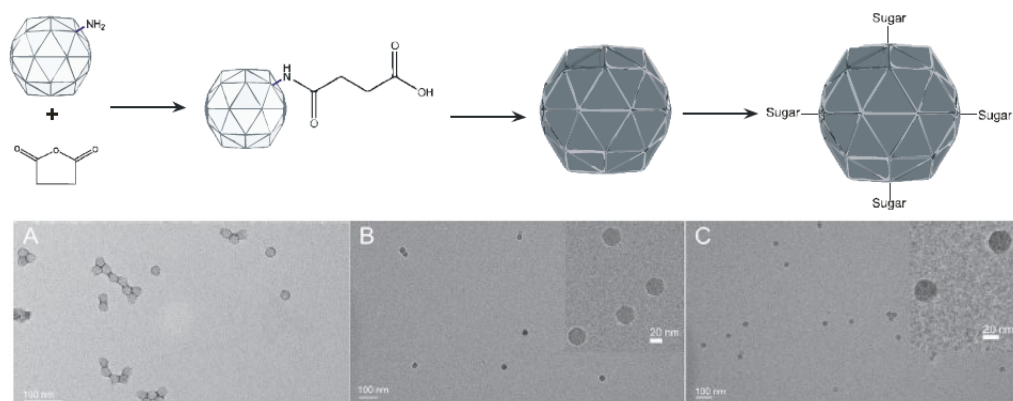


Figure 7: (top) Synthetic pathway for the modification of CPMV with succinamate followed by mineralisation of a nanoshell, (bottom) TEM micrographs of (A) CPMV-succinate, (B) CPMV with cobalt shell, and (C) CPMV with iron oxide shell.⁷ [37]

Modification of a virus coat can cause it to dissociate into subunits if an energetically unfavourable state emerges. Artificial templates can however be presented to these coat proteins, such that these can reassemble the coat protein. CCMV modified with polyethylene glycol (PEG) chains shows such dissociation into subunits. By presenting polystyrene sulphonate (PSS) as a template for the coat proteins, a smaller T=1 capsid is formed, see figure 8. [38]

7 Charge Modified Cowpea Mosaic Virus Particles for Templated Mineralization, Aljabali, A.A.A., et al., Advanced Functional Materials, 21(21). Copyright © 2011 WILEY-VCH Verlag GmbH & Co. KGaA, Weinheim

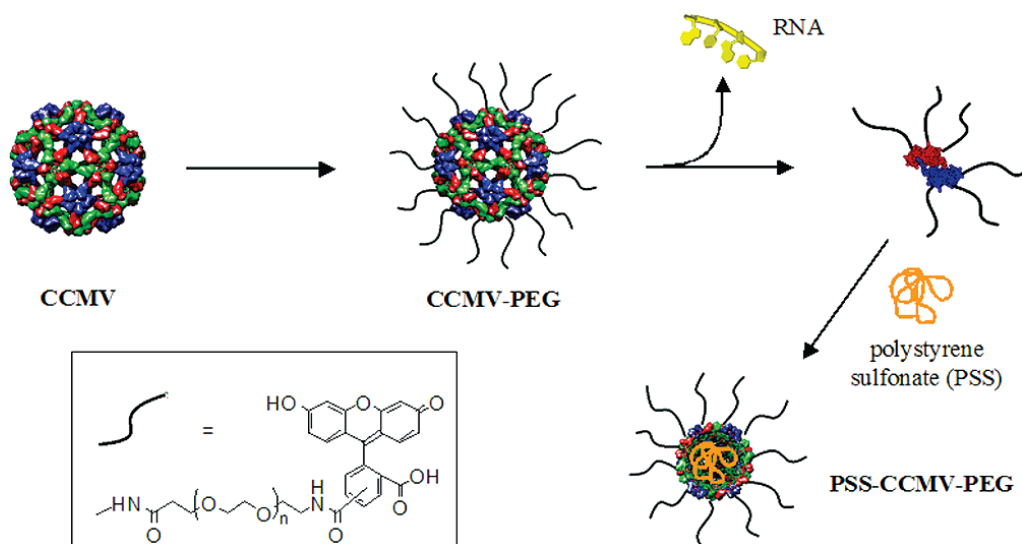


Figure 8: PEG chains on CCMV can render subunits unable to form capsid structures; however the addition of an anionic template for the capsid assembly can overcome this energetic barrier.⁸ [38]

Genetic modifications

One drawback for chemical modifications is that it relies on finding reaction conditions suitable for the capsid. Genetic modifications make use of natural mechanisms to introduce functionality to protein cages. A key issue here is to make a modification in the protein sequence without disrupting its tertiary structure or ability to form a capsid shell. General strategies for such modifications have used either point mutations on the surface of the protein, modifications to the N-terminus or altering the composition of surface exposed loops.[39] These modifications have allowed the charge alteration of protein cages[40, 41], gold or nickel binding protein cages[42-45] and as anchoring points for further chemical modification[32].

Introducing cysteine residues in the protein structure is perhaps the most common modification.[39, 46] This enables the protein cage to selectively bind to gold and maleimide functionalised species, and has been used to anchor cages to surfaces[47] and nanoparticles[43]. The symmetry of the capsid ensures an even spacing of these modifications on the virus surface, which allows for the organisation gold nanoparticles when they are mixed with the modified virus and bind to the surface cysteines. Using TEM, it was shown by Blum et al., that gold

⁸ Reprinted (adapted) with permission from (Comellas-Aragonès et al.,2009) [38] Copyright 2009 American Chemical Society.

particles of different size form a tight arrangement based on the position of the cysteine thiol groups, see figure 9.[43] Taking this a step further, the regular spacing of these gold nanoparticles make such VLPs excellent candidates to fabricate conductive networks. Upon connecting the bound gold nanoparticles with 1,4-C₆H₄[trans-(4-AcSC₆H₄C≡C)Pt-(PBu₃)₂C≡C]₂ (di-Pt) and oligophenylenevinylene (OPV), the formation of distinctive conductive networks on the virus surface was revealed. The conductive properties of the networks are dependent on the size and spacing of the nanoparticles.[48]

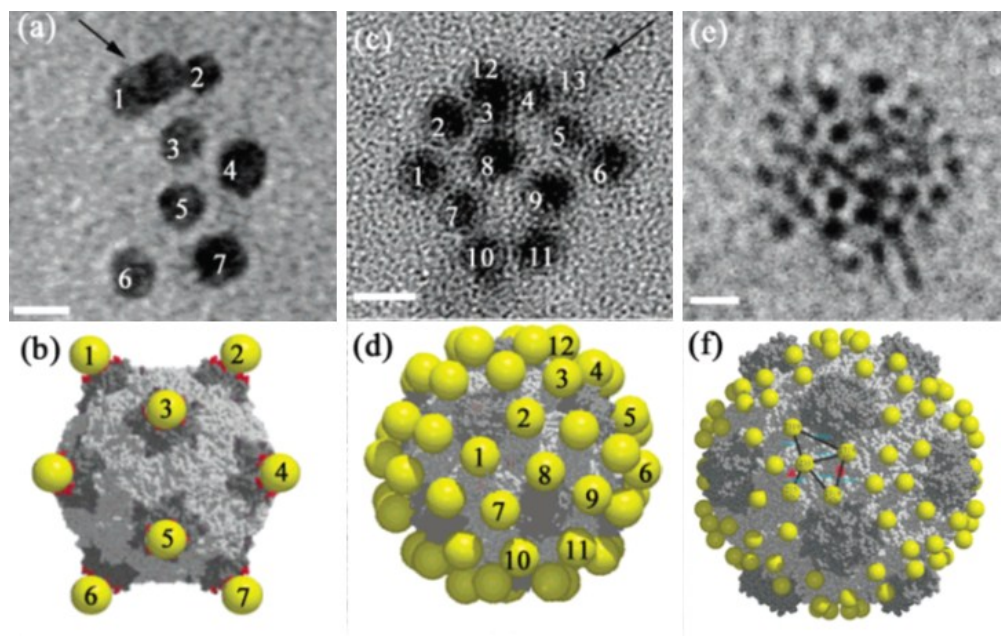


Figure 9: Three different cysteine mutants of CPMV (left to right: BC, DE and EF) show good agreement between experimental TEM images of gold nanoparticle binding and theoretical predictions based on the capsid symmetry.⁹ [43]

Genetically modified viruses can be used as anchoring points for a variety of species as the location of the introduced surface group as well as its nature and orientation can be easily tuned. This allows for the use of the virus as a scaffold to organise functional materials in a controlled manner. An example of this can be found in CPMV with His-tags engineered on several places by Chatterji et al. [44] This modification enables CPMV to bind nickel in various positions on the capsid, each of which has different binding efficiencies and electrostatic properties. In this

⁹ Reprinted (adapted) with permission from (Blum et al.,2009) [43] Copyright 2009 American Chemical Society.

manner protein shells with similar compositions and overall morphology can be given distinctly different properties, like control over the electrostatics by altering the protonation of the histidine sequence.[44]

Introducing genetic modifications onto the surface also allows for the ability to localize and orient the interactions on the coat proteins. Despite being composed of identical building blocks and having a high degree of symmetry in their structure, protein engineering can, in this way, be used to mono functionalise a virus coat protein. This is achieved by co-assembling modified and unmodified protein building blocks into a capsid, as is demonstrated by Li et al. They engineered cysteine and histidine tags onto the surface of simian virus 40 (SV40). Coassembling these with native proteins and subsequently selecting the monofunctionalised VLPs with a nickel column yielded VLPs that could selectively bind a single gold nanoparticle using its surface exposed cysteine group.[45]

Recent studies have revealed that more complex modifications to virus capsids can take functionality even further. Combining not only genetic and chemical modifications, but coupling inorganic materials to them generates complex nanoarchitectures. Martinez-Morales et al. used this technique to anchor iron oxide nanoparticles to the surface of the CPMV-T184C mutant. To achieve this, they chemically functionalised the exposed cysteine group with an amine group and used carbodiimide chemistry to couple the carboxylic acid coated iron oxide particles to the virus mutant. This enabled them to obtain hybrids, linking multiple iron oxide nanoparticles to the virus surface. These hybrids showed an enhanced magnetic response due to dipole coupling between the regularly spaced iron oxide particles, showing the potential of such constructs as MRI contrast agents.[49]

Qazi et al. used this approach by introducing a cysteine group to the capsid interior of bacteriophage p22 and coupling N-propargyl bromoacetamide to the capsid to act as the starting point for the synthesis of a branched oligomer, see figure 10. This was possible due to p22's 'wiffleball' morphology that ensured sufficiently large holes for the reagents to flow through freely. The oligomeric components doubled the Gd^{3+} content with each branching step, thus quickly filling the capsid with the paramagnetic ions. A total of 1,900 Gd^{3+} ions can be loaded into the capsid, ensuring a significant improvement on particle relaxivity compared to previous systems.[32]

P22 'wiffleball' viral capsid

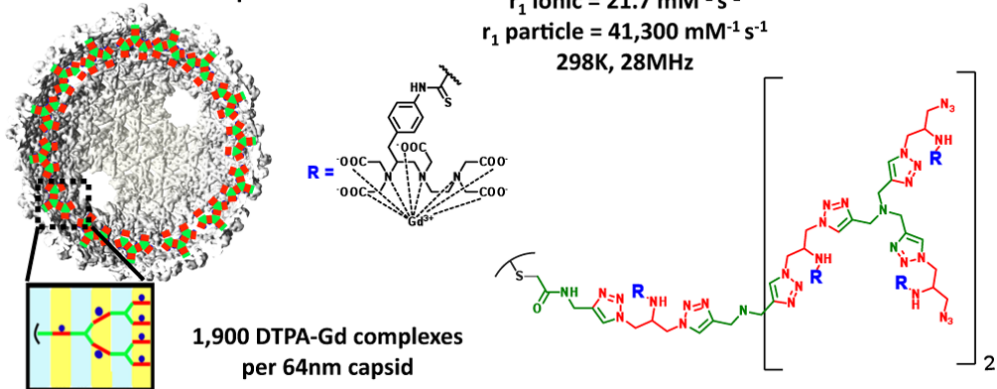


Figure 10: The whiffleball morphology of a mature bacteriophage P22 capsid allows for the growth of a branched oligomer due to diffusion through holes in its structure.¹⁰ [32]

Protein engineering can be taken a step further in another direction. By creating a fusion protein comprising a capsid subunit and another (functional) protein it becomes possible to encapsulate these secondary proteins within the confinement of a virus shell. This can be done by mixing the fusion protein with unmodified subunits and triggering capsid formation. Depending on the ratio it would even allow different, albeit statistical encapsulations, of protein into the capsid. Patterson et al. demonstrated this for the encapsulation of CelB glycosidase inside P22. Furthermore, these VLPs demonstrated conservation of enzyme activity, unlike previous encapsulations of enzymes which reported an enhancement. [50]

Biomaterialisation

Genetic manipulation also introduces biological functionality into a virus cage, which plays a role in biomaterialisation. The synthesis of monodisperse, well-defined nanoparticles and materials is a field in which biomaterialisation offers an interesting perspective. Biological organisms have adapted a wide variety of means of controlling the crystallisation of inorganic minerals on various length scales. Using empty virus protein cages as a scaffold for such crystallisation is therefore no far leap. And whilst certain nanoparticles grow in native virus capsids, others can be fabricated using recombinant capsid proteins, with examples given below. This biomaterialisation inside the protein follows two main strategies; either a specific protein motive is engineered into the virus genome that facilitates the nucleation of a specific mineral or nonspecific diffusion mechanics are used.

¹⁰ Reprinted (adapted) with permission from (Qazi et al., 2009)[32] Copyright 2009 American Chemical Society.

The interior of a virus protein cage is designed by nature to interact with RNA or DNA. However, this environment is also ideally suited for the mineralisation of various inorganic nanoparticles provided the conditions for mineralisation are conform to those present in the protein cage. Biomineralisation of this kind in viral capsids takes its original inspiration in the iron binding properties of the ferritin protein capsid. This protein cage facilitates the reduction of iron salts to form iron oxide inside its cavity. Douglas et al. used CCMV capsids as a mimic of ferritin. It shows a good affinity for the biomineralisation of tungsten, vanadium and molybdenum salts. The key to this process seems to be the ability of virus capsids to have material diffuse through their pores and present a template for the crystal growth. [51-53] Diffusion mechanics are greatly enhanced when negatively charged precursors are used, such as is the case for the Prussian blue $(\text{NH}_4\text{Fe}^{\text{II}}(\text{Fe}^{\text{III}}(\text{CN})_6))$ nanoparticles synthesised inside CCMV reported by de la Escosura et al., where the local apparent concentration of iron inside the capsid far exceeded the concentration of the precursor solution. These VLPs are generally size and shape controlled by the templating virus capsid, see figure 11.[31]

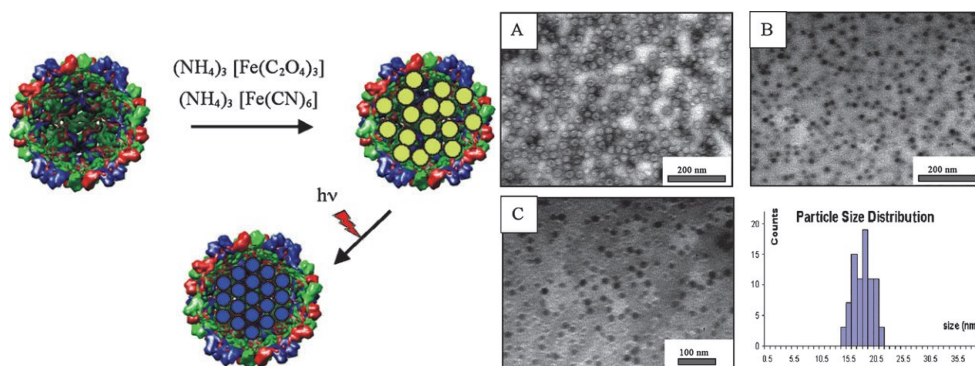


Figure 11: (Left) Synthetic pathway for the diffusion of monomers into CCMV and subsequent synthesis of Prussian blue particles inside the capsid; (right) uranyl acetate stained (A) and unstained (B,C) TEM micrographs reveal that the size distribution of the particles approximates the interior diameter of CCMV.¹¹ [31]

Still diffusion does not always require charged precursors. An empty, unmodified CPMV protein mantle has been shown to facilitate the growth of iron oxide and cobalt. This simply uses the permeability of the protein coat to small ions. After incubation for 30 minutes (for CoCl_2) or overnight (for iron sulphates) a reducing agent can be added for 30-40 minutes after which the crystals are formed inside

¹¹ Reproduced from Ref. 31 with permission from The Royal Society of Chemistry.

the protein cage. The protein cage can then be modified afterwards, for instance by biotinylation, to allow for further interaction. [54]

Protein cages prove to be highly robust structures that can be genetically engineered to alter the interior environment without losing its structure and external functionality. This was applied by Douglas et al. on CCMV to create a true mimic of ferritin in which an iron oxide particle was mineralised inside a genetically modified cavity. To achieve this, 9 basic residues on the N-terminus were substituted for glutamic acid (the subE mutant). This sub E mutant therefore displayed an acidic, rather than a basic interior cavity, which enabled the growth of monodisperse iron oxide nanoparticles. In this, the CCMV cavity was modified to act similar to some natural iron binding ferritin protein cages. [40]

By engineering specific protein sequences onto virus capsids they can act as a scaffold for the mineralization of inorganic nanoparticles. These sequences are designed to act as a template for one specific compound. Steinmetz, Shah et al. have used a surface exposed loop on the small subunit of the CPMV coat protein as the insertion point for such mineralization sequences which enabled them to grow thin shells of iron-platinum and silica. These particles are potentially of interest in magnetic and optical studies due to the well-defined monodisperse template that the shells of those materials form. Furthermore, these crystallization processes can be performed in aqueous media without the need for organic solvents, allowing for green chemistry.[55, 56]

Biohybrid structures of virus-like particles

As discussed virus protein cages can be modified and altered in different ways to facilitate a variety of interactions. To build on this, and to introduce further interactions, biohybrid structures can be created out of artificial (synthetic) templates and capsid proteins to form a new class of nanomaterials. In this way, they combine the advantages of viruses, like monodispersity, symmetry and ease of modification, with a wide variety of physical properties. Amongst other things, this has led to functional nanoreactors and plasmonic crystals and it has enabled that the capsid size and morphology can be controlled.[57-60]

Electrostatic loading

In 1969, Bancroft already showed that CCMV, CPMV and BBMV (Broad Bean Mottle Virus) all display the ability to form a spherical shell when presented with a large variety of flexible charged polyanions. Rigid polyanions, such as double stranded DNA, can sometimes even trigger assembly of tubes or other non-spherical assemblies. [61] Therefore, whilst a virus coat protein is designed to encapsulate

negatively charged RNA or DNA, it seems equally suited to encapsulate anionic polymers and organic molecules that mimic this genetic material. For instance, anionic PSS and polyacrylic acid (PAA) are encased in Hibiscus Chlorotic Ringspot Virus (HCRSV), whereas neutral dextran polymers of similar length do not. The formed VLPs showed similar electrostatic and size properties compared to native viruses.[62]

Controlling the morphology of a virus capsid with a polyanion enables the formation of new protein architectures induced by this the template. For instance, Caspar Klug symmetry predicts that coat proteins of virus particles can form stable capsid shells of various sizes, which differ from their native conformation. This was investigated by introducing short anionic polymers to virus coat proteins. For example, Sikkema et.al. found that PSS of 9.9kDa could assemble CCMV coat protein into a stable 16-18nm monodisperse T=1 capsid.[59] Further work on the encapsulation of PSS in CCMV reveals that for higher mass polymers ($m_w > 400k$) the capsid can form the T=2 and even the native T=3 morphology if the mass is above 2000kDa.[63] As such RNA viruses are shown to undergo electrostatic assembly upon the addition of a charged polymer.

As discussed, for the encapsulation of genomic material most RNA viruses require a charge ratio of 1.6 negative charges to compensate each positive charge. When Cadena-Nava and Hu et al. used fluorescently labelled PSS to track the amount of PSS to be encapsulated, they found CCMV can encapsulate an undercharge of 0.6 or 0.45 negative charges for each positive charge, whilst 400kDa+ PSS displayed 9 to 1 overcharge. These results indicate that other factors also contribute significantly to the encapsulation process. [63, 64] Theoretical simulations predict that the initial amount of polymer needed ($\langle \phi \rangle^*$) scales with the surface charge of the capsid interior (σ) and is indirectly proportional to the charge on the polymer (α) and the interior radius of the capsid (R), following $\langle \phi \rangle^* = 6 \sigma / (R^* \alpha)$. [65] Alternatively, this could be explained in part by the entropy factor present in the encapsulation as theoretically simulated by Castelnovo.[18]

Usually the formation of a protein shell follows Caspar Klug symmetry, however, when an incompressible template is presented, the protein shell can be forced to assume additional symmetries due to the size and curvature of the template and naturally occurring kinetic traps. This was shown by assembling CCMV coat proteins around nanoemulsion droplets that were stabilized by anionic surfactants, see figure 12. Depending on the size and curvature of these droplets the protein either followed Caspar Klug symmetry or showed locally disordered states, such as hexagonal sheets of protein.[66] Similarly, a rigid template can force CCMV to be

organised into tubular nanostructures. Mukherjee et al. showed that double stranded DNA can cause such assembly. This assembly is dependent on the ratio of CP to DNA base pairs (BP), with excess of CP forming short 17nm in diameter tubes (similar to the diameter of T=1 capsids), while an excess of 10 BP per CP affords longer, but narrower tube like structures. [67]

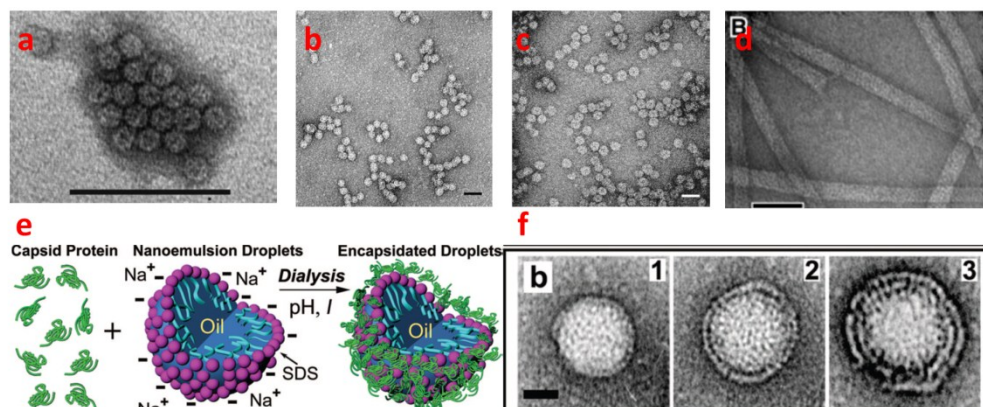


Figure 12: CCMV can be assembled into a variety of architectures based on the template presented: (a) 16nm T1 capsid using PSS* [59], (b) 22nm T2 capsid using PSS**, (c) 27nm T3 capsid using PSS** [63], and (d) 17nm diameter tubes using double stranded DNA*** [67]. (e) Scheme showing the encapsulation of a nanoemulsion droplets in CCMV****, (f) TEM images of nanoemulsion droplets encapsulated by 1,2 or 3 protein shells depending on buffer conditions****.¹² [66]

The principles applied to the encapsulation of polymers also hold true for other molecules. Anionic molecules can provide a template and cause the capsid to assemble. As such, the electrostatic loading of a virus shell is also a strategy that can be employed to change the nature of the virus cavity. For instance, micelles or DNA-amphiphiles can be introduced into the capsid. This effectively creates a hydrophobic cavity that is stabilised by the virus shell. [68]

Nanoparticle encapsulation

Electrostatic encapsulation is not merely limited to organic molecules and polymers. The same can be applied to rigid inorganic nanoparticles, enabling the creation of biohybrid structures that combine protein cages with inorganic physical

¹² *Reproduced (adapted) from Ref .59 with permission of The Royal Society of Chemistry.

Reprinted from Packaging of a polymer by a viral capsid, 94(4), Hu et al., Biophysical Journal, p.1354-1359, Copyright 2007, with permission from Elsevier. *Reprinted (adapted) with permission from (Mukherjee et al.,2006)⁶⁷ Copyright 2006 American Chemical Society. ****Reprinted (adapted) with permission from (Chang et al.,2008)⁶⁶ Copyright 2008 American Chemical Society.

properties and states, like superparamagnetism, plasmon absorption and similar confined electromagnetic states. [60, 69]

Dragnea et al. first showed the ability for citrate or tannic acid capped gold nanoparticles to be trapped inside the virus capsid of BMV upon reassembling a capsid in the presence of these particles. Small particles were shown to be tightly bound inside the capsid and exhibited a change in the spectroscopic properties.[70] Though these surface ligands carry negative charge, the role of surface charge is more prominent when DNA linkers are attached to the gold particle prior to encapsulation.[71] By using a small DNA or RNA chain bound to a nanoparticle it is possible to form a nucleation site for the coat protein shell. After incubation of this complex with the coat protein of redclover necrotic mottle virus, lowering the pH to trigger capsid formation is sufficient to enable this nucleation point to fully encapsulate the nanoparticle. The relative density can then be used to separate the full and empty protein shells.[72]

Encapsulation of a rigid gold nanoparticle core might thus be stimulated by either the electrostatic interaction between the coat protein and the scaffold, or via a specific origin of assembly (OAS). This is done through a two-step encapsulation pathway. It involves first lowering the ionic strength in a neutral buffer to facilitate aggregation of proteins on the nanoparticle surface and secondly to lower pH to trigger capsid shell formation. As such, only a fraction of the anionic AuNP is encapsulated. The efficiency of this encapsulation is often defined as $N_{\text{AuVLP}} / N_{\text{AuTotal}}$ and is normally only 2% or 3% for citrate ligands on the gold. A flexible linker molecule can be attached to the nanoparticle surface to act as nucleation sites for capsid assembly, increasing the efficiency up to 95%. Furthermore, by tuning the gold nanoparticle size, different core morphologies can be selected conforming to the T=3, T=1 and even metastable T=2 morphologies, see figure 13. The encapsulation efficiency does tend to vary with particle size as a competition between empty and filled capsid shells occurs. The resulting capsids are comparable to the native virus in that they show similar exterior characteristics and can be crystallised. These VLP crystals show interesting optical properties that differ from the free VLPs, likely due to electromagnetic interactions that are enhanced by the close proximity of the particles.[58, 73]

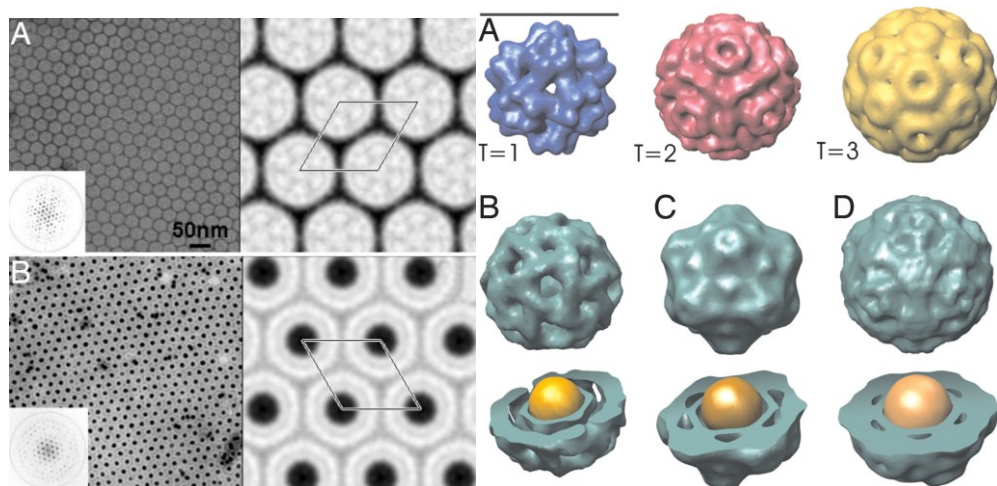


Figure 13: Encapsulation of AuNPs in CPMV leads to core controlled polymorphism (left) TEM micrographs of (A) CPMV and (B) CPMV-AuNP; (right) (A) T=1, T=2 and T=3 models from the VIPER database structures for CPMV and 3D cryo-TEM reconstructions showing (B) pseudo T=1, pseudo T=2 and pseudo T=3 morphologies for different sized AuNP encapsulated in the capsid.¹³ [58]

Carboxylic acid terminated triethylene glycol (TEG) coated AuNPs can also be introduced into CCMV via the two step encapsulation pathway. Similar to BMV, the VLP size depends on the core size presented. Surprisingly, it was found that N-terminus deleted CCMV, which lacks many of the positively charged residues associated with electrostatic binding of RNA or polyelectrolytes, still showed an encapsulation efficiency of 72%. The authors believe this could be of use in the creation of biomedicine by replacing such sequences with functional handles. [41] To us, this also indicates that the (re)assembly of the virus coat protein is favoured by the presence of a template.

13 Reprinted (adapted) from (Sun et al.,2007) [58] Copyright 2007 National Academy of Sciences, USA.

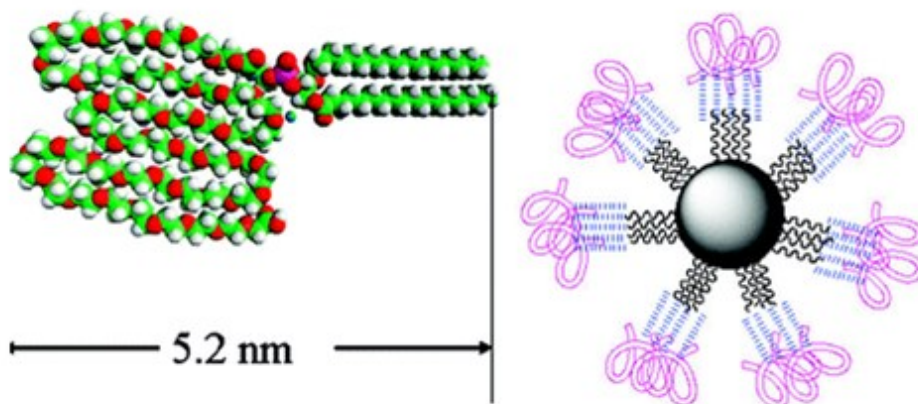


Figure 14: (left) A carboxylic acid terminated polyethylene glycol (PEG) chain is attached to a phospholipid. (right) This lipid intercalate with oleic acid groups on the surface of an iron oxide nanoparticle to enable the encapsulation in BMV (COOH-PEG-PL is shown in pink (PEG) and blue (PL) with black oleic acid covering the iron oxide nanoparticle).¹⁴[74]

Besides gold nanoparticles, BMV also has the potential to assemble around other inorganic cores. The key here is to selectively manipulate the surface ligand to create an anionic surface around the nanoparticle. For instance, oleic acid iron oxide nanoparticles were modified by adding a carboxylic acid terminated polyethylene glycol (PEG) chain attached onto a phospholipid onto their exterior surface, see figure 14. Subsequent assemblies showed the potential for core controlled polymorphism even beyond the native T=3 symmetry and displayed superparamagnetic behaviour in the particles. Still the encapsulation efficiency for the 10.5 and 8.5 nm particles was rather low (5% to 3%) compared to similar sized gold nanoparticles. This likely results from the rather spacious linker, which reduced the overall surface charge density due to folding of the PEG chain.[74] Anionic quantum dots can also be encapsulated inside BMV. Dixit et al. have coated these particles with the same PEG and DNA ligands that were used to encapsulated gold nanoparticles. Unlike the gold nanoparticles, however, multiple quantum dots were observed inside the virus shell. [75]

Studies employing gold nanoparticles displaying a mixture of COOH and OH terminated PEG chains as surface ligands showed that the surface charge density plays an important role in the templated assembly of the BMV protein cage. Below a critical surface charge concentration little encapsulation is observed, above it the

¹⁴ Reprinted (adapted) with permission from (Huang et al.,2007) [74] Copyright 2007 American Chemical Society.

efficiency increases drastically with increasing surface charge. VLP assembly is initiated at neutral pH where the nanoparticles are fully charged and afterward brought to acidic pH to trigger shell formation. These results indicate the necessity to form a critical nucleus of coat proteins through electrostatic association, thus enabling further growth and encapsulation upon pH lowering.[76]

Recent work by Tsvetkova et al. shows that both cooperative and non-cooperative absorption of protein subunits can promote the assembly of a virus capsid around a nanoparticle, but the pathway is dependent on the surrounding medium. These studies indicate that the organisation of BMV proteins around anionic AuNP shows such behaviour. At acidic pH initially little capsid formation is observed, until a critical concentration is reached. Presumably, at that point, the coat protein has a sufficiently large nucleus to promote further cooperative assembly. At neutral pH, when the AuNP charge is far higher, the protein readily absorbs onto the nanoparticle, until it is saturated. This is likely due to a greater charge interaction with the nanoparticle surface, in that way excluding the need for a nucleus that facilitates cooperative encapsulation.[77]

Gold nanoparticles can be coated with PEG or DNA to prepare them for encapsulation into simian virus 40 (SV40) capsids. DNA coated particles of all sizes can be encapsulated, but neutral PEG coated particles are only encapsulated if their core size is at least 15nm. This size dependency is in contrast to the normal electrostatic interaction and seems to be dependent on the total size of the PEG-AuNP construct, not merely the gold core.[78] This furthermore suggests that a charged template is not always needed. Li et al. have also shown that SV40 can encapsulate both anionic and cationic quantum dots with similar efficiencies. This might be attributed to the difference in the charge landscape of its coat protein. Whereas the isoelectric points of the inner coat for most virus capsids that have been studied are well above the pH of the assembly conditions used, SV40 has an isoelectric point close to this pH. This could explain the ability to encapsulate particles regardless of charge, indicating that the type of virus protein coat has a significant effect on the encapsulation.[79]

For encapsulation of anionic AuNP cores in animal alpha viruses the encapsulation efficiency was never found to be above 62%.[80] Yet, in simpler viruses, such as Red clover necrotic mosaic virus (RCNMV), capsid formation is also sometimes induced by more than electrostatics. In this case an origin of assembly (OAS) is required, comprised of a small RNA or DNA sequence found within the viral genome, that preorganizes some of the monomers, which subsequently triggers the further capsid formation. Loo et al. showed that by attaching this sequence to a

variety of nanoparticles, such as Au, CdSe and CoFe₂O₄ capsid formation around the nanoparticle will occur. This encapsulation process is limited by the size of the nanoparticle as particles in excess of the natural cavity cannot be encapsulated.[81]

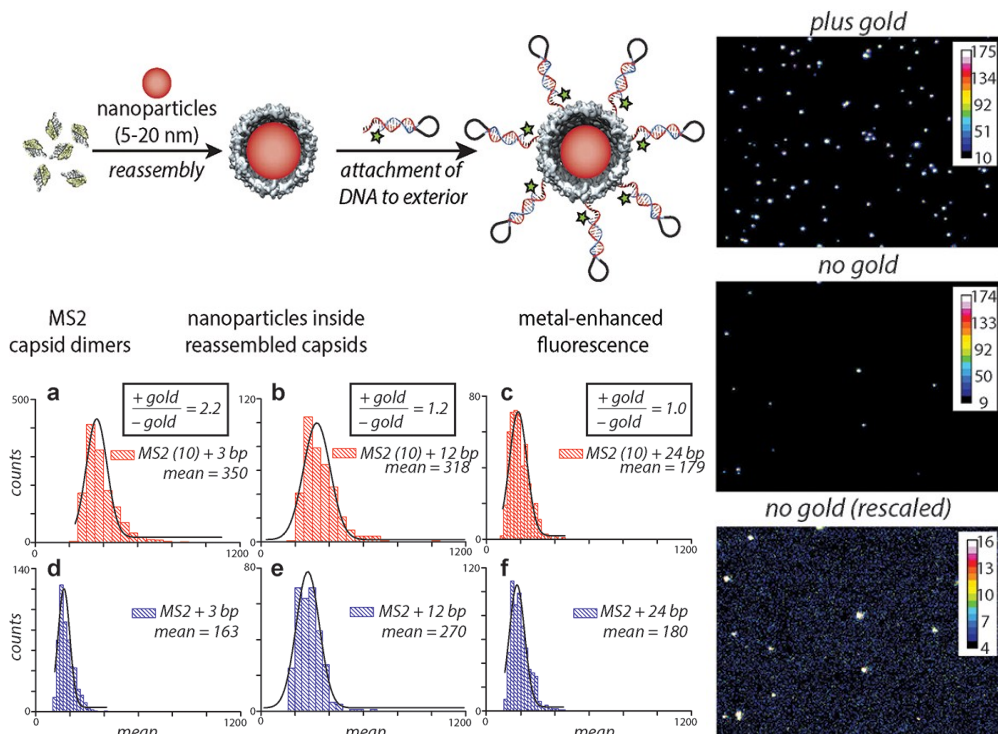


Figure 15: (Top, left) Encapsulation of NP inside and attachment of fluorescent dye to the exterior of MS2; (right) total internal reflection microscopy (TIRF) on CPMV-dye with and without a gold core; (bottom, left) TIRF intensity histograms for MS2 with AuNP (red) and without (bleu) with dye at 3, 12 or 24 distance spacing showing the relative increase of fluorescence.¹⁵ [82]

In the end, gold nanoparticles encapsulated in a viral coat protein present a stable scaffold with a large plasmon response. These physical properties can be exploited for their plasmon properties as the virus shell provides sufficient spacing to prevent quenching effects. Instead, a dye that is positioned on the surface of such a particle is expected to show an enhanced fluorescence as the dipole is enlarged due to interaction with the electric field of the gold plasmon. Capehart et al. used such gold nanoparticle based VLPs and attached a fluorophore with a DNA linker to the surface and showed that the fluorescence enhancement depended on the linker length and thus the spacing of the fluorophore to the gold nanoparticle, see figure

¹⁵ Reprinted (adapted) with permission from (Capehart et al.,2013) ⁸² Copyright 2013 American Chemical Society.

15.[82] Similar results have been achieved with other nano structures.[83-85] However, the virus capsids allow for a scaffold that is easily formed around a variety of nanoparticles and yet maintains similar surface functionality and chemical addressability.

Simulations

Simulations by Hagan confirm that strong core-shell interactions can lead to core controlled polymorphism. Yet, these simulations predict that the stability of the assembly can be undermined if the curvature of the core is incompatible with the subunit-subunit interaction that results in the lowest free energy. Therefore, whilst core-controlled polymorphism is allowed, it leads to the formation meta-stable particles. Additionally, chemisorption of subunits could lead to kinetically trapped states that prevent proper shell formation. More flexible cores overcome the curvature issues, but kinetic traps might occur more frequently.[86]

As shown by these simulations the ability of protein subunits to self-assemble around a rigid electrostatic core is dominated primarily by the surface charge density of the nanoparticle. After a certain threshold value is reached, the encapsulation efficiency is nearly 100%, though before that encapsulation is stunted. The theory is incomplete in that it does not account for the meta-stable phases, that seem to occur in experimental results before the threshold, which explain a gradual increase in efficiency with increased surface charge. As the early stages of the assembly are dominated by electrostatic absorption onto the nanoparticle surface, an excess of the coat protein is needed to allow for rapid encapsulation as otherwise the process requires desorption of coat protein before the capsid shells can be completed.[87]

A minimal charge density on the surface of a nanoparticle is required to trigger the assembly of a coat protein into a core controlled sized VLP. Sifers' simulations, see figure 16, show that not only the core diameter of the inorganic nanoparticle core affects the size of the final assembly, but also that the surface charge density plays an important role. In particular the flexible N-terminus that contains the positive charge, such as found in CCMV, can act as a spacer for sufficiently charged particles, in which the energy landscape will favour a different size assembly. Depending on particle diameter and surface charge, multiple transitions between smaller and larger VLP assemblies are observed.[88]

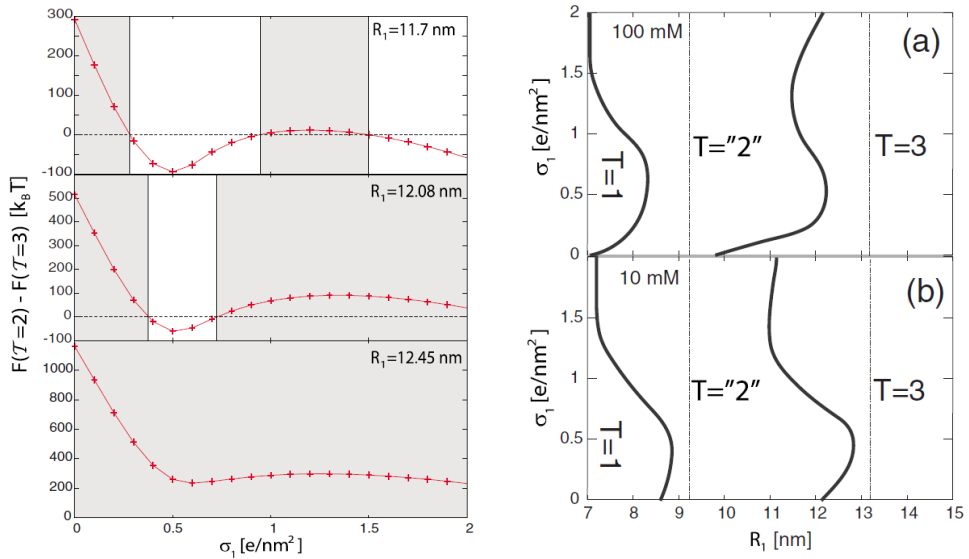


Figure 16: (left) The difference between the T=2 and T=3 capsid free surface energies for different core radii as a function of core surface charge density, showing either T=2 (white) or T=3 (grey) as being the energetically favoured assembly; (right) the energetically most favoured capsid morphology as a function of both charge (σ_1) and core radius (R_1) at (a) 100mM and (b) 10mM of monovalent salt.¹⁶ [88]

Anionic nanoparticles are typically stabilized by weakly acidic groups. Additionally, virus proteins tend to be stable and assemble around physiological pH or slightly acidic pH (5-7). As such, most encapsulation experiments have been performed around the pKa of the acidic groups, which in the case of small particles can lead to significant charge variation between the particles; an effect that is less pronounced for larger nanoparticles. Simulations by Line et al. show that this accounts for the gradual increase of encapsulation efficiency beyond the critical charge density, rather than an immediate sharp rise as was predicted by Hagan. [89]

Outer surface electrostatics

Whilst the inner surface might readily and controllably promote the encapsulation of a wide variety of species, the outer surface too carries the potential for electrostatic interaction. Similar to genetic and chemical modifications, the outer charged shell is dependent on the locally available groups and is highly symmetrical. In effect, this creates a surface which, more than the inner surface,

¹⁶ Reprinted figure with permission from A. Šiber, R. Zandi, and R. Podgornik, Physical Review E, 81(5), 051919, 2010. Copyright (2010) by the American Physical Society.

carries patches of charge in a highly symmetrical pattern. Comparable to the inner surface, these patches can be used to bind polyelectrolytes or nanoparticle.

Binding polymers to the surface of a virus can be used to transform the virus particle into a template for the synthesis of an inorganic shell. For instance, Evans has electrostatically bound poly(allylamine) hydrochloride (PAH) to the surface of CPMV to promote the absorption of gold nanoparticles. These particles could be subsequently incubated with gold salts, which after reduction form a gold shell around the virus particle. [90]

Due to the capsid symmetry, the electrostatic interactions of protein cages with small metallic nanoparticles has allowed for the creation of organised nanostructures. Not only does the symmetry of the protein cage result in the symmetrical distribution of charges, but often these charges are concentrated in patches on the surface, that, depending on pH and ionic strength, allow for multivalent electrostatic interactions at specific sites. Kale et.al used this to organise 5nm CdS quantum dots on the surface of P22 bacteriophage capsids. In this case, structures with hexagonal and pentagonal organisation of quantum dots on the 60nm capsid were obtained at pH 4, below the isoelectric point of 4.97, where the subunits appear to pop out of the capsids. The organisation was lost at around pH 9. [91]

Both internal and external functionalization of the capsids can be combined in the same structure. For instance, a protein mantle can be formed around a nanoparticle and subsequently coated with different nanoparticles, adhering to the outer shell to create complex architectures. Due to the supramolecular nature of the interactions in these architectures, these can be easily manipulated using pH and ionic strength. SV40 capsids have been used to demonstrate this for gold nanoparticles adhering to amine rich spots on the surface of an SV40 VLP containing a variety of different nanoparticles inside the VLP, see figure 17.[92]

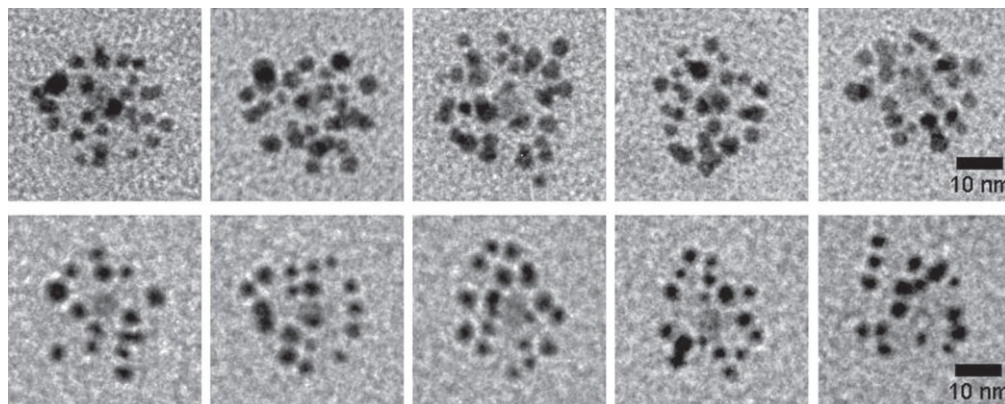
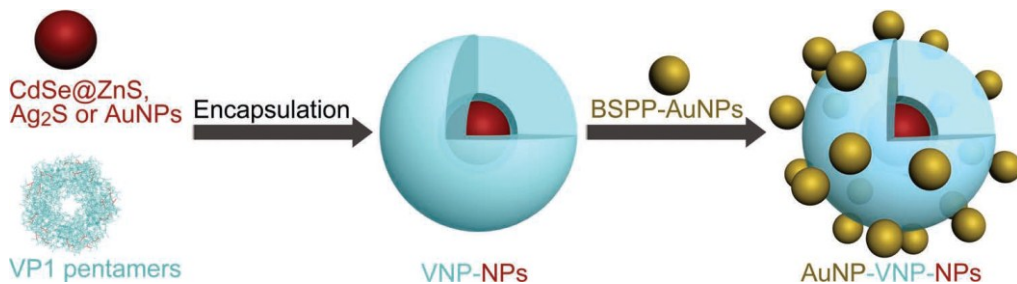


Figure 17: (top) Scheme for combining internal and external electrostatic assembly for the creation of complex architectures; (bottom) TEM micrographs of AuNP assembling around a SV40 capsid containing a CdSe/ZnS quantum dot.¹⁷ [92]

Organisation of viruses

As is shown above, the organisation of particles or molecules on viruses allows for the fabrication of organised nanostructures on a single VLP. This can be taken a step further, by for example linking multiple VLPs to a single surface, by layer-by-layer assembly or by non-covalent clustering. These architectures range from simple monolayers to layered structures and even complex hierarchical 3D crystals. These virus-based nanomaterial assemblies can be separated into two broad groups based on the particle interaction; either as covalent and biomolecular assembly, or as electrostatic assembly.

Covalent and biomolecular assembly

Using chemical linkers to direct viruses to assemble onto surfaces in 2D or layer-by-layer into 3D assemblies allows for strong binding and precise control over the composition of the layers that are formed. Either the virus is crystallised first and

¹⁷ Three-Dimensional Gold Nanoparticle Clusters with Tunable Cores Templated by a Viral Protein Scaffold, Li, F., et al., *Small*, 8(24). Copyright © 2012 WILEY-VCH Verlag GmbH & Co. KGaA, Weinheim

subsequently stabilised using chemical crosslinkers or, to promote a specific interaction, a recombinant VLP can be used, containing for instance cysteine residues or his-tag loops. Two approaches to control this organisation exist; i) a top down (pre)patterning of a surface or scaffold, or ii) dynamic self-assembly at an interface or by inter-particle interaction. The later generally shows a greater degree of control over the structure's size and order. We attribute this to the symmetry of the virus, which in dynamic self-assembly becomes an important structural and packaging parameter.

Under well-chosen conditions virus particles can be crystallised, however, these crystals often need to be stabilised using chemical crosslinking. For example, Russel et al. have shown that CPMV particles can be organised on the interface in a mixture of perfluorodecalin or chloroform and water. The resulting close packing of virus nanoparticles was cross-linked using glutaraldehyde. No disruption of the virus nanoparticle integrity was observed, however, the resulting membranes would crumple upon the removal of the solvents. [93, 94] These cross-linked systems can be used as porous scaffolds for the synthesis of nano-composites. To demonstrate this, Falkner et al. incubated such a crystal with a precursor solutions containing palladium ions and subsequently platinum ions, which were catalytically reduced to generate metal deposits inside the virus scaffold.[95]

Genetically modified CPMV that presents a cysteine group on the exterior surface of the capsid can be attached to a gold surface that has been modified with maleimide groups; as is shown by the formation of a layer of cysteine labelled CPMV. Using a top down strategy, this layer can be patterned subsequently, using e-beam lithography, leaving 30nm wide lines of CPMV on the surface, in effect showing a pseudo 1D pattern of the viruses.[47] As an alternative strategy the surface itself can be pre-patterned. To do this Cheung et al. further modified the CPMV cysteine with 6 His tags. This enabled them to form a surface pattern with lines of Ni-NTA, allowing binding of the modified CPMV to the surface onto these lines. [96] In both cases no higher order organisation within the lines can be observed, nor in the 2D patterns that they were made from them.

Using a self-assembly approach may thus make it easier to organise viruses on a surface, by controlling and limiting the number of interactions. Klem et al. used A163C genetically modified CCMV virus capsids and self-assembled them onto Au surfaces. They found that capsids which have a limited number of surface exposed thiols show a greater degree of organisation compared to capsids that have all of its 180 thiol groups exposed.[42]

Moving towards a 3D pattern an interlayer can help with the organisation of virus particles without the need to modify viruses separately. Steinmetz et al. used biotinylated CPMV for the creation of alternating layers of CPMV linked by streptavidin molecules. Before assembly into layers, different dyes were coupled to CPMV to monitor the process. The layer-by-layer process was thus demonstrated to create unique and separate layers that showed no intermixing, see figure 18.[97] To further enhance the biotin-CPMV-streptavidin assembly, the effect of the density and spacer length of the biotinylation on CPMV was studied. Depending on these factors, the order within each layer can be affected. More importantly, shifts in the frequency in the quartz crystal microbalance measurements show that this also affects the mechanical properties of the array.[98]

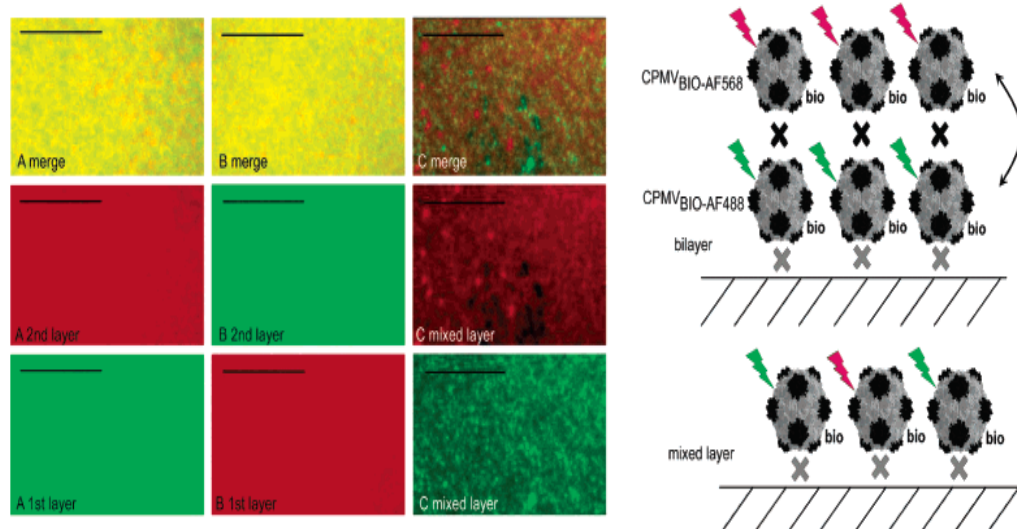


Figure 18: (left) Fluorescence microscopy images of biotin-streptavidin-CPMV bilayers of (A) AF488 labelled CPMV layer followed by AF568 labelled CPMV layer, (B) AF568 labelled CPMV layer followed by AF488 labelled CPMV layer, (C) both AF-568 and AF-488 dye labels attached to CPMV in each layer, top images show the merged images of the red and green filtered images shown below; (right) scheme showing the biotin-streptavidin-CPMV-dye assembly.¹⁸ [97]

Interestingly, the aggregation of coat proteins can also be achieved purely using coat protein alone, if suitable conditions and modifications are chosen. Porta et al. found that expression of foreign peptides, genetically engineered into an exposed surface loop, resulted in the aggregation of protein cages within infected plant

¹⁸ Reprinted (adapted) with permission from (Steinmetz et al., 2006) [97] Copyright 2006 American Chemical Society.

tissue. This behaviour was only observed in certain chimeric particles, but never for the wild type virus.[99]

The organisation of viruses and VLPs is attractive as such particles are naturally designed to interact with biological cells. A large research effort is on-going towards the use of these particles as a drug delivery vesicles, however, this is beyond the scope of this chapter.[100] , a similar interaction principle can be used for other purposes when combined with surface growth. In a study by Lin et al. CPMV was used to promote cell adhesion to a surface. To achieve this poly(diallyldimethylammonium chloride) (PDDA) was used to adhere CPMV to a Ag coated wafer by alternating PDDA and CPMV in a layer-by-layer fashion. The coverage of CPMV in this case is dependent simply on both time and pH, favouring a pH near the isoelectric point. Cells grown on this layer show good adhesion and are still biologically active.[101]

Ultimately, the goal we envision is to generate a large 3D architecture of viruses and integrate functional components into this structure. In work by Cigler et al. this has been achieved by using a DNA programmed assembly technique to form binary crystals of Q β phage capsids and gold nanoparticles. To this end opposing strands of DNA were grafted on the capsid, using surface modification techniques similar to those described above, and the gold nanoparticle, using a thiol ligand exchange. Upon combination of these two particles DNA, base pairing allows for the formation of NaCl lattice crystal structures for particles with similar radii. As an open structure with regularly spaced plasmonic gold nanoparticles, such structures can be vital in the design of the next generation of nano-photonic materials.[102] Furthermore, we feel that this example also demonstrates the broad potential of viruses as a structural nano building block in forming highly organised structures as it is likely that the virus symmetry and monodispersity improved the degree of crystallinity found by the authors.

Electrostatic assembly

As described, the exterior surface of a virus is decorated with symmetrically placed patches of charge. In general, to compensate for the cationic N-terminus found inside most virus capsids the exterior tends to be anionic. This enables viruses and VLPs to be used as a substitute for other anionic species in many systems. The potential to assemble virus in alternating multilayers of opposing charge was observed when PSS could be substituted by Carnation Mottle Virus as the anionic species in an alternating PSS and poly(allylamine) (PAA) multilayer. [103]

Electrostatic interactions can have a profound influence on the ability of viruses to absorb onto and later assemble on surfaces. Little to no absorbance was shown by

Suci et al. for CCMV on bare silica or formvar surfaces. After the surface charge was changed by coating the surface with polylysine a change in the coverage is observed, with greater positive charge inducing a greater coverage. Variations in the pH after surface modification can be further used to alter the surface interaction. [104] The electrostatic absorption of CCMV on a charged surface, such as cysteamine on gold or amines on silica, can thus be used to pre-organise a 2D layer of virus nanoparticles (see above).

Not all viruses show similar behaviour, a markedly different behaviour between spherical and rod-like species is observed. In experiments by Yoo et al. a layer of polyelectrolytes was grown and subsequently either rod-like (TMV, M13) or spherical viruses (CCMV, CPMV) were deposited on these layers. The spherical particles show rapid surface absorption compared to the rod-like ones, but both eventually showed close packing of the particles. To achieve further growth, alternating layers of polyelectrolytes and virus nanoparticles were deposited. Spherical viruses are integrated successfully in this structure, though rod-like viruses are excluded from the layers and are found to float to the top of the polyelectrolyte layer. [105, 106]

Going beyond surface bound techniques might allow for control over crystallisation directly in solution. To achieve this, the electrostatic interaction of CCMV with a variety of positively charged polymers was studied by Kostianen et al. Amine functionalised Newcombe type dendrons, PANAM and poly- λ -lysine all have shown the ability to induce aggregation of CCMV. An increased charge on the macromolecules allows for a more efficient clustering, with 4 or less positive charges showing no clustering at all. Both the salt concentration and pH have a significant effect on this type of clustering. Furthermore, the clustering is also shown to work with Prussian blue containing CCMV based VLPs, showing the general applicability of this method to generate nanomaterial arrays.[107]

The assembly of viruses and VLPs into large clusters by itself may make for an interesting nano-array, but dynamic systems that allow control over this clustering can also be created. Kostianen et al. created such dynamic systems that allow the reversible assembly and disassembly of densely packed and highly ordered arrays to be studied, see figure 19. These systems are based on same the Newcombe type dendrimers as before, only now containing a photolabile group. After clustering, UV irradiation can be used to break up the dendrimers, thus dropping the overall charge to 4 or less positive charges per polyelectrolyte, and disrupting the array. [108] Similarly, temperature responsive block- copolymers can be electrostatically bound to CCMV. Upon applying an external stimulus by raising the temperature,

the mantle of these polymers collapses and causes the CCMV-polymer complex to cluster. A subsequent lowering of the temperature releases the virus-polymer complexes back into solution.[109]

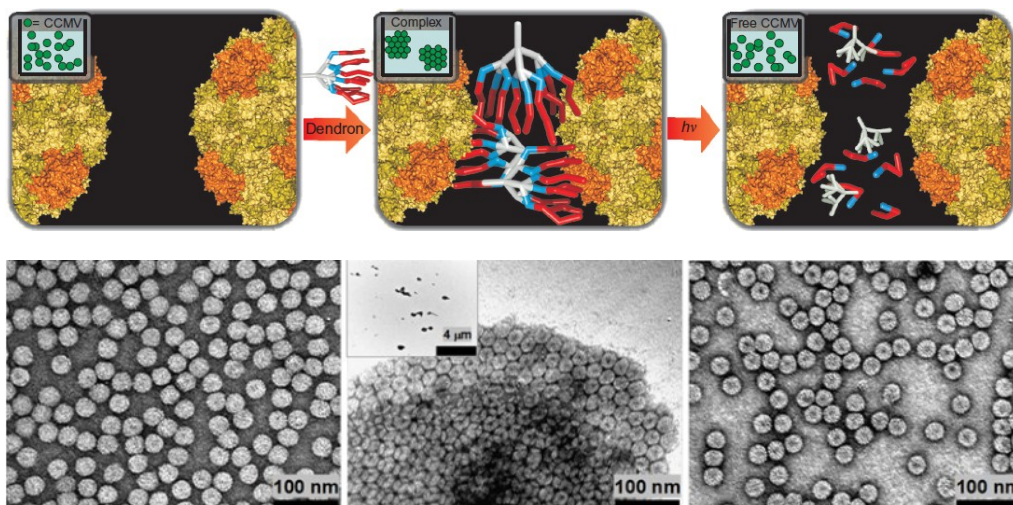


Figure 19: (top) Schematic representation and (bottom) TEM images of: (left) Free CCMV before any clustering agent is added. (centre) Clustered CCMV due to the addition of spermine (red) terminated Newcombe type dendrimers containing a photolabile group (blue). (right) CCMV released from clustering by UV irradiation to disrupt the photolabile group.¹⁹[108]

This clustering behaviour is not limited to polymeric soft materials. Using the electrostatic interaction between anionic CCMV protein cages and cationic gold nanoparticles, Kostianen et al. were able to fabricate complex architectures. These architectures resulted from the naturally occurring patches of negative charge found on the CCMV surface. The spacing and position of these 60 patches is defined by the structure of the protein cage, and they are found near the naturally occurring pores on the trifold axis of the icosahedral structure. Allowing space for electrostatic repulsion between the gold nanoparticles, and thus leaving an empty patch between each nanoparticle binding site, it was found that 24 of these patches could be used to bind the gold nanoparticles. [110]

Besides proper clustering conditions, other factors could explain why Kostianen found clusters rather than single VLPs decorated with gold nanoparticles. De et al. demonstrated that nanoparticles and proteins interactions are partially dominated by the relative size of these particles. If proteins are much larger than the

¹⁹ Reprinted by permission from Macmillan Publishers Ltd: Nature Chemistry, from (Kostianen, M.A., et al., 2010)[108], copyright 2010.

nanoparticle the protein complexes multiple nanoparticles, the reverse is true if the nanoparticle is much larger than the protein. If they are of similar size, however, the particles are capable of forming extended networks and form complex self-assembled structures.[111]

VLP clustering might even lead to an energetically favoured state due to the patchy nature of the surface. For viral capsids, due to the symmetry in the protein shell these surface charge variations are especially pronounced. Božić and Podgornik show that these variations can lead to a reduction in the interaction energy between the shells of two equally charged virus particles. Furthermore, if the particles allow sufficient orientation variation to minimise the interaction energy, this can even lead to a short range attractive force between the particles. If multiple symmetrical axis can be defined on a particle, such as on larger VLPs with increased Caspar Klug symmetries, these effects are even more outspoken. Additionally, such symmetrical concerns can of course influence the interaction of virus shells with other charged species, such as polyelectrolytes or multivalent ions.[112]

Concluding remarks

Viruses and virus-like nanoparticles offer a highly adaptable scaffold for nanotechnology. They combine important natural characteristics, such as symmetry, chemical addressability and versatility and genetic modifiability. Furthermore, through manipulation and templating they can be tuned in size and shape. These properties can be utilised to build a wide variety of functional systems from paramagnetic contrast agents and mineralisation templates to nanoreactors and containers. More importantly, the nature of a virus capsid allows different modifications to be combined into complex systems and, when needed, arrays of these materials can be made through a variety of chemical and electrostatic clustering techniques.

It is in the last decades that VLPs have been studied to be used in nanotechnological applications, and still the research interest in the field is far from depleted. After all, there are both new challenges to be addressed and steps to be taken to improve upon the existing work. These challenges range from the structural scaling towards larger, organised clusters of these particles to seeking control over interactions between materials confined in or in the proximity of these protein cages.

There are, however, natural limitations to these particles, as they are and remain based on soft protein matter. Though generally more robust than other biological

or soft materials, their biological nature limits the range of conditions such as solvents, pH and temperature that they will thrive in. The recent discovery of other, non-viral, protein cages, like encapsulins from bacteria, proves that these limits could be stretched quite significantly if needed. Other opportunities lie, for instance, in combined hard-soft materials like core-shell systems where the proteins monodispersity and symmetry form the template for materials with radically different properties.

Ultimately, we feel that though an extensive library of different VLPs and techniques for organising exists, so far few research papers have studied the properties of VLPs in materials and the effect of the protein cage upon the resulting physical properties. This, however, will be a next crucial step in the future of this field as it holds the promise of modular nanomaterials with a uniform VLP building block. An endeavour that will allow us to create nanostructured materials with a wide variety of new physical properties. Key to the success of this endeavour will be a clear understanding of the properties, parameters and limitations that govern these structures combined with exhaustive synthetic tools for their creation.

Bibliography

1. Lars, O.L., et al., *Structural transitions in Cowpea chlorotic mottle virus (CCMV)*. Physical Biology, 2005. **2**(4): p. S166.
2. Carrillo-Tripp, M., et al., *VIPERdb2: an enhanced and web API enabled relational database for structural virology*. Nucleic Acids Research, 2009. **37**(suppl 1): p. D436-D442.
3. Lee, K.K. and J.E. Johnson, *Complementary approaches to structure determination of icosahedral viruses*. Current Opinion in Structural Biology, 2003. **13**(5): p. 558-569.
4. Baker, T.S. and R.H. Cheng, *A model-based approach for determining orientations of biological macromolecules imaged by cryoelectron microscopy*. J Struct Biol, 1996. **116**(1): p. 120-30.
5. Makino, D.L., et al., *Investigation of RNA structure in satellite panicum mosaic virus*. Virology, 2006. **351**(2): p. 420-431.
6. Comellas-Aragones, M., et al., *Solution scattering studies on a virus capsid protein as a building block for nanoscale assemblies*. Soft Matter, 2011. **7**(24): p. 11380-11391.
7. Speir, J.A., et al., *Structures of the native and swollen forms of cowpea chlorotic mottle virus determined by X-ray crystallography and cryo-electron microscopy*. Structure, 1995. **3**(1): p. 63-78.
8. Caspar, D.L.D. and A. Klug, *Physical principles in the construction of regular viruses*. Cold Spring Harbor Symp. Quant. Biol, 1962: p. 27,1-24.

9. Caspar, D.L.D.K., A., *Structure and assembly of regular virus particles*. *Virus, nucleic acids and cancer*. 17th Annual Symposium on Fundamental Cancer Research, University of Texas, Williams and Wilkins, Baltimore,, 1963 . . p. pp. 27-39.
10. Bruinsma, R.F., et al., *Viral Self-Assembly as a Thermodynamic Process*. *Physical Review Letters*, 2003. **90**(24): p. 248101.
11. Zandi, R., et al., *Origin of icosahedral symmetry in viruses*. *Proceedings of the National Academy of Sciences of the United States of America*, 2004. **101**(44): p. 15556-15560.
12. Nguyen, H.D. and C.L. Brooks, *Generalized Structural Polymorphism in Self-Assembled Viral Particles*. *Nano Letters*, 2008. **8**(12): p. 4574-4581.
13. Nguyen, H.D., V.S. Reddy, and C.L. Brooks, *Invariant Polymorphism in Virus Capsid Assembly*. *Journal of the American Chemical Society*, 2009. **131**(7): p. 2606-2614.
14. Johnson, J.E. and J.A. Speir, *Quasi-equivalent viruses: A paradigm for protein assemblies*. *Journal of Molecular Biology*, 1997. **269**(5): p. 665-675.
15. Zlotnick, A. and S.J. Stray, *How does your virus grow? Understanding and interfering with virus assembly*. *Trends in Biotechnology*, 2003. **21**(12): p. 536-542.
16. Belyi, V.A. and M. Muthukumar, *Electrostatic origin of the genome packing in viruses*. *Proceedings of the National Academy of Sciences*, 2006. **103**(46): p. 17174-17178.
17. Linger, B.R., et al., *Sindbis virus nucleocapsid assembly: RNA folding promotes capsid protein dimerization*. *RNA*, 2004. **10**(1): p. 128-38.
18. Castelnovo, M., D. Muriaux, and C. Faivre-Moskalenko, *Entropic control of particle sizes during viral self-assembly*. *New Journal of Physics*, 2013. **15**(3): p. 035028.
19. Johnson, J.M., et al., *Interaction with Capsid Protein Alters RNA Structure and the Pathway for In Vitro Assembly of Cowpea Chlorotic Mottle Virus*. *Journal of Molecular Biology*, 2004. **335**(2): p. 455-464.
20. Zlotnick, A., et al., *Mechanism of Capsid Assembly for an Icosahedral Plant Virus*. *Virology*, 2000. **277**(2): p. 450-456.
21. Zhao, X., et al., *In Vitro Assembly of Cowpea Chlorotic Mottle Virus from Coat Protein Expressed in Escherichia coli and in Vitro-Transcribed Viral cDNA*. *Virology*, 1995. **207**(2): p. 486-494.
22. Bancroft, J.B., C.E. Bracker, and G.W. Wagner, *STRUCTURES DERIVED FROM COWPEA CHLOROTIC MOTTLE AND BROME MOSAIC VIRUS PROTEIN*. *Virology*, 1969. **38**(2): p. 324-&.
23. Lavelle, L., et al., *Phase Diagram of Self-assembled Viral Capsid Protein Polymorphs*. *Journal of Physical Chemistry B*, 2009. **113**(12): p. 3813-3819.
24. Loo, L., et al., *Infusion of dye molecules into Red clover necrotic mosaic virus*. *Chemical Communications*, 2008. **0**(1): p. 88-90.

25. Basu, G., et al., *Metal binding to cowpea chlorotic mottle virus using terbium(III) fluorescence*. Journal of Biological Inorganic Chemistry, 2003. **8**(7): p. 721-725.
26. Allen, M., et al., *Paramagnetic Viral Nanoparticles as Potential High-Relaxivity Magnetic Resonance Contrast Agents*. Magnetic Resonance in Medicine, 2005(54): p. 807-812.
27. Lee, L.A., H.G. Nguyen, and Q. Wang, *Altering the landscape of viruses and bionanoparticles*. Organic & Biomolecular Chemistry, 2011. **9**(18): p. 6189-6195.
28. Strable, E. and M.G. Finn, *Chemical Modification of Viruses and Virus-Like Particles*, in *Viruses and Nanotechnology*, M. Manchester and N. Steinmetz, Editors. 2009, Springer Berlin Heidelberg. p. 1-21.
29. Young, M., et al., *Plant Viruses as Biotemplates for Materials and Their Use in Nanotechnology*. Annual Review of Phytopathology, 2008. **46**(1): p. 361-384.
30. Steinmetz, N.F., G.P. Lomonosoff, and D.J. Evans, *Decoration of Cowpea Mosaic Virus with Multiple, Redox-Active, Organometallic Complexes*. Small, 2006. **2**(4): p. 530-533.
31. de la Escosura, A., et al., *Viral capsids as templates for the production of monodisperse Prussian blue nanoparticles*. Chemical Communications, 2008. **0**(13): p. 1542-1544.
32. Qazi, S., et al., *P22 Viral Capsids as Nanocomposite High-Relaxivity MRI Contrast Agents*. Molecular Pharmaceutics, 2012. **10**(1): p. 11-17.
33. Barnhill, H.N., et al., *Turnip Yellow Mosaic Virus as a Chemoaddressable Bionanoparticle*. Bioconjugate Chemistry, 2007. **18**(3): p. 852-859.
34. Wang, Q., et al., *Natural Supramolecular Building Blocks: Wild-Type Cowpea Mosaic Virus*. Chemistry & Biology, 2002. **9**(7): p. 805-811.
35. Wang, Q., et al., *Icosahedral Virus Particles as Addressable Nanoscale Building Blocks*. Angewandte Chemie International Edition, 2002. **41**(3): p. 459-462.
36. Anderson, E.A., et al., *Viral Nanoparticles Donning a Paramagnetic Coat: Conjugation of MRI Contrast Agents to the MS2 Capsid*. Nano letters, 2006. **6**(6): p. 1160-1164.
37. Aljabali, A.A.A., et al., *Charge Modified Cowpea Mosaic Virus Particles for Templated Mineralization*. Advanced Functional Materials, 2011. **21**(21): p. 4137-4142.
38. Comellas-Aragonès, M., et al., *Controlled Integration of Polymers into Viral Capsids*. Biomacromolecules, 2009. **10**(11): p. 3141-3147.
39. Wang, Q., et al., *Natural Supramolecular Building Blocks: Cysteine-Added Mutants of Cowpea Mosaic Virus*. Chemistry & Biology, 2002. **9**(7): p. 813-819.
40. Douglas, T., et al., *Protein Engineering of a Viral Cage for Constrained Nanomaterials Synthesis*. Advanced Materials, 2002. **14**(6): p. 415-418.

41. Aniagyei, S.E., et al., *Synergistic Effects of Mutations and Nanoparticle Templating in the Self-Assembly of Cowpea Chlorotic Mottle Virus Capsids*. Nano Letters, 2009. **9**(1): p. 393-398.
42. Klem, M.T., et al., *2-D Array Formation of Genetically Engineered Viral Cages on Au Surfaces and Imaging by Atomic Force Microscopy*. Journal of the American Chemical Society, 2003. **125**(36): p. 10806-10807.
43. Blum, A.S., et al., *Cowpea Mosaic Virus as a Scaffold for 3-D Patterning of Gold Nanoparticles*. Nano Letters, 2004. **4**(5): p. 867-870.
44. Chatterji, A., et al., *A Virus-Based Nanoblock with Tunable Electrostatic Properties*. Nano Letters, 2005. **5**(4): p. 597-602.
45. Li, F., et al., *Monofunctionalization of Protein Nanocages*. Journal of the American Chemical Society, 2011. **133**(50): p. 20040-20043.
46. Hooker, J.M., E.W. Kovacs, and M.B. Francis, *Interior Surface Modification of Bacteriophage MS2*. Journal of the American Chemical Society, 2004. **126**(12): p. 3718-3719.
47. Cheung, C.L., et al., *Fabrication of assembled virus nanostructures on templates of chemoselective linkers formed by scanning probe nanolithography*. Journal of the American Chemical Society, 2003. **125**(23): p. 6848-6849.
48. Blum, A.S., et al., *An Engineered Virus as a Scaffold for Three-Dimensional Self-Assembly on the Nanoscale*. Small, 2005. **1**(7): p. 702-706.
49. Martinez-Morales, A.A., et al., *Synthesis and Characterization of Iron Oxide Derivatized Mutant Cowpea Mosaic Virus Hybrid Nanoparticles*. Advanced Materials, 2008. **20**(24): p. 4816-+.
50. Patterson, D.P., et al., *Virus-like particle nanoreactors: programmed encapsulation of the thermostable CelB glycosidase inside the P22 capsid*. Soft Matter, 2012. **8**(39): p. 10158-10166.
51. Douglas, T. and M. Young, *Virus particles as templates for materials synthesis*. Advanced Materials, 1999. **11**(8): p. 679-+.
52. Allen, M., et al. (2002) *Protein Cage Constrained Synthesis of Ferrimagnetic Iron Oxide Nanoparticles*. Advanced Materials, 1562-1565 DOI: 10.1002/1521-4095(20021104)14:21<1562::AID-ADMA1562>3.0.CO;2-D.
53. Douglas, T. and M. Young, *Host-guest encapsulation of materials by assembled virus protein cages*. Nature, 1998. **393**(6681): p. 152-155.
54. Aljabali, A.A.A., et al., *Cowpea Mosaic Virus Unmodified Empty Viruslike Particles Loaded with Metal and Metal Oxide*. Small, 2010. **6**(7): p. 818-821.
55. Shah, S.N., et al., *Environmentally benign synthesis of virus-templated, monodisperse, iron-platinum nanoparticles*. Dalton Transactions, 2009(40): p. 8479-8480.
56. Steinmetz, N.F., et al., *Virus-Templated Silica Nanoparticles*. Small, 2009. **5**(7): p. 813-816.
57. Comellas-Aragones, M., et al., *A virus-based single-enzyme nanoreactor*. Nature Nanotechnology, 2007. **2**(10): p. 635-639.

58. Sun, J., et al., *Core-controlled polymorphism in virus-like particles*. Proceedings of the National Academy of Sciences, 2007. **104**(4): p. 1354-1359.
59. Sikkema, F.D., et al., *Monodisperse polymer-virus hybrid nanoparticles*. Organic & Biomolecular Chemistry, 2007. **5**(1): p. 54-57.
60. Liu, Z., et al., *Natural supramolecular building blocks: from virus coat proteins to viral nanoparticles*. Chemical Society Reviews, 2012. **41**(18): p. 6178-6194.
61. Bancroft, J.B., E. Hiebert, and C.E. Bracker, *The effects of various polyanions on shell formation of some spherical viruses*. Virology, 1969. **39**(4): p. 924-930.
62. Ren, Y., S.-M. Wong, and L.-Y. Lim, *In vitro-reassembled plant virus-like particles for loading of polyacids*. Journal of General Virology, 2006. **87**(9): p. 2749-2754.
63. Hu, Y.F., et al., *Packaging of a polymer by a viral capsid: The interplay between polymer length and capsid size*. Biophysical Journal, 2008. **94**(4): p. 1428-1436.
64. Cadena-Nava, R.D., et al., *Exploiting Fluorescent Polymers To Probe the Self-Assembly of Virus-like Particles*. Journal of Physical Chemistry B, 2011. **115**(10): p. 2386-2391.
65. van der Schoot, P. and R. Bruinsma, *Electrostatics and the assembly of an RNA virus*. Physical Review E, 2005. **71**(6): p. 061928.
66. Chang, C.B., et al., *Curvature Dependence of Viral Protein Structures on Encapsidated Nanoemulsion Droplets*. ACS Nano, 2008. **2**(2): p. 281-286.
67. Mukherjee, S., et al., *Redirecting the Coat Protein of a Spherical Virus to Assemble into Tubular Nanostructures*. Journal of the American Chemical Society, 2006. **128**(8): p. 2538-2539.
68. Kwak, M., et al., *Virus-like Particles Templated by DNA Micelles: A General Method for Loading Virus Nanocarriers*. Journal of the American Chemical Society, 2010. **132**(23): p. 7834-+.
69. Aniagyei, S.E., et al., *Self-assembly approaches to nanomaterial encapsulation in viral protein cages*. Journal of Materials Chemistry, 2008. **18**(32): p. 3763-3774.
70. Dragnea, B., et al., *Gold Nanoparticles as Spectroscopic Enhancers for in Vitro Studies on Single Viruses*. Journal of the American Chemical Society, 2003. **125**(21): p. 6374-6375.
71. Chen, C., et al., *Packaging of Gold Particles in Viral Capsids*. Journal of Nanoscience and Nanotechnology, 2005. **5**(12): p. 2029-2033.
72. Loo, L., et al., *Controlled Encapsidation of Gold Nanoparticles by a Viral Protein Shell*. Journal of the American Chemical Society, 2006. **128**(14): p. 4502-4503.
73. Chen, C., et al., *Nanoparticle-Templated Assembly of Viral Protein Cages*. Nano Letters, 2006. **6**(4): p. 611-615.

74. Huang, X., et al., *Self-Assembled Virus-like Particles with Magnetic Cores*. NANO LETTERS 2007. **7**(8): p. 2407-2416.
75. Dixit, S.K., et al., *Quantum Dot Encapsulation in Viral Capsids*. Nano Letters, 2006. **6**(9): p. 1993-1999.
76. Daniel, M.C., et al., *Role of Surface Charge Density in Nanoparticle-Templated Assembly of Bromovirus Protein Cages*. ACS Nano, 2010. **4**(7): p. 3853-3860.
77. Tsvetkova, I., et al., *Pathway switching in templated virus-like particle assembly*. Soft Matter, 2012. **8**(17): p. 4571-4577.
78. Wang, T.J., et al., *Encapsulation of gold nanoparticles by simian virus 40 capsids*. Nanoscale, 2011. **3**(10): p. 4275-4282.
79. Li, F., et al., *Viral Coat Proteins as Flexible Nano-Building-Blocks for Nanoparticle Encapsulation*. Small, 2010. **6**(20): p. 2301-2308.
80. Goicochea, N.L., et al., *Core-like Particles of an Enveloped Animal Virus Can Self-Assemble Efficiently on Artificial Templates*. Nano Letters, 2007. **7**(8): p. 2281-2290.
81. Loo, L., et al., *Encapsidation of Nanoparticles by Red Clover Necrotic Mosaic Virus*. Journal of the American Chemical Society, 2007. **129**(36): p. 11111-11117.
82. Capehart, S.L., et al., *Controlled Integration of Gold Nanoparticles and Organic Fluorophores Using Synthetically Modified M52 Viral Capsids*. Journal of the American Chemical Society, 2013. **135**(8): p. 3011-3016.
83. Schneider, G., et al., *Distance-Dependent Fluorescence Quenching on Gold Nanoparticles Ensheathed with Layer-by-Layer Assembled Polyelectrolytes*. Nano Letters, 2006. **6**(3): p. 530-536.
84. Bardhan, R., et al., *Fluorescence Enhancement by Au Nanostructures: Nanoshells and Nanorods*. ACS Nano, 2009. **3**(3): p. 744-752.
85. Acuna, G.P., et al., *Fluorescence Enhancement at Docking Sites of DNA-Directed Self-Assembled Nanoantennas*. Science, 2012. **338**(6106): p. 506-510.
86. Hagan, M.F., *Controlling viral capsid assembly with templating*. Physical Review E, 2008. **77**(5): p. 051904.
87. Hagan, M.F., *A theory for viral capsid assembly around electrostatic cores*. Journal of Chemical Physics, 2009. **130**(11).
88. Siber, A., R. Zandi, and R. Podgornik, *Thermodynamics of nanospheres encapsulated in virus capsids*. Physical Review E, 2010. **81**(5).
89. Lin, H.K., P. van der Schoot, and R. Zandi, *Impact of charge variation on the encapsulation of nanoparticles by virus coat proteins*. Physical Biology, 2012. **9**(6).
90. Aljabali, A.A.A., G.P. Lomonossoff, and D.J. Evans, *CPMV-Polyelectrolyte-Templated Gold Nanoparticles*. Biomacromolecules, 2011. **12**(7): p. 2723-2728.

91. Anup, K., et al., *Directed self-assembly of CdS quantum dots on bacteriophage P22 coat protein templates*. *Nanotechnology*, 2013. **24**(4): p. 045603.
92. Li, F., et al., *Three-Dimensional Gold Nanoparticle Clusters with Tunable Cores Templated by a Viral Protein Scaffold*. *Small*, 2012. **8**(24): p. 3832-3838.
93. Russell, J.T., et al., *Self-assembly and cross-linking of bionanoparticles at liquid-liquid interfaces*. *Angewandte Chemie-International Edition*, 2005. **44**(16): p. 2420-2426.
94. Boker, A., et al., *Self-assembly of nanoparticles at interfaces*. *Soft Matter*, 2007. **3**(10): p. 1231-1248.
95. Falkner, J.C., et al., *Virus Crystals as Nanocomposite Scaffolds*. *Journal of the American Chemical Society*, 2005. **127**(15): p. 5274-5275.
96. Cheung, C.L., et al., *Physical Controls on Directed Virus Assembly at Nanoscale Chemical Templates*. *Journal of the American Chemical Society*, 2006. **128**(33): p. 10801-10807.
97. Steinmetz, N.F., et al., *Plant Viral Capsids as Nanobuilding Blocks: Construction of Arrays on Solid Supports*. *Langmuir*, 2006. **22**(24): p. 10032-10037.
98. Steinmetz, N.F., et al., *Assembly of Multilayer Arrays of Viral Nanoparticles via Biospecific Recognition: A Quartz Crystal Microbalance with Dissipation Monitoring Study*. *Biomacromolecules*, 2008. **9**(2): p. 456-462.
99. Porta, C., et al., *Cowpea mosaic virus-based chimaeras: Effects of inserted peptides on the phenotype, host range, and transmissibility of the modified viruses*. *Virology*, 2003. **310**(1): p. 50-63.
100. Ma, Y., R.J.M. Nolte, and J.J.L.M. Cornelissen, *Virus-based nanocarriers for drug delivery*. *Advanced Drug Delivery Reviews*, 2012. **64**(9): p. 811-825.
101. Lin, Y., et al., *Layer-by-layer assembly of viral capsid for cell adhesion*. *Acta Biomaterialia*, 2008. **4**(4): p. 838-843.
102. Cigler, P., et al., *DNA-controlled assembly of a NaI lattice structure from gold nanoparticles and protein nanoparticles*. *Nat Mater*, 2010. **9**(11): p. 918-922.
103. Lvov, Y., et al., *Successive Deposition of Alternate Layers of Polyelectrolytes and a Charged Virus*. *Langmuir*, 1994. **10**(11): p. 4232-4236.
104. Suci, P.A., et al., *Influence of Electrostatic Interactions on the Surface Adsorption of a Viral Protein Cage*. *Langmuir*, 2005. **21**(19): p. 8686-8693.
105. Yoo, P.J., et al., *Spontaneous assembly of viruses on multilayered polymer surfaces*. *Nature Materials*, 2006. **5**(3): p. 234-240.
106. Steinmetz, N.F., et al., *Layer-by-layer assembly of viral nanoparticles and polyelectrolytes: The film architecture is different for spheres versus rods*. *ChemBioChem*, 2008. **9**(10): p. 1662-1670.
107. Kostianen, M.A., et al., *Electrostatic self-assembly of virus-polymer complexes*. *Journal of Materials Chemistry*, 2011. **21**(7): p. 2112-2117.

108. Kostianen, M.A., et al., *Self-assembly and optically triggered disassembly of hierarchical dendron–virus complexes*. Nat Chem, 2010. **2**(5): p. 394-399.
109. Kostianen, M.A., et al., *Temperature-Switchable Assembly of Supramolecular Virus-Polymer Complexes*. Advanced Functional Materials, 2011. **21**(11): p. 2012-2019.
110. Kostianen, M.A., et al., *Electrostatic assembly of binary nanoparticle superlattices using protein cages*. Nat Nano, 2013. **8**(1): p. 52-56.
111. De, M., et al., *Size and geometry dependent protein-nanoparticle self-assembly*. Chemical Communications, 2009(16): p. 2157-2159.
112. Bozic, A.L. and R. Podgornik, *Symmetry effects in electrostatic interactions between two arbitrarily charged spherical shells in the Debye-Huckel approximation*. Journal of Chemical Physics, 2013. **138**(7).

Chapter 3: Encapsulation of nanoparticles

One-step electrostatic encapsulation of gold nanoparticles in CCMV

Abundant and highly diverse, viruses offer new scaffolds in nanotechnology for the encapsulation, organization or even synthesis of novel materials. Using a single-step process, Cowpea Chlorotic Mottle Virus (CCMV) was used to encapsulate as-synthesised and commercially available gold nanoparticles (AuNPs) without prior modification of the surface with up to 97% efficiency. The resulting gold containing virus-like particles (VLPs) were clustered by poly- λ -lysine, which, interestingly, does not cause plasmon coupling between the particles. Therefore, this might be employed to create a new class of nanomaterials that have a dense packing of individual plasmon states.

Introduction

Simple, AuNP-cored VLPs (Au-VLPs) present an ideal building block for supramolecular crystals that have plasmon properties. Ideally, these functional, hybrid materials could constitute a new generation of targeted therapeutics or optically active materials.[1-3] However, before this can become a reality, several challenges remain to be addressed. Foremost is the need to understand the assembly process that creates the Au-VLP to increase encapsulation efficiency. Although modifications on the gold nanoparticle to maximise the assembly efficiency have been studied in great detail,[4-6] the effect of the virus protein coat itself is also of great interest.

Current methods to synthesise AuNP-cored VLPs involve the coupling of RNA, DNA or extended, anionic, thiol-based ligands to AuNPs that facilitate interaction with the coat protein.[4-6] Furthermore, studies on AuNP-cored Brome Mosaic Virus (BMV) based VLPs have revealed that the hydrodynamic diameter of the core can control the polymorphism of the final VLP. As with the native BMV, these VLPs can be crystallised. However, these VLP crystals are smaller than BMV crystals and reveal additional plasmon bands when compared to the original AuNPs.[7]

The process of encapsulation developed for the encapsulation of AuNP in virus capsids by Dragnea et al. involves two stages.[8] Firstly, anionic AuNPs are incubated with disassembled proteins at neutral pH. This ensures that the carboxylic acid groups on the AuNP stabilizing ligands are negatively charged, while the capsids' N-terminal lysine residues will be protonated and thus positively charged. The resulting electrostatic attraction pre-organises the capsid proteins on the nanoparticle surface. Secondly, these proto-VLPs are dialysed to a lower pH in a high salt concentration buffer to reduce the electrostatic binding strength, thus allowing capsid shell formation to occur on the nanoparticle surface; trapping the AuNP inside the capsid.[8]

The efficiency of this encapsulation process has been defined by the ratio between encapsulated AuNP and the total AuNP ($N_{Au,enc}/N_{Au,tot}$) as counted in TEM microscopy images of the sample. Initially, the encapsulation of these particles in BMV had an efficiency around 2-3%. [4] However, in further work these investigators managed to improve this to 95% by changing from citrate to more flexible carboxylate-terminated thiolalkylated tetra(ethylene glycol) (TEG) surface ligands on the AuNP.[5] Similarly, Aniagyei et al. used the two-step method to encapsulate these AuNP in CCMV, revealing no free AuNP after encapsulation in TEM. [9]

CCMV is a well-studied bromovirus that, in its native conformation, has a T=3 icosahedral Caspar-Klug capsid symmetry. The CCMV capsid can be disassembled following removal of the RNA (at pH 7.5 and 0.5M Ca²⁺) and subsequently reassembled in vitro (at pH 5.0 and >0.3M NaCl) or around a template. As such, CCMV has been shown to efficiently encapsulate a wide variety of species, including polyanions, proteins, enzymes, micelles and nanoparticles. It is noteworthy that many of these species are formed at near neutral pH in a simple one -step encapsulation process.[9-12]

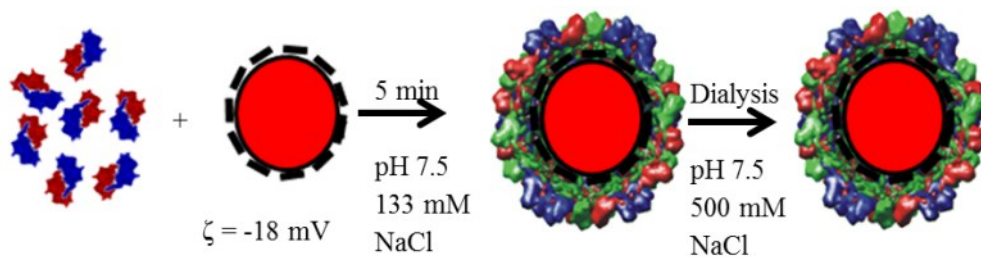
Additionally, the CCMV capsid in the absence of a template can be assembled into a wide variety of structures by varying the pH and ionic strength of the assembly buffer. These structures such as tubes, multi-layered structures or dumbbells, differ from similar viruses such as BMV that only forms spherical assemblies.[13, 14] Unlike BMV, CCMV is known to have a flexible N-terminus, which might account for these differences in assembly behaviour.[15, 16]

The flexibility of the N-terminus might improve the encapsulation of nanoparticles in CCMV, eliminating the need for a flexible ligand on the surface. Therefore, we present a study on the encapsulation of as-synthesised and commercial gold nanoparticles of varying sizes inside wild-type CCMV. Furthermore, we hypothesize that since the flexibility in the system lies in the coat protein, the encapsulation can be performed entirely at near neutral pH in a one-step process.

Results and Discussion

Formation of virus-like particles (Characterising the encapsulation)

The encapsulation of AuNP by the CCMV coat protein is dependent on several factors. The charge on the proteins and the AuNP, the relative concentration of these particles and their stability under the conditions used. Fortunately, the N-terminus of the coat protein is positively charged under disassembly conditions (pH 7.5, 500mM NaCl), the same holding true for the surface of commonly used citrate stabilised AuNP. In our experience coat proteins stable under disassembly conditions for several hours or even days, though the citrate capped AuNP will quickly aggregate under at this ionic strength, due to electrostatic shielding of the surface ligands. Therefore, we hypothesize that an excess of coat protein is needed for efficient encapsulation, as the encapsulated AuNP will be shielded from aggregation.



Scheme 1: Schematic representation of the AuNP encapsulation process by disassembled CCMV coat proteins.

To study the basis for encapsulation, citrate stabilised gold nanoparticles were added to a slight excess of disassembled CCMV coat proteins to see if VLP formation would occur. To start with, the CCMV capsid can be disassembled into 90 coat protein (CP) dimers in a pH 7.5 aqueous buffered solution (50mM Tris or PO₄; 500mM NaCl). Under these conditions no capsid formation has been observed without the aid of a template. Upon the addition of 12nm citrate stabilised gold nanoparticles (Au12C), such a template is presented and capsid formation can take place, leading to a CCMV-based VLP containing Au12C (CAu12C) (scheme 1). However, TEM images of the resulting VLPs (figure 1) shows some polydispersity in the size and shape of the encapsulated nanoparticles.

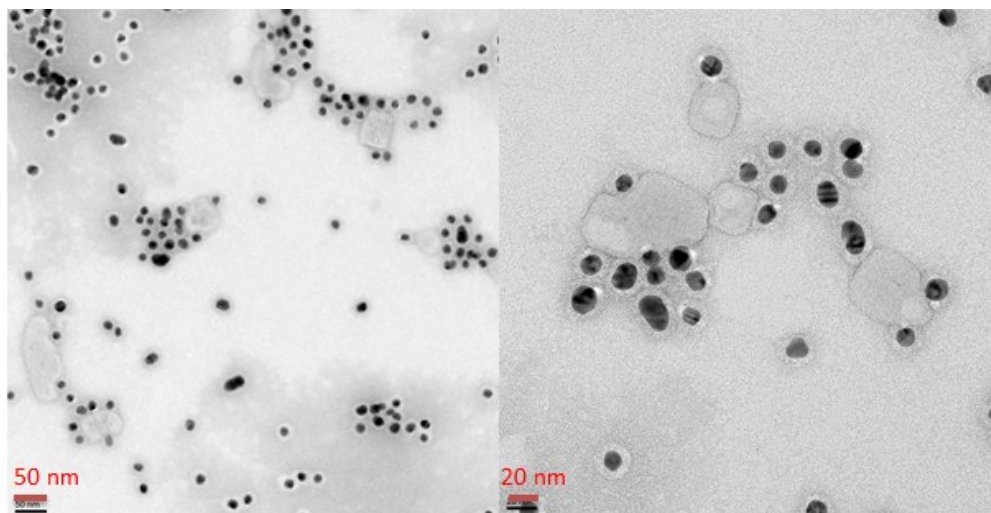


Figure 1: TEM micrographs of 1% uranyl acetate stained CAu12C nanoparticles at two different magnifications.

Even though sufficient CP is present, some partially aggregated particles are observed (figure 1). These aggregated particles are larger than the 12 nm AuNP in the original sample (figure 2d), but still appear to be encapsulated. Therefore,

preparative FPLC size exclusion chromatography can be used to separate them from the sample. The FPLC chromatogram of CAu12C (figure 2a) shows three distinct peaks at $V = 8$ ml, 11 ml and 18 ml elution volume. If collected, these peaks yield purple, red and colourless samples respectively. The TEM images reveal that the $V = 8$ ml peak represents a mixture of aggregated and partially encapsulated gold nanoparticles particles (Figure 2b), whilst the $V = 11$ ml peak represents the single encapsulated particles (Figure 2c) with residual protein dimers represented by the 18ml peak, lacking the $\lambda = 520$ nm plasmon absorption. This reinforces the idea that electrostatic shielding initially aggregates some of the gold nanoparticles, but the encapsulation shields the particles from further aggregation.

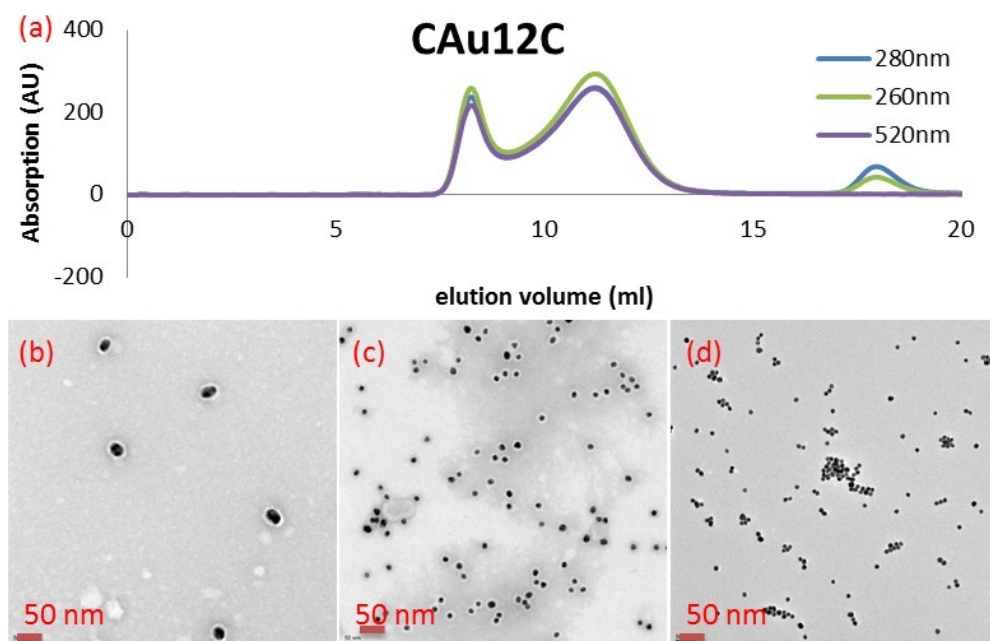


Figure 2: (a) FPLC chromatogram of the encapsulation mixture of CAu12C measured at $\lambda = 260$ nm, 280 nm and 520 nm, revealing three different particle sizes, corresponding to aggregated AuNP (8ml), CAu12C (11ml) and CP dimers (18ml); (b) TEM image of 8ml FPLC peak showing encapsulated aggregated AuNP, (c) TEM image of 11.2ml FPLC peak showing encapsulated single AuNP; and (d) TEM image of unencapsulated Au12C as a reference.

The polydispersity could have resulted from the partial aggregation of some of these nanoparticles due to the NaCl in the buffer. Indeed, a quick study on the stability of Au12C under increasing NaCl concentration reveals aggregation behaviour at NaCl concentrations greater than 50mM. This makes successful encapsulation easy to observe by the naked eye. If sufficient CP is present, the

solution retains its bright red colour from the $\lambda = 520$ nm plasmon absorption. However, if too little or no CP is present, the solution turns purple immediately and after one or more days shows a black precipitate. This shows that the encapsulation efficiency of AuNP is dependent on the CP concentration.

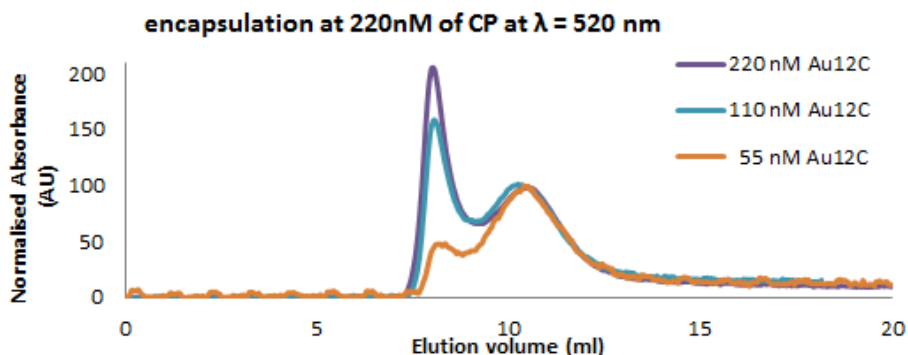


Figure 3: FPLC chromatogram at the $\lambda = 520$ nm AuNP absorption of Au12C encapsulated by 220nM of CCMV coat protein (CP) at 1:1, 2:1 and 4:1 CP to AuNP ratio. The peaks were normalised at the CAu12C peak maximum. Note that at 520 nm no CP peak at 18 ml is observed.

To study this, in figure 3, the encapsulation of AuNP at increasing AuNP/CP ratio's is presented. This shows that as the relative amount of AuNP increases, so does the aggregation of these particles, seen by the increasing $V = 8$ ml peak. Considering this, it is indeed likely that two processes compete during the encapsulation process. One process is the association of CP to AuNP, the other involves the aggregation of AuNP due to the electrostatic shielding of the AuNP stabilizing ligands at 500mM NaCl.

As the TEM data (figures 1, 2b and 2c) shows few to no unencapsulated particles, it is inconclusive with regard to the encapsulation efficiency, previously calculated according to $N_{Au,enc}/N_{Au,tot} = 100\%$. Instead, the relative height of two peaks at 8ml and 11ml from the $\lambda = 520$ nm absorption can be seen as a measure for the efficiency for the AuNP encapsulation.²⁰ Doing so will exclude the aggregated AuNP observed in TEM micrographs from being counted as encapsulated. Additionally, this efficiency discounts the protein material, with any free CP dimers eluting at $V = 18$ ml (figure 2a), and using only the gold plasmon absorption at $\lambda = 520$ nm. Thereby making this a measure for encapsulation efficiency, not VLP formation. This enables us to quantify the efficiency of the encapsulation process as ranging

²⁰ Minor shifts in the plasmon absorption spectra due to aggregation of particles are not taken into account.

from 32.5% for a 1:1 CP:AuNP ratio to 69.5% for a 4:1 ratio for CAu12C (figure 3). Thus, by providing a large excess of CP to AuNP, efficient encapsulation can be achieved, presumably by allowing for more rapid encapsulation of the nanoparticles before aggregation can take place.

Core size and ligand variation

CCMV is known to be able to assemble in a variety of different size and symmetries, based upon the core material presented. The stability of these VLPs varies, with those following Caspar Klug symmetry structures being energetically favoured, which should lead to a higher encapsulation efficiency.[17] We have therefore tested the above approach for four nanoparticle sizes (7nm, 12nm, 17nm and 30nm) with three different capping ligands (citrate, tannic acid and poly vinyl pyridine). We found that core size was the single most important factor in the encapsulation efficiency of AuNP in CCMV VLPs.

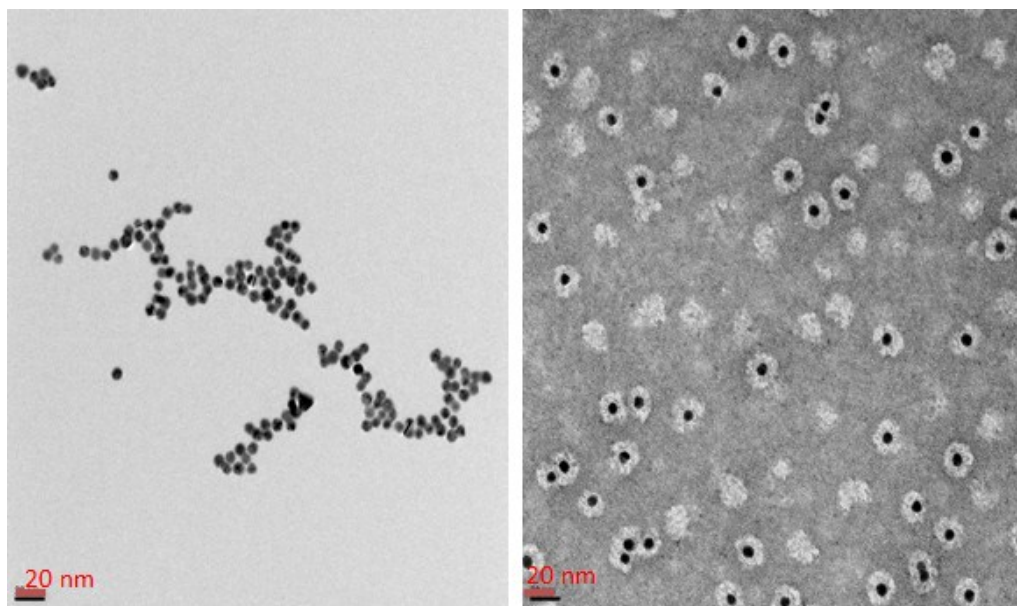


Figure 4: TEM micrographs of (a) unencapsulated Au7T and (b) CAu7T.

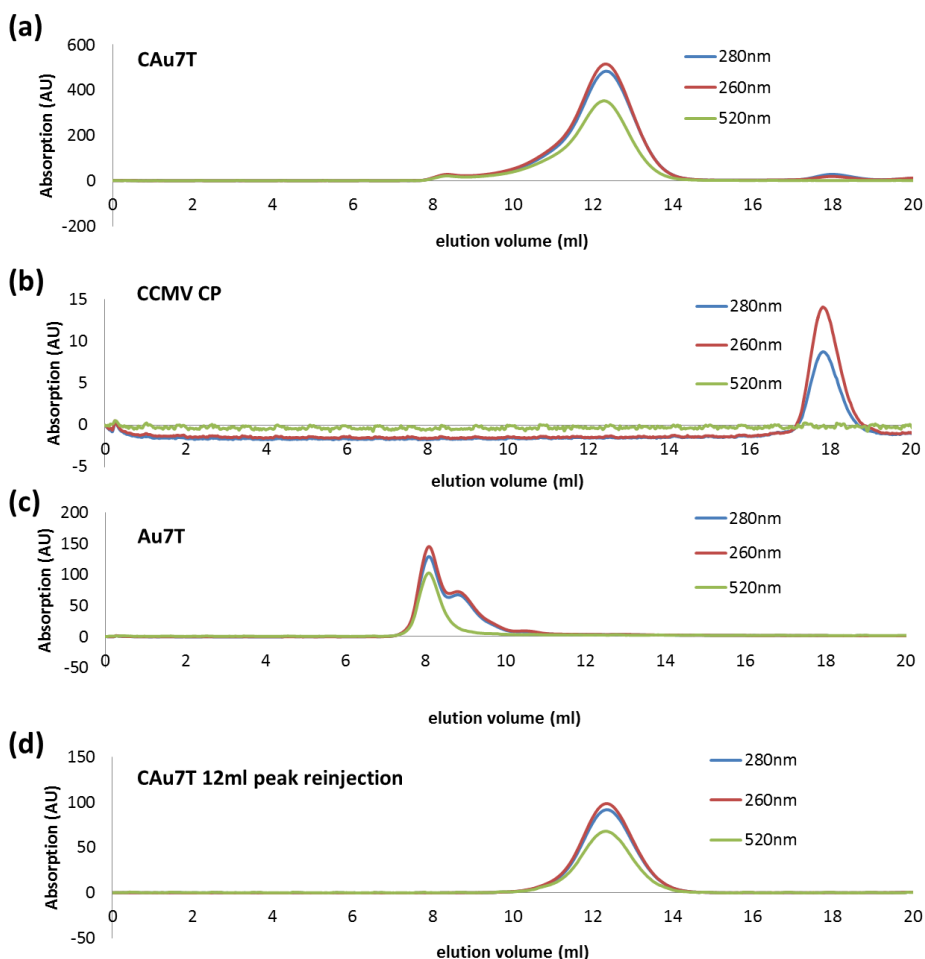


Figure 5: FPLC chromatogram at $\lambda = 280 \text{ nm}$, 260 nm and 520 nm of (a) CAu7T showing peaks for the partially, aggregated and unencapsulated gold (8 ml), fully encapsulated CAu7T (12 ml) and CCMV CP (18 ml); (b) CCMV CP showing a single peak; (c) unencapsulated Au7T; and (d) CAu7T reinjected after several days eluting again at 12ml and showing no deterioration.

The stability of the Au-cored VLPs varies with size, but most remain stable at pH 7.5 for several days. As with CAu12C, the existence of core-shell particles is verified by TEM images (figure 4) of the 7nm tannic acid capped AuNP (Au7T) and CCMV-encapsulated Au7T (CAu7T). Indeed, the FPLC chromatogram of CCMV-encapsulated the CAu7T VLPs shows three peaks (figure 5). In fact, for Au7T, the encapsulation efficiency is very high (97%) compared to the Au12C (53%), based on FPLC. Furthermore, by comparing the FPLC chromatogram of CAu7T (figure 5a) to that for CP (figure 5b) and AuNP (figure 5c), the origin of the 8ml and 18ml peaks can quickly be identified as aggregated, unencapsulated or partially encapsulated

Au7T and CP, respectively. In fact, reinjecting the second peak (12ml) after several days (figure 5d) shows a single peak at 12ml, showing the particles remain stable.

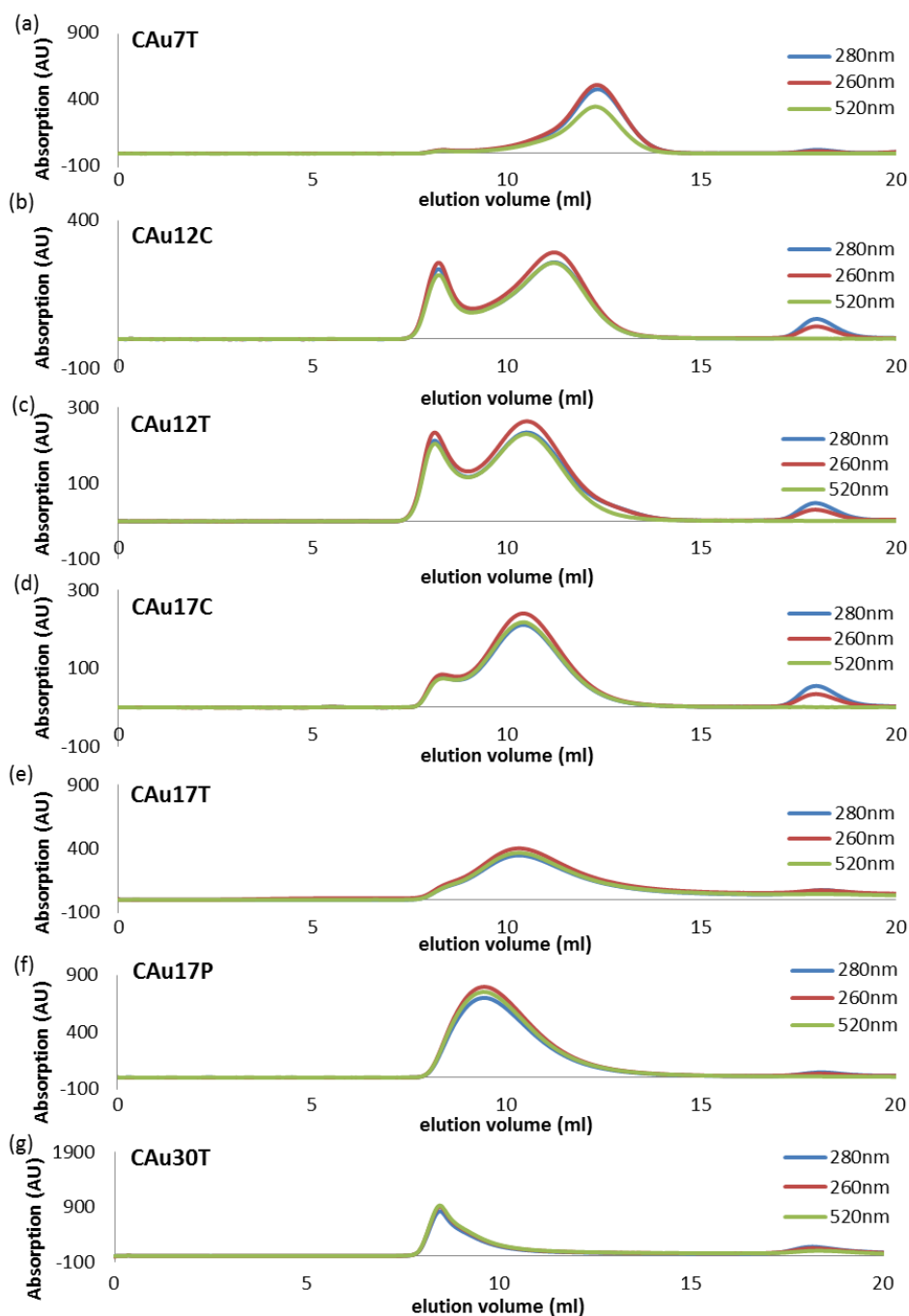


Figure 6: (top to bottom) FPLC chromatograms for increasing size of AuNP encapsulated by CCMV at >10 fold excess of CP to AuNPs.

Similar encapsulation results, as for Au7T, were obtained for commercial Au12T, Au12C, Au17T, and Au17C (table 1). Depending on the nanoparticle size a shift can be observed in the position of second FPLC elution peak (figure 6 a to e) from around $V = 10.3$ ml for 17 nm and $V = 10.6$ ml (tannic acid) or $V = 11.2$ ml (citrate) for 12 nm particles to $V = 12.3$ ml for 7 nm particles. The encapsulation efficiency appears to vary with size, from 97% for 7 nm CAu7T; to 53% and 54% for CAu12C and CAu12T respectively; to 75% and 82% CAu17C and CAu17T respectively; and only seems to slightly favour tannic acid over citrate ligands. After dialysis to pH 5 the 7 nm and 17 nm cored VLPs remain in solution, while both 12 nm cored VLPs precipitate.

Gold nanoparticle				Encapsulation by CCMV			
Name	Diameter (nm)	Capping Ligand	ζ -potential (mV)	Name	Efficiency (%)	Elution Volume (ml)	Casper-Klug Symmetry
Au7T	6.7	Tannic Acid	[-18]*	CAu7T	97	12.3	T=1
Au12T	12.0	Tannic Acid	-22.6	CAu12T	54	10.6	[T=2]**
Au12C	12.0	Citrate	-17.6	CAu12C	53	11.2	[T=2]**
Au17T	16.1	Tannic Acid	-32.7	CAu17T	82	10.3	T=3
Au17C	15.1	Citrate	-18.4	CAu17C	75	10.3	T=3
Au17P	16.8	PVP	-12.8	CAu17P	***	[9.5]***	[T=3]***
Au30T	28.8	Tannic Acid	-35.4	N/A	N/A	N/A	N/A

Table 1: Overview of AuNP and resulting encapsulations. *Surface potential for 7nm AuNPs is estimated from other particles; **The T=2 symmetry is considered meta-stable; *** The 17nm PVP particles show no separation peak separation, thus the elution volume might be an overlap between the 8 nm aggregation peak and an encapsulation peak.

Combining all these results with the STEM images (figure 7) which show 18 nm CAu7T, 24 nm CAu12T and CAu12C and 30 nm CAu17C, we can draw parallels with other CCMV based VLPs. First, wild-type CCMV elutes at $V = 10.5$ ml and is known to have a T=3 confirmation, is approximately 29 nm in diameter and has an 18 nm cavity, which corresponds to the stable VLP assembly found for the 17 nm cored

nanoparticles. Second, CCMV containing 70kDa polystyrene sulphonate (PSS) elutes at $V = 12.5\text{ml}$ and is known to have a $T=1$ confirmation, is approximately 18 nm in diameter and has an 8 nm cavity, which corresponds to the stable VLP assembly found for the 7nm cored nanoparticles.[10] Finally, a $T=2$ CCMV capsid, having been previously observed for the encapsulation of 400kDa PSS, is known to have a diameter close to 23 nm, but according to Caspar-Klug symmetry should not be as stable as the $T=1$ or $T=3$ capsids, which correlates to the reduced encapsulation efficiency found for the 12nm particles.[18]

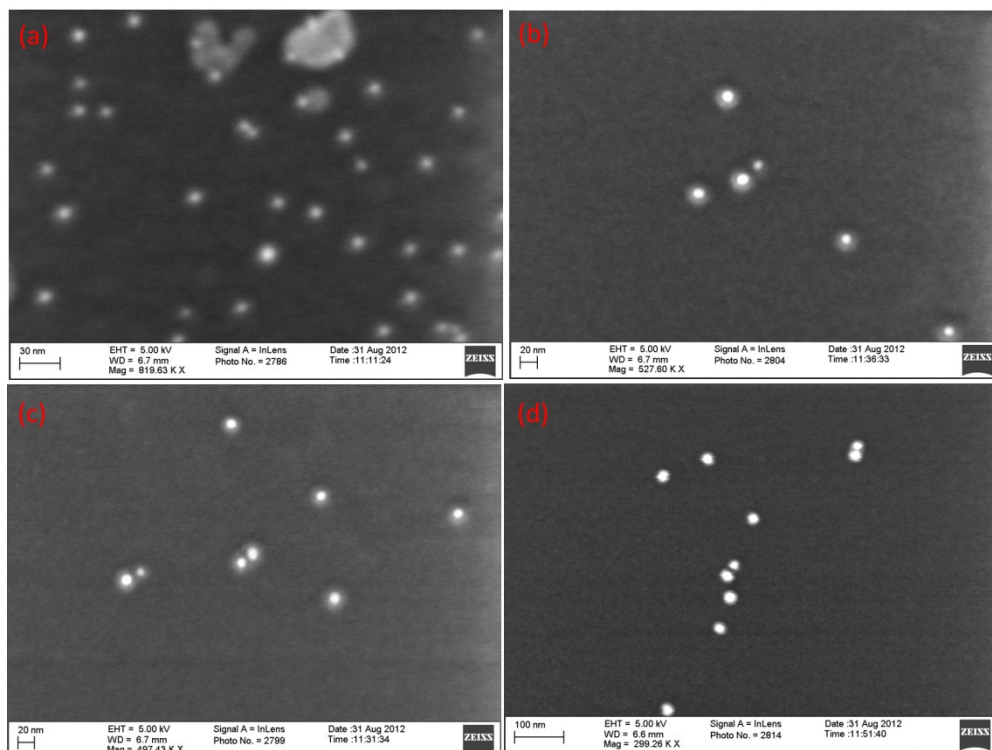


Figure 7: STEM images showing the core-shell morphology of: (a) CAu7T; (b) CAu12C; (c) CAu12T; (d) CAu7T.

However, attempts at encapsulating polyvinyl pyridine (PVP) coated AuNP (Au17P), and Au30T did not yield usable VLPs. Instead, FPLC chromatograms (figure 6 f and g) showed elution volumes of 9ml (Au17P) and 8ml (Au30T) and no secondary peaks that are comparable to $T=1$, $T=2$ or $T=3$ morphologies. As a basic polymer, PVP would not be likely to be encapsulated and showed stability even in the presence of $>50\text{mM}$ NaCl without CP. Also the 30nm AuNP, likely too large to be encapsulated, did not yield any $T=3$ or smaller sized VLP.

Conservation of plasmon properties

The surface plasmon absorbance peak of AuNPs is subject to shift following modification of the particle surface. This occurs for two main reasons: disruption of the surface electrons and the disruption of the plasmon electric field, caused by altering the surrounding refractive index, which in its turn is due to a change in the dielectric constant of the surrounding medium. As the anionic ligands on the gold surface are thought to promote the assembly as a result of the electrostatic interaction with the CCMV N-terminus, it is likely that direct contact between the proteins and the gold particle surface will be limited. Thus any change in surface plasmons should arise mostly from the change in refractive index. As the effect of the protein layer is small compared to that of the surrounding solution, the expected change in surface plasmon absorption should be minimal.

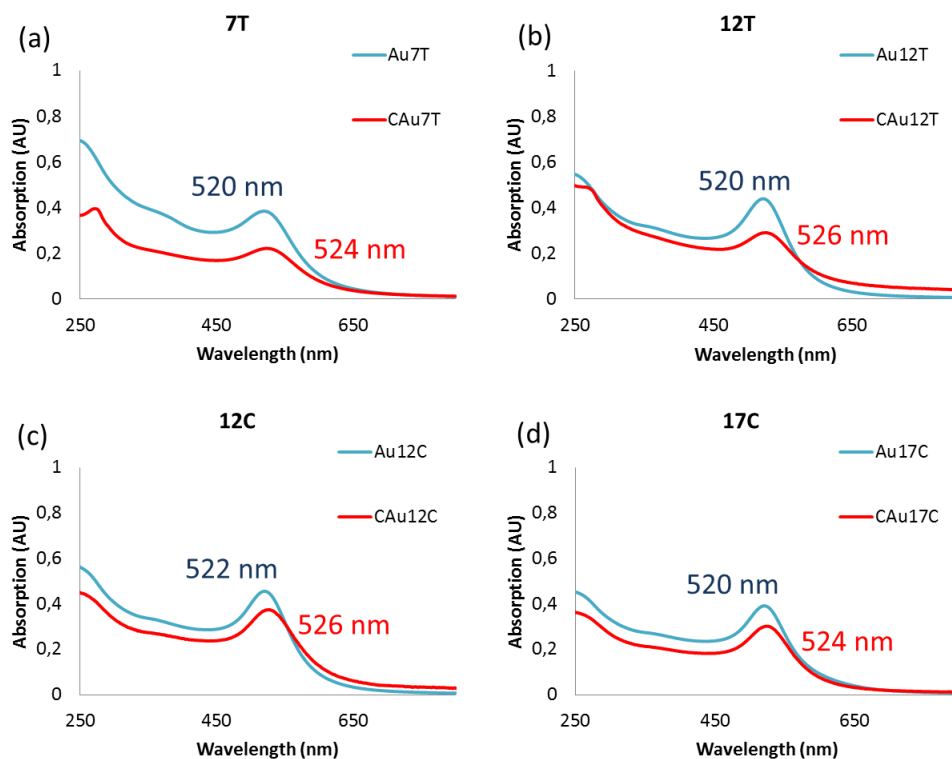


Figure 8: UV visible spectrograms and plasmon absorption maximums of AuNP before and after encapsulation of (a) CAu7T and Au7T, (b) CAu12C and Au12C, (c) CAu12T and Au12T, (d) CAu17C and Au17C.

Indeed, the UV-Visible spectra of Au7T, Au12T, Au12C and Au17C and their respective CCMV-based VLPs (figure 8) show a shift of 4 to 6 nm in their plasmon absorbance (Table 2) after encapsulation by the coat protein. As the shift is similar

in all cases, it indicates that the protein shell has a uniform thickness. Furthermore, there appears to be little or no peak broadening indicating that the AuNP within each sample has a similar coverage of protein, which considering the excess of coat protein along with the size differentiation observed in FPLC suggests the formation of a full protein shell around each gold nanoparticle.

Plasmon behaviour upon clustering

Since the VLPs show conservation of plasmon properties, it allows us a preliminary investigation into the behaviour of these VLPs upon clustering. A prospective use for these particles is in metamaterials, in which the collective properties of the nanoparticles could promote other new or different behaviour. However, the difficulty with respect to plasmonic nanoparticles arises from the inter-particle coupling of the plasmon states, which results in a shift and broadening of the plasmon absorption band. Fortunately, the strength of this coupling is dependent on the distance between the nanoparticles, which typically lies in nanometre range. As the capsid protein shell of CCMV has a thickness of 5nm, the separation of the AuNPs by 10nm should be sufficient to prevent this plasmon coupling upon cluster formation.

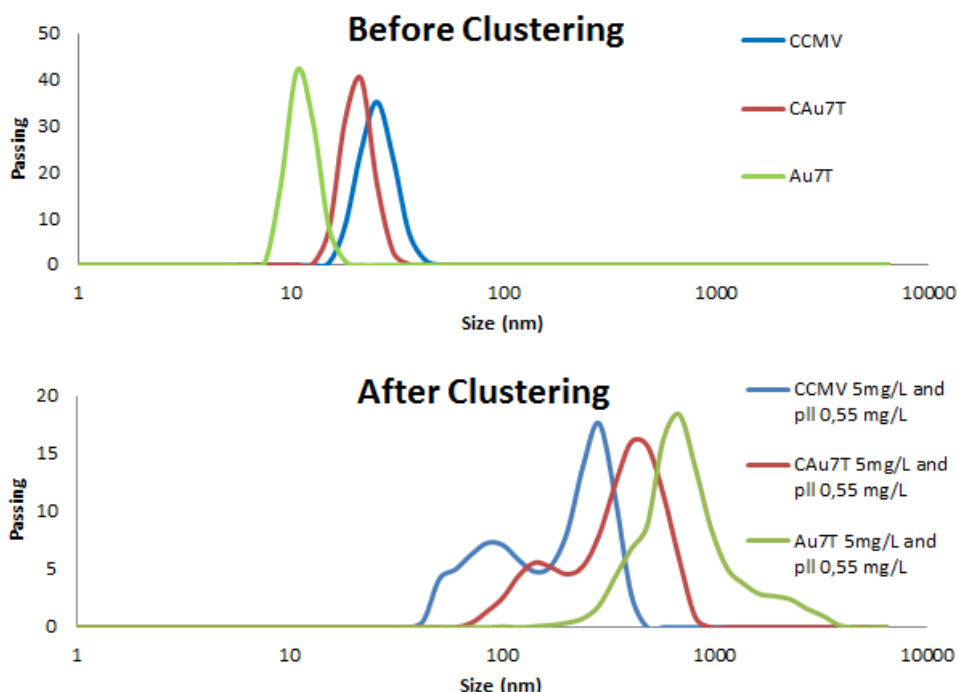


Figure 9: Dynamic light scattering size analysis of CCMV, CAu7T and Au7T (a) before clustering with p11 and (b) after clustering with p11. Concentrations for CAu7T were estimated.

To further study the plasmon behaviour, CCMV, CAu7T and Au7T were clustered using poly- λ -lysine (pll) according to the procedure for CCMV developed by Kostiainen and co-workers.[19] Dynamic light scattering (DLS) data (figure 9) shows that upon addition of pll, clustering is observed after 2 minutes of incubation. The clusters obtained for the reference Au7T particles were generally larger and more uniform for a similar amount of pll compared to those obtained for CCMV and CAu7T, both of which show clustering behaviour comparable to that reported by Kostiainen et. al.

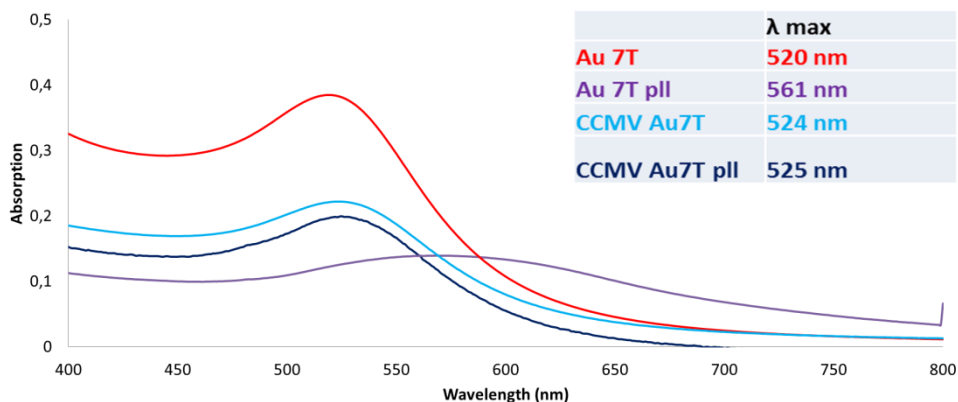


Figure 10: UV visible spectrograms of Au7T and CAu7T both before and after clustering; (inset) plasmon peak absorption maximums for the spectra shown.

The UV-visible spectrum of CAu7T (figure 10) does not change significantly following clustering with pll. On the other hand, the unencapsulated Au7T shows a distinctive redshift in the absorption maximum of the plasmon peak. We suspect that two factors play a part: clustering efficiency and inter particle distance. The clustering efficiency for Au7T is much higher than for CAu7T, as seen in DLS, with relatively smaller clusters for CAu7T thus limiting the number of interacting particles. Yet, this does not explain the lack of a shift or broadening resulting from the smaller clusters in CAu7T. Therefore, it is more likely that the difference in inter-particle distance, caused by the protein shell around CAu7T, leads to minimizing of the plasmon coupling.

Conclusions

CCMV has been shown to facilitate the encapsulation of commercial AuNP without the need for prior modification of the surface ligand. Furthermore, these particles were able to maintain their individual character as nanoparticles following clustering without plasmon coupling. Therefore, the fabrication of nanomaterials with a narrow plasmon band and a dense packing of states is potentially possible.

Currently, research is focussed on improving the assembly of these clusters along with a detailed study of their optical properties. Additionally, the presented method can be extended to other as-synthesized and commercially available negatively charged nanoparticles, such as quantum dots and iron oxides, which is expected to eventually lead to a new class of virus based nanomaterials.

Experimental

CCMV coat protein dimers isolation

CCMV coat protein dimers (CP) were prepared as described by Verduin and adapted by Comellas Aragonés et al.[20, 21] 500µl of a solution containing CCMV (5 to 15 mg/ml) in virus buffer (H₂O; pH 5.0; 200mM Sodium Acetate; 10mM EDTA; 1mM NaN₃) is dialysed for 2x 2 hours against 500ml of RNA buffer (H₂O; pH 7.5; 50mM Tris; 500mM CaCl₂). This results in a white precipitate. Ultracentrifugation at 40,000 rpm (sorval, F-50-TL rotor) is used to pellet the precipitate. The supernatant (~500µl) is dialysed for at least 2x 2 hours against 500ml clean buffer (H₂O; pH 7.5; 50mM Tris; 500mM NaCl). The resulting solution can be analysed using UV-Visible to determine the concentration of the CP. For storage, the CP solution (~500µl) can be dialysed for 2x 2 hours to capsid storage buffer (H₂O; pH 5.0; 100mM Sodium Acetate; 500mM NaCl) which causes the empty capsid shell to form and protects the capsid from proteases.

Gold Nanoparticle encapsulation in CCMV

Gold nanoparticles were encapsulated into a CCMV-based VLP by assembling the coat protein of the virus around anionic gold nanoparticles. In a typical experiment, 4,5ml of a Gold Nanoparticle solution (H₂O; 0,05 mg/ml) is concentrated to 450µl. To this, 150µl of CCMV coat protein solution (H₂O; pH 7.5; 50mM Tris or PO₄; 500mM NaCl) is added and allowed to incubate for 5 minutes at room temperature. The reaction mixture is subsequently dialysed overnight to the aqueous buffer conditions of the CCMV coat protein (H₂O; pH 7.5; 50mM Tris or PO₄; 500mM NaCl). The resulting VLPs are purified using preparative FPLC chromatography (superpose 6, 24ml column).

VLP Clustering

Spin filtration (30k MWCO, 5krpm, eppendorf 5415 R centrifuge) was used to replace the phosphate buffer with a pH 5 acetate buffer (50mM NaCl, 10mM sodium acetate, 1 mM EDTA, 1mM NaN₃). Samples of 1000µl were prepared by diluting the protein solutions to a fixed concentration of 5µg/ml of protein. To cluster these samples, 5µl of a 1mg/ml PLL solution was added to 995µl of protein solution, after which the samples were mixed on a roller bank for 2 minutes.

FPLC

FPLC size exclusion chromatography samples, ranging from 100µl up to 500µl were measured on a 24ml column stacked with superose-6 and collected by fractionation.

UV-Vis

UV-Visible samples are prepared from 500 µl fresh sample solutions. They were measured in a 1cm quartz cuvette in a PerkinElmer Lambda 850 UV/VIS Spectrometer.

(S)TEM

The TEM samples are prepared by leaving 5µl of a freshly made sample solution on a formvar carbon coated copper grid for 5 minutes and subsequently removing it by tipping the grid onto low lint paper (Kimtech science precision wipes). Stained samples use 5ul of a 1% Uranyl Acetate solution which is removed after 30 seconds to provide optimal contrast. Samples are imaged using a Philips CM300ST-FEG TEM or a Zeiss Merlin (S)TEM.

DLS

Each 1000ul sample was measured five times for 120 seconds using an Anaspec nanotrack wave dynamic light scattering instrument with the best of these five measurements selected.

Bibliography

1. Giljohann, D.A., et al., *Gold Nanoparticles for Biology and Medicine*. Angewandte Chemie International Edition, 2010. **49**(19): p. 3280-3294.
2. Dreaden, E.C., et al., *The golden age: gold nanoparticles for biomedicine*. Chemical Society Reviews, 2012. **41**(7): p. 2740-2779.
3. Gramotnev, D.K. and S.I. Bozhevolnyi, *Plasmonics beyond the diffraction limit*. Nat Photon, 2010. **4**(2): p. 83-91.
4. Dragnea, B., et al., *Gold Nanoparticles as Spectroscopic Enhancers for in Vitro Studies on Single Viruses*. Journal of the American Chemical Society, 2003. **125**(21): p. 6374-6375.
5. Chen, C., et al., *Nanoparticle-Templated Assembly of Viral Protein Cages*. Nano Letters, 2006. **6**(4): p. 611-615.
6. Loo, L., et al., *Encapsidation of Nanoparticles by Red Clover Necrotic Mosaic Virus*. Journal of the American Chemical Society, 2007. **129**(36): p. 11111-11117.
7. Sun, J., et al., *Core-controlled polymorphism in virus-like particles*. Proceedings of the National Academy of Sciences, 2007. **104**(4): p. 1354-1359.

8. Tsvetkova, I., et al., *Pathway switching in templated virus-like particle assembly*. *Soft Matter*, 2012. **8**(17): p. 4571-4577.
9. Aniagyei, S.E., et al., *Synergistic Effects of Mutations and Nanoparticle Templating in the Self-Assembly of Cowpea Chlorotic Mottle Virus Capsids*. *Nano Letters*, 2009. **9**(1): p. 393-398.
10. Sikkema, F.D., et al., *Monodisperse polymer-virus hybrid nanoparticles*. *Organic & Biomolecular Chemistry*, 2007. **5**(1): p. 54-57.
11. Minten, I.J., et al., *Controlled Encapsulation of Multiple Proteins in Virus Capsids*. *Journal of the American Chemical Society*, 2009. **131**(49): p. 17771-17773.
12. Kwak, M., et al., *Virus-like Particles Templated by DNA Micelles: A General Method for Loading Virus Nanocarriers*. *Journal of the American Chemical Society*, 2010. **132**(23): p. 7834-+.
13. Bancroft, J.B., E. Hiebert, and C.E. Bracker, *The effects of various polyanions on shell formation of some spherical viruses*. *Virology*, 1969. **39**(4): p. 924-930.
14. Lavelle, L., et al., *Phase Diagram of Self-assembled Viral Capsid Protein Polymorphs*. *Journal of Physical Chemistry B*, 2009. **113**(12): p. 3813-3819.
15. Speir, J.A., et al., *Structures of the native and swollen forms of cowpea chlorotic mottle virus determined by X-ray crystallography and cryo-electron microscopy*. *Structure*, 1995. **3**(1): p. 63-78.
16. Douglas, T., et al., *Protein Engineering of a Viral Cage for Constrained Nanomaterials Synthesis*. *Advanced Materials*, 2002. **14**(6): p. 415-418.
17. Nguyen, H.D. and C.L. Brooks, *Generalized Structural Polymorphism in Self-Assembled Viral Particles*. *Nano Letters*, 2008. **8**(12): p. 4574-4581.
18. Hu, Y.F., et al., *Packaging of a polymer by a viral capsid: The interplay between polymer length and capsid size*. *Biophysical Journal*, 2008. **94**(4): p. 1428-1436.
19. Kostianinen, M.A., et al., *Electrostatic self-assembly of virus-polymer complexes*. *Journal of Materials Chemistry*, 2011. **21**(7): p. 2112-2117.
20. Verduin, B., *The preparation of CCMV-protein in connection with its association into a spherical particle*. *FEBS letters*, 1974. **45**(1): p. 50-54.
21. Aragones, M.C., *The cowpea chlorotic mottle virus as a building block in nanotechnology*. 2010, Radboud University: Nijmegen

Chapter 4: Clustering with soft macromolecules

The effect of VLP size on the electrostatic clustering of virus-like particles

Being able to organise materials at the nanoscale via self-assembly at a large scale remains the most challenging aspect in the field of nanotechnology. Virus-like particles (VLPs) present a natural building block that could be used as a scaffold to organise a wide variety of nanoparticles in such a manner. This chapter investigates the role of the VLPs size and resulting Caspar Klug symmetry in forming electrostatic clusters out of these building blocks, showing that the onset point for clustering is determined by steric considerations of the binding site and binding agent and requires that multiple binding sites per capsid are used. The clustering is shown to be independent of cargo and the data suggests that rotational symmetry in the $T=3$ capsid allows for hexagonal close packed structures, whereas the $T=1$ capsid that lacks a six-fold and twofold rotational axis does not show such organisation.

Introduction

Scientific scope

The organisation of nanoparticles into assembled materials has the potential to form new devices with biomedical, optoelectronic, catalytic, structural or even combined applications. All of these, however, rely on an ordered structure and large scale combination of different nanoparticles with various properties to achieve the desired result. The degree of organisation and scale are also where the principle challenges in this field lie, as due to the multitude of nanoscale forces, so far, no single technique can cover both challenges for different particles.[1] Therefore, we believe in simplifying the problem by limiting the number of different particles that need to be organised by using virus protein shells to first encapsulate the desired nanoparticle before forming the assembly.

Nano-assemblies of virus-like particles

Many techniques exist to form assemblies based on viruses and virus-like particles (VLPs) from protein crystallisation techniques [2, 3] to using covalent linkers [4, 5] and electrostatics [6-8]. The first two, however, are techniques that require a great deal of time and effort as they rely on slow crystallisation processes or layer-by-layer material deposition. Electrostatic assembly can, however, be achieved in solution rather than on a surface or through layer-by-layer assembly by using cationic polyelectrolytes. [9, 10] This opens up the possibility of rapidly assembling different materials contained inside the capsid into large scale organised structures. As discussed in the previous chapter, not all VLPs with encapsulated particles conform to the native size and thus symmetry, which, despite using the same protein, will affect their ability to cluster.[3]

Size and symmetry in virus capsids

Formation of VLP clusters by electrostatics is affected by virus Caspar Klug symmetry structures. Recent experimental studies and theoretical simulations confirm that symmetrically placed patches of electrostatic charge aid and guide the clustering of viruses.[11, 12] However, under Caspar Klug symmetry laws, the virus proteins can also form different sized VLPs that do not have the same symmetry as the native virus.[13] Therefore, the symmetrical charge distribution can differ in different sized VLPs, even though the overall charge density is similar as the same proteins are used. Clustering could thus be controlled by controlling the capsid size and resulting symmetry.

Coat proteins (CP) can fold into these different symmetrical architectures following the size of a presented template. This allows for the encapsulation of functional materials into a variety of capsid sizes and resulting symmetries. Spherical

symmetry sizes follow Caspar Klug symmetry laws, with stable capsid shells being formed at discreet intervals, governed by the triangulation (T) number, and containing $60 \cdot T$ proteins.²¹ CCMV makes an excellent model system, as its CP have been shown to adopt T=1, pseudo 'T=2' and T=3 as well as rod-like symmetries using the right template. Furthermore the clustering of the T=3 symmetrical structure is well studied by Kostianen et al.[9, 10, 14] In this experimental study we have combined CCMV CP with anionic templates to study the difference in clustering behaviour between T1, T3 and mixed VLPs.

Chapter content

In this chapter, the clustering of T=1 and T=3 CCMV based VLPs is studied and analysed to understand the effect of different size and symmetry VLPs on cluster formation. First, the formation of the T=1 and T=3 VLPs according to procedures adapted from literature and earlier work is briefly described with emphasis on the relevant differences between the VLPs. Subsequently, the effect of the ionic strength, polymer shape, VLP core and clustering dynamics are presented to further understand these systems. This interplay between ionic strength and symmetry is shown to be a dominant force in the clustering of these particles. Finally, a comparison to a model that shows the different electrostatic binding pockets for the T=1 and T=3 CCMV capsids is used to explain this behaviour.

Results and Discussion

Formation of T=1 and T=3 VLPs

In order to study the clustering of different sized VLPs, several model VLPs are selected and synthesised using known procedures. In this, the native T=3 CCMV, having a resolved crystal structure and known clustering properties with different soft macromolecules, serves as the model for T=3 sized capsids.[10] To compliment this, two known T=1 VLPs, CCMV with a 70kDa polystyrene sulphonate core (CPPS) and CCMV with a 7nm gold nanoparticle core (CAu7T), are synthesised following known encapsulation procedures (figure 1). [15] In brief, these procedures are detailed below, with emphasis given to the clustering-relevant properties of these different VLPs.

²¹ Note that not all T numbers form stable, symmetrical capsids shells, as explained in chapter 3.

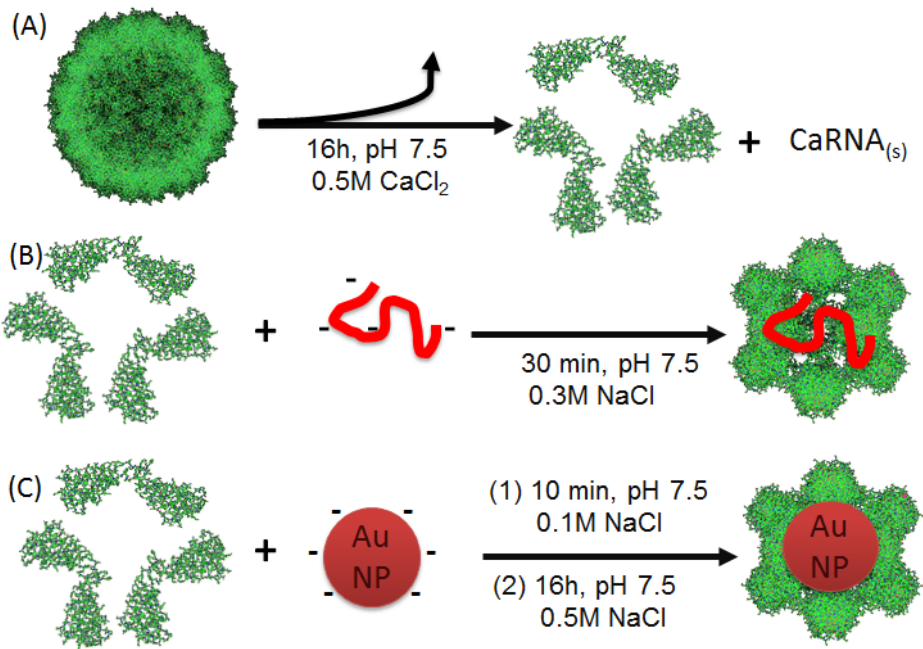


Figure 1: Scheme showing; (A) the disassembly of the T=3 native CCMV using precipitation of RNA by calcium at pH 7,5; (B) encapsulation of 70kDa polystyrene sulphonate by CCMV coat protein to form a T=1 VLP; (B) encapsulation of tannic acid stabilized 7nm gold nanoparticles to form a T=1 VLP.

The native T=3 capsid of CCMV can be extracted from infected cowpea plants and subsequently disassembled into 90 protein dimers by removing the RNA both following established procedures.[16] These dimers can be reassembled into well studied T=1 capsid VLPs by encapsulating negatively charged gold nanoparticles (AuNP) or polystyrene sulphonate (PSS). The efficient formation of T=1 capsids using PSS, as described by Sikkema et al., requires a precise ratio between polymer and protein, such that for each protein monomer 40 sulphonate groups are available.[15] Encapsulation of AuNP, as described in the previous chapter, is done by adding an excess of CP to solution of 7nm AuNP, taking care to keep the NaCl concentration around 0.1 M.

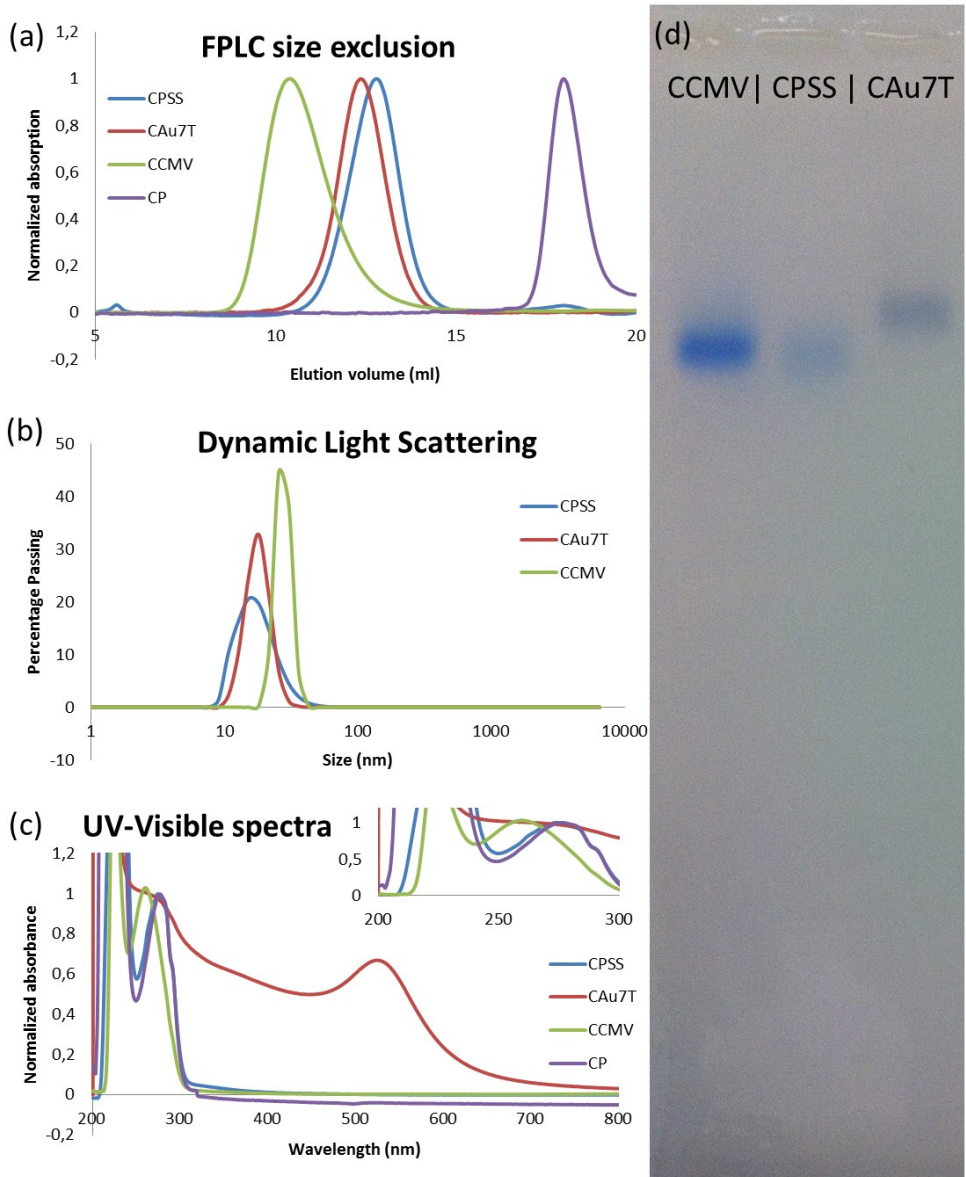


Figure 2: (a) FPLC size exclusion chromatograms at $\lambda = 280\text{nm}$ absorption for CCMV, CCMV CP, CPSS and CAu7T. (b) Dynamic light scattering plots for CCMV, CPSS and CAu7T. (c) Normalised UV-visible spectra for CPSS, CAu7T, CCMV and CCMV CP, with inset showing an expansion of the range relevant for RNA, PSS and protein absorptions. (d) Agarose Gel electrophoresis of T=3 CCMV (left), T=1 CPSS (middle) and T=1 CCMV AuNP (right).

The resulting VLPs were characterised using FPLC, DLS, agarose gel electrophoresis (figure 2) and TEM (figure 3) to check for successful VLP formation and confirm their size correlates with either a T=3 or T=1 VLP. The FPLC size exclusion

chromatograms show the expected elution volumes of $V = 10.3$ ml for CCMV (T=3), $V = 12.7$ ml for CPSS (T=1) and $V = 12.3$ ml for CAu7T (T=1) with any leftover CP residue eluting at 18 ml.²² The DLS and TEM confirm relatively monodisperse particles have formed, with an approximate of 28 nm for the CCMV T=3 particle and 18nm for both the CPPS and CAu7T T=1 VLPs. Finally, agarose gel electrophoresis shows a uniform electrophoretic mobility, and thus charge/mass ratio, for all VLP, as expected from particles that have the same type of proteins forming the outer shell.

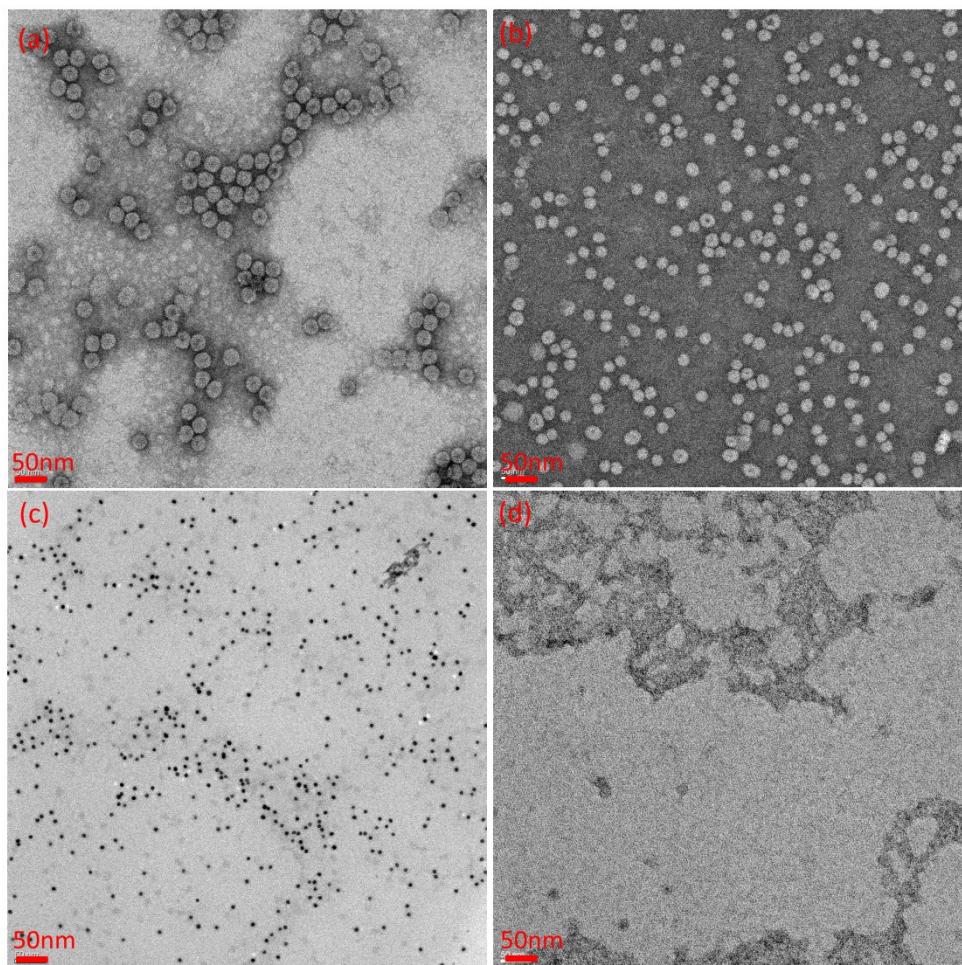


Figure 3: TEM images of (a) virus particles (CCMV), (b) T=1 polymer cored virus capsids (CPSS), (c) gold cored T=1 virus capsids (CAu7T), (d) disassembled CCMV coat protein (CP).

²² The small difference in elution volume, $\Delta V = 0.4$, between CPSS and CAu7T VLPs can be attributed to the hard AuNP encapsulated in the CAu7T VLP, making this VLP slightly less compressible and malleable in the FPLC column compared to soft macromolecule (PSS) cored VLP.

UV-Vis spectroscopy was used to further characterise the VLPs (figure 2c). The native CCMV is known to have a large characteristic UV-Vis absorption at $\lambda = 260$ nm due to the presence of RNA ($\epsilon_{260} = 2.78 \cdot 10^7 \text{ M}^{-1}\text{cm}^{-1}$) with little contribution of the protein absorbance peak at $\lambda = 280$ nm ($\epsilon_{280} = 2.41 \cdot 10^4 \text{ M}^{-1}\text{cm}^{-1}$), which is confirmed for the isolated CCMV T=3 particles. [17] After the encapsulation of PSS or Au7T the characteristic $\lambda = 260$ nm peak is lost, instead the CPPS shows a shift to $\lambda = 280$ nm and the CAu7T VLPs show the characteristic gold plasmon absorbance peak at $\lambda = 520$ nm. Due to their spectral overlap the relative absorptions of the CCMV-CP and PSS at $\lambda = 260\text{nm}$ and $\lambda = 280\text{nm}$ ($\epsilon_{260,\text{PSS}} = 2.17 \cdot 10^6 \text{ M}^{-1}\text{cm}^{-1}$, $\epsilon_{280,\text{PSS}} = 4.96 \cdot 10^5 \text{ M}^{-1}\text{cm}^{-1}$) have been used to calculate the concentrations of CPSS. For CAu7T the gold plasmon peak at $\lambda = 506\text{nm}$ (for 7nm AuNP, $\epsilon_{506,7\text{nmAuNP}} = 2.73 \cdot 10^7 \text{ M}^{-1}\text{cm}^{-1}$) is used to determine particle concentration after purification as the change in the plasmon peak is negligible.[18]

Ionic strength dependence of clustering different sized VLPs

When examining the interaction of particles and polymers through electrostatic forces, the ions in solution must be considered. These can screen charges and lead to an effective reduction of interaction strength. By tuning this interaction strength, the speed of clustering can be tuned from rapid aggregation with little order to slow formation of periodic crystals or even an altogether stop of the clustering. The Debye screening length (κ), the distance at which electrostatic interactions become meaningful, is indicative of this effect and is given by:[19]

$$\kappa^{-1} = \sqrt{\frac{\epsilon_0 \epsilon_r k_b T}{e^2 \sum_i c_i z_i^2}}$$

Clusters of CCMV and CPSS are formed by adding an increasing concentration of poly- λ -lysine (PLL) to a fixed concentration of VLPs (figure 4). In an ideal system the minimum amount of polymer needed to cluster the VLP is such that all electrostatic binding sites on one VLP share one polymer with one binding site on another VLP. These binding sites are known to occur on the threefold axis, with the T=3 CCMV thus having 60 such binding sites, which, assuming the T=1 VLPs have a similar binding site, means 20 such binding sites on the T=1 VLPs. Significant variation from the amount of polymer being needed per two binding sites (i.e. one), indicates that the anionic binding sites of the system are screened by the ionic strength of the solution.

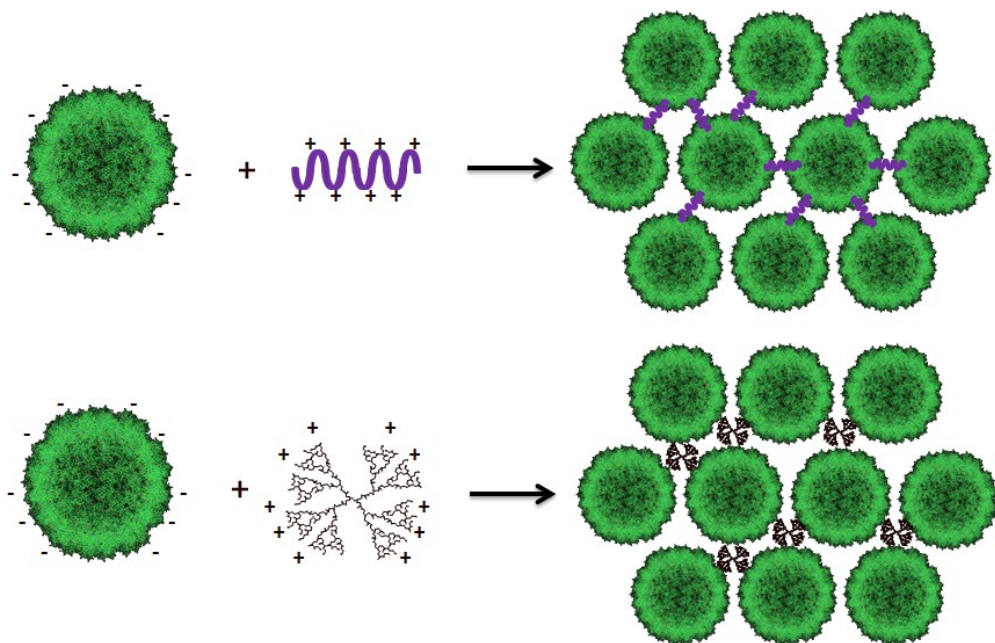


Figure 4: Schematic representation of VLP clustering with (top) linear poly- λ -lysine (PLL) and (bottom) spherical PAMAM G-3 dendrimers (PG3).

The formation of clusters of these VLPs and PLL is followed by DLS at different ionic strengths to characterize the dependence on the ionic strength. Buffered solutions with 150 mM NaCl (165 mM Na^+ , so $\kappa \approx 0.8$ nm), 50mM NaCl (65 mM Na^+ , so $\kappa \approx 1.2$ nm) and 0 mM NaCl (15 mM Na^+ , so $\kappa \approx 2.5$ nm) show varying onset points for the formation of polymer-VLP clusters. In this, we consider the onset point of clustering, an indication of how many polymers are needed per binding site, to be the point at which the DLS intensity signal indicates the presence of particles significantly larger than the capsid used. Two things become immediately apparent from the DLS results: firstly, the onset point for clustering is dependent on the ionic strength as expected, and, secondly, the two capsids behave different as the concentration of NaCl increases.

The 60 binding sites of the T=3 capsid and 20 of the T=1 capsid allow for 30 or 10 polymers respectively to interact with the capsid assuming two binding sites per polymer, an effective ratio of 6 proteins per polymer regardless of symmetry. Thus 50 $\mu\text{g}/\text{ml}$ of protein ($Mw_{\text{of protein}} = 20\text{kDa}$, 2.5mM) would require 3.96 $\mu\text{g}/\text{ml}$ of PLL ($Mw_{\text{average}} = 9500\text{kDa}$, 0.417 mM) to allow for an optimal interaction assuming no competing ions shield the electrostatic binding sites. At first glance the DLS data (figure 5) shows that for T=3 capsids this holds at 0mM and 50mM, but the ionic strength is too high for optimal cluster formation at 150mM. For the T=1 particles this seems to require a further analysis as their clustering already seems hindered

from 50mM NaCl onwards, even though the surface charge density of both T=3 and T=1 VLPs should be similar.

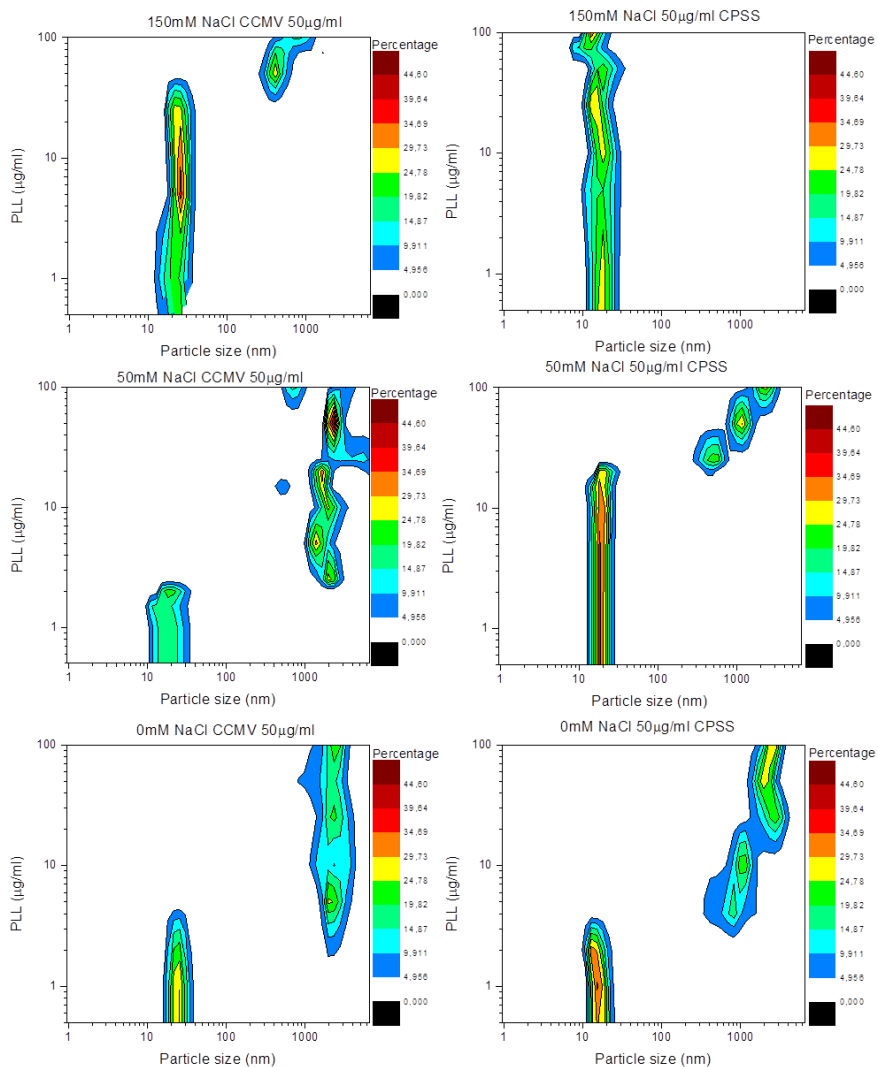


Figure 5: Dynamic light scattering intensity plots of 50 µg/ml (left) T=3 virus particles (CCMV) and (right) T=1 polymer cored virus capsids (CPSS) at (top to bottom) 150mM, 50mM and 0mM of NaCl. Note that a fictive $1 \cdot 10^{-6}$ µg/ml concentration of PLL was used to plot the measurements for the capsid stock capsid solutions.

At 0mM NaCl the number of competing ions is lowest and the DLS data (figure 5) indeed shows an onset point of clustering between 1 and 5 µg/ml of PLL for both the T=1 and the T=3 capsids. TEM micrographs taken at 5 µg/ml of PLL at 0mM

NaCl (figure 6 A and C), however, do not show any signs of organised structures. In fact, the T=3 capsids form a random colloidal assembly (figure 6A), whilst the T=1 capsids are packaged closely but with a clear fluctuation in the density of capsid particles (figure 6C). It is likely that these assemblies are the result of extremely rapid aggregation of the particles upon exposure to the polymer possibly leading to kinetically trapped states.

As stated, at $[\text{NaCl}] > 50\text{mM}$ there is a clear difference between the T=1 and T=3 VLPs clustering behaviour, as evident from the DLS data (figure 5). Most importantly, the T=3 particles seem to still be able to form clusters near the calculated $3.94\ \mu\text{g/ml}$ calculated for optimal interaction. Furthermore TEM micrographs for T=3 capsids cluster with $5\ \mu\text{g/ml}$ of PLL (figure 6B), close to this optimal interaction, show the formation of organised nanostructures. Unlike the T=3 VLPs, the T=1 VLPs do not show this desired organisation and clustering behaviour, and instead require concentrations of $25\ \mu\text{g/ml}$ PLL ($2.63\ \text{mM}$) or greater before clustering is initiated. This effectively means that an average of more than 1 polymer per protein, or 3 polymers per binding site, is needed before clustering starts. This is confirmed by TEM micrographs (figure 6D) which show loose strips of protein cages not unlike those found without the presence of a clustering polymer. It should, however, be noted that the quality of the staining of these T=1 samples is poor, which, despite similar conditions to the other samples and several attempts, did not allow for better contrast. This is likely caused by the PLL, that screens the carboxylic acid groups in the binding sites on the surface from the uranyl acetate staining, resulting in a reduced level of staining and thus contrast.

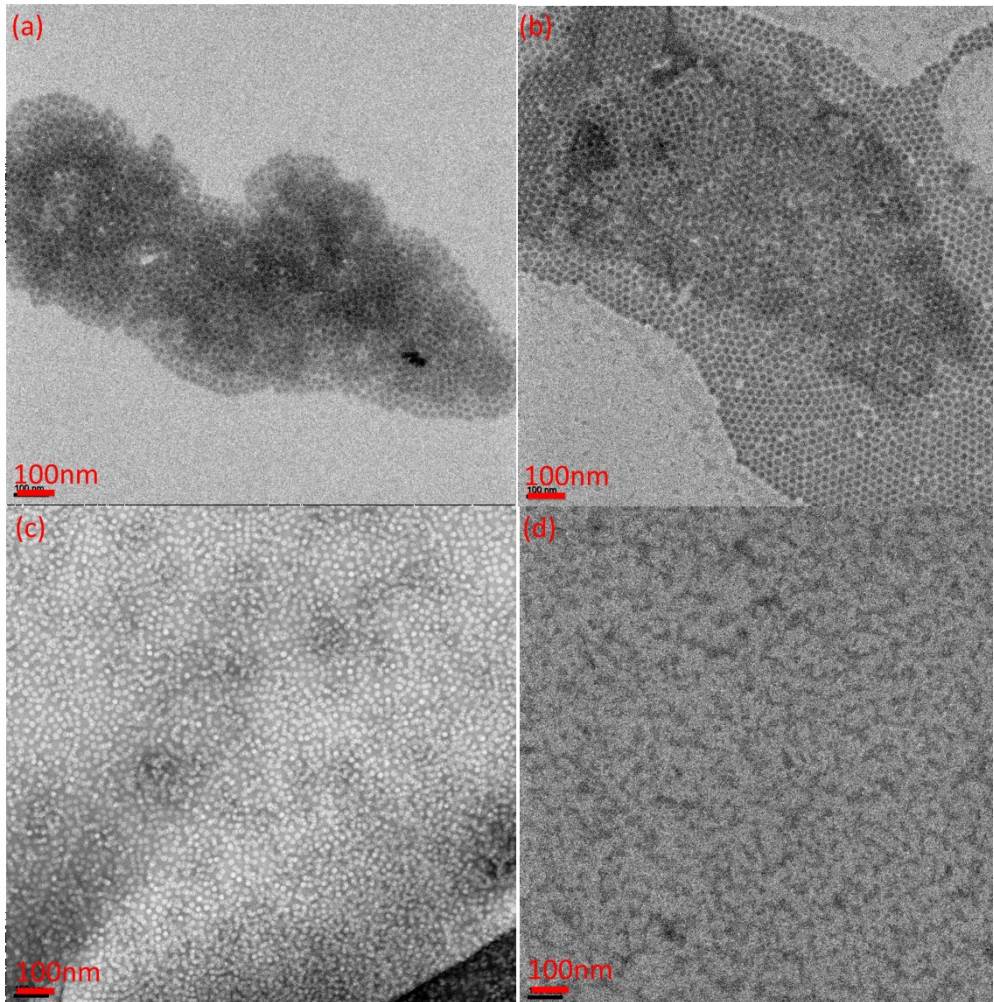


Figure 6: Transmission electron micrographs of 50 $\mu\text{g}/\text{ml}$ VLPs, protein mass only, and 5 $\mu\text{g}/\text{ml}$ of PLL of (a) T=3 CCMV VLPs at 0mM NaCl, (b) T=3 CCMV VLPs at 50mM NaCl, (c) T=1 CPSS VLPs at 0mM NaCl, and (d) T=1 CPSS VLPs at 50mM NaCl.

Binding of Poly- λ -Lysine by the T=1 capsid

The differences in the binding of PLL by the T=1 CPSS compared to the T=3 CCMV requires further examination. Therefore, the DLS and TEM results are compared to agarose gel electrophoresis and models for the T=1 and T=3 VLP capsid, to investigate the nature of the binding between the T=1 CPSS VLP and PLL. As stated, the effect of ionic strength on this binding is more pronounced in the T=1 CPSS VLP compared to the T=3 VLP, which we feel can be attributed to the capsid symmetry itself and not to the change from an RNA type core to a PSS type core. Both are, after all, relatively soft macromolecules and PSS is a well-studied RNA mimic for

virus assembly.[15] As seen in the structural model (figure 7), the relevant change between the T=1 and T=3 symmetrical structures lies in a structural change of the negatively charged electrostatic binding site near the threefold axis, which could explain the difference in binding.

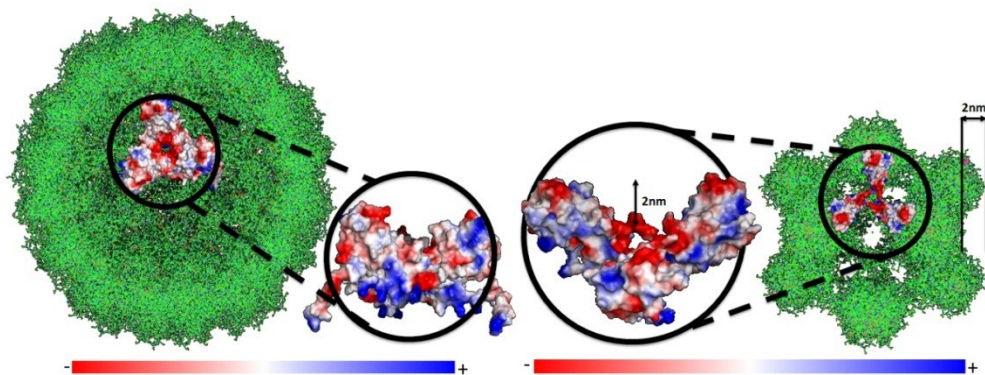


Figure 7: To scale reconstruction of T=3 (left) and T=1 (right) symmetry capsids with electrostatic potential map of the 3-fold symmetry axis for both symmetries.

The VLP binding site (figure 7) changes from a pocket, formed by two proteins from two different hexamers and one from a pentamer, for T=3 VLPs, to a 2nm groove formed by three proteins derived solely from three different pentamers for T=1 VLPs. Assuming the binding site has in fact changed as suggested; two key parameters can change in the protein shell electrostatics, namely the surface charge density and the charge distribution. Agarose gel electrophoresis (figure 2c) confirms that the overall surface charge to mass ratio does not change from the T=3 to the T=1 VLPs as both capsids show an equal electrophoretic mobility on the gel. On the other hand, the above model shows a change in the distribution of charge within each binding site, which could explain the effect of the ionic strength contribution to the electrostatic clustering. After all starting at 50mM NaCl ionic strength the Debye screening length is comparable to the depth of the groove, ensuring that charges inside the groove have little interaction with charge outside. At 0mM NaCl there is little charge screening allowing polymers to fully interact with neighbouring particles, whereas at 150mM all interaction outside of the groove is quenched.

This is supported by agarose gel electrophoresis analysis of the T=1 and T=3 VLP clusters at increasing concentration of PLL (figure 8). In this, T=3 CCMV clusters show only two possible protein bands, whilst the T=1 CPSS clusters show three distinct protein bands. The top band/smear for both the T=3 CCMV and T=1 CPSS

clusters can be attributed to clusters of particles slowly breaking up under the applied electric field. The lower bands for the T=3 CCMV clusters slowly decrease in electrophoretic mobility as the PLL concentration increases, an effect likely caused by reversible interaction with PLL. Unlike the T=3 clusters, the lowest band for the T=1 particles does not change in electrophoretic mobility and merely decreases in intensity as the PLL concentration increases with a second band appearing halfway and again remains at constant electrophoretic mobility. This indicates a system where either a T=1 capsid has PLL bound or it has not, and no reversible interaction between the two occurs. At 50mM of NaCl the linear PLL is most likely bound by the T=1 capsid groove, lying, as it were, flat in the groove at 2nm depth and not be able to have meaningful interactions with charges on any neighbouring capsid due to a Debye screening length of only 1.2nm. At higher concentrations it could compete with other PLL polymer chains, to weaken interaction and allow for clustering at concentrations greater than 25 $\mu\text{g/ml}$ PLL (2.63 mM) for 50 $\mu\text{g/ml}$ CPSS seen in DLS.

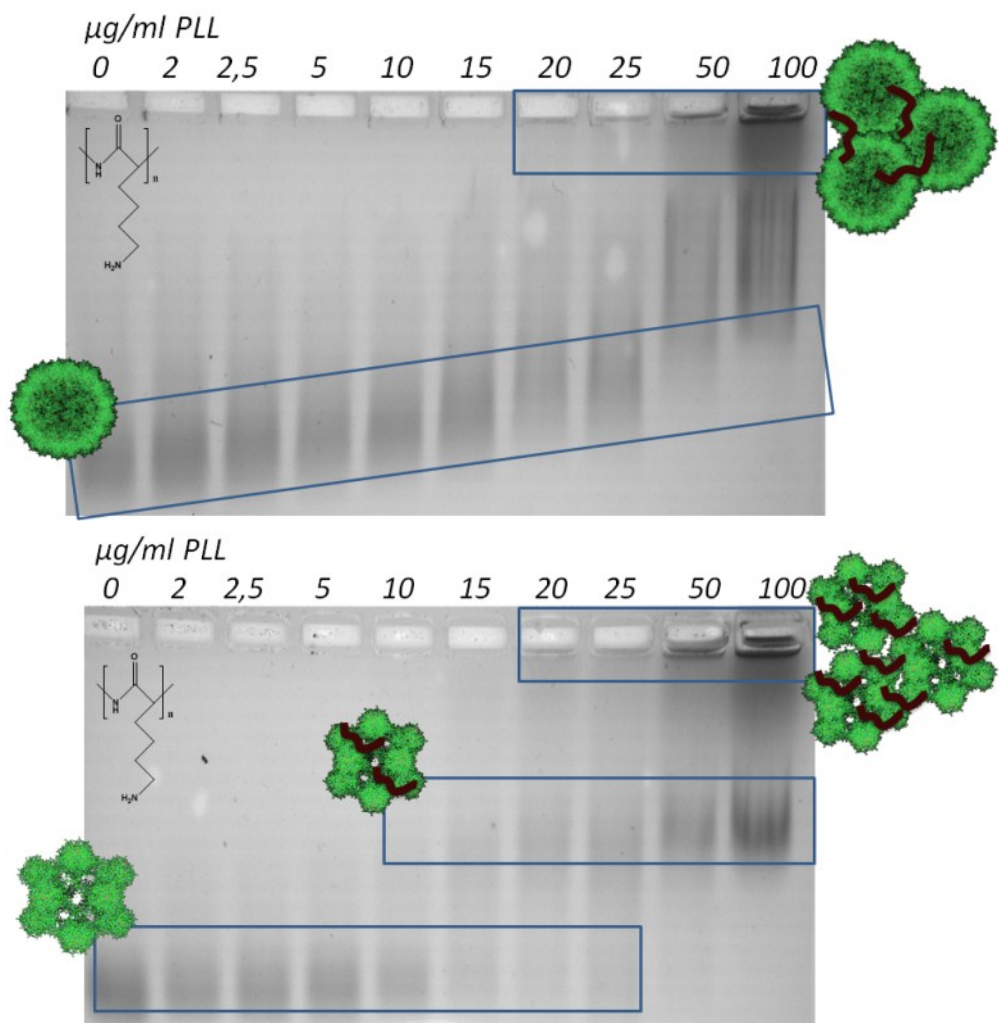


Figure 8: Agarose Gel Electrophoresis of T=3 (top) and T=1 (bottom) of protein cage clusters formed in 50mM of NaCl at 100 µg/ml of protein and increasing PLL concentration.

These results indicate a stronger binding between the PLL and T=1 CPSS VLPs compared to the T=3 CCMV VLPs, which should allow the T=1 CPSS VLP to outcompete the T=3 CCMV for PLL if both are mixed. To test this hypothesis, competition experiments between the two VLPs were carried out, in which equal quantities of VLP protein were mixed in different order at 50mM of NaCl (figure 9). Initially, 25 µg/ml of T=3 CCMV and 5 µg/ml of PLL is used to form clusters, upon the addition of either more buffer solution or 25 µg/ml of T=3 CCMV a conservation of clustered particles is observed by DLS. However, upon addition of 25 µg/ml of T=1 CPSS, instead of buffer or T=3 CCMV, there is a loss of most of the clustered

state, with a broad peak appearing around 20nm that indicates a mixture of free T=1 and T=3 particles. Similarly, addition of 25 $\mu\text{g/ml}$ of T=3 to a solution of 25 $\mu\text{g/ml}$ of T=1 CPSS and 5 $\mu\text{g/ml}$ of PLL does not show anything but a broad peak for free particles. A control experiment, the addition of 25 $\mu\text{g/ml}$ of T=1 CPSS to a solution of 25 $\mu\text{g/ml}$ of T=1 CPSS and 5 $\mu\text{g/ml}$ of PLL, also shows a peak for free particles, but distinctly narrower as no T=3 sized particles are present. The loss of a signal for clustered materials indicates a decreased clustering, caused by a scavenging of the available PLL clustering agent by the T=1 capsid.

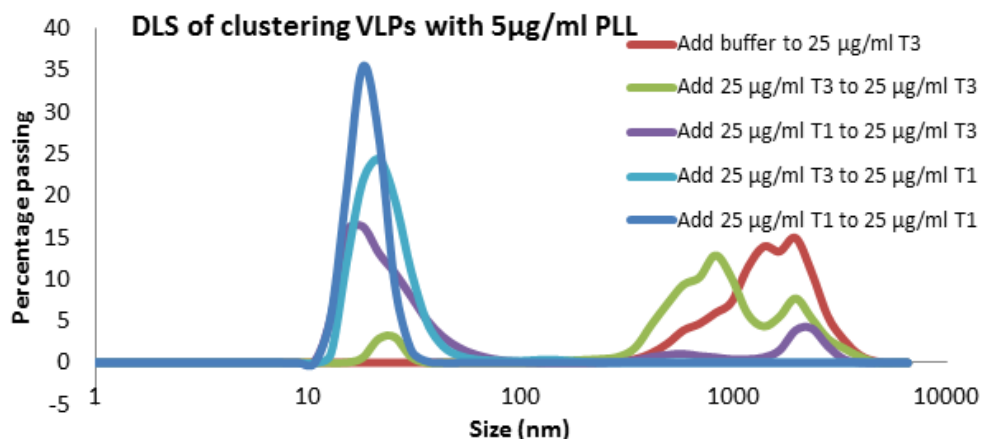


Figure 9: Competition experiments between T=3 CCMV and T=1 CPSS monitored by dynamic light scattering. Starting at 25 $\mu\text{g/ml}$ of protein the sample was subsequently diluted by the addition of a second solution as indicated in the figure above.

The effect of the polymer shape on the clustering

If indeed there is a binding pocket that traps the linear PLL, a polymer of a different shape might show a different interaction with this pocket. To investigate this, spherical PAMAM-G3 (PG3) dendrimers are used in clustering experiments, as they are an established alternative means of clustering T=3 CCMV capsids.[10] The overall mass of the PG3 dendrimer ($M_{w_{PG3}}=6,909$) is within the range of the PLL ($M_{w_{PLL}}= 4,000-15,000$) and it has a similar amine to mass ratio resulting in a similar charge density. Furthermore, the diameter of this spherical dendrimer is around 3.3 nm,²³[20] excluding containment in any surface groove. As evident from the dynamic light scattering data (figure 10), the dendritic PG3 has a very different interaction with the two different VLP symmetries compared to the linear PLL.

²³ This diameter is two times the radius derived from the solvent accessible surface area, $R_{SASA} = 16.43 \text{ \AA}$, as computed by Maiti et al.[20]

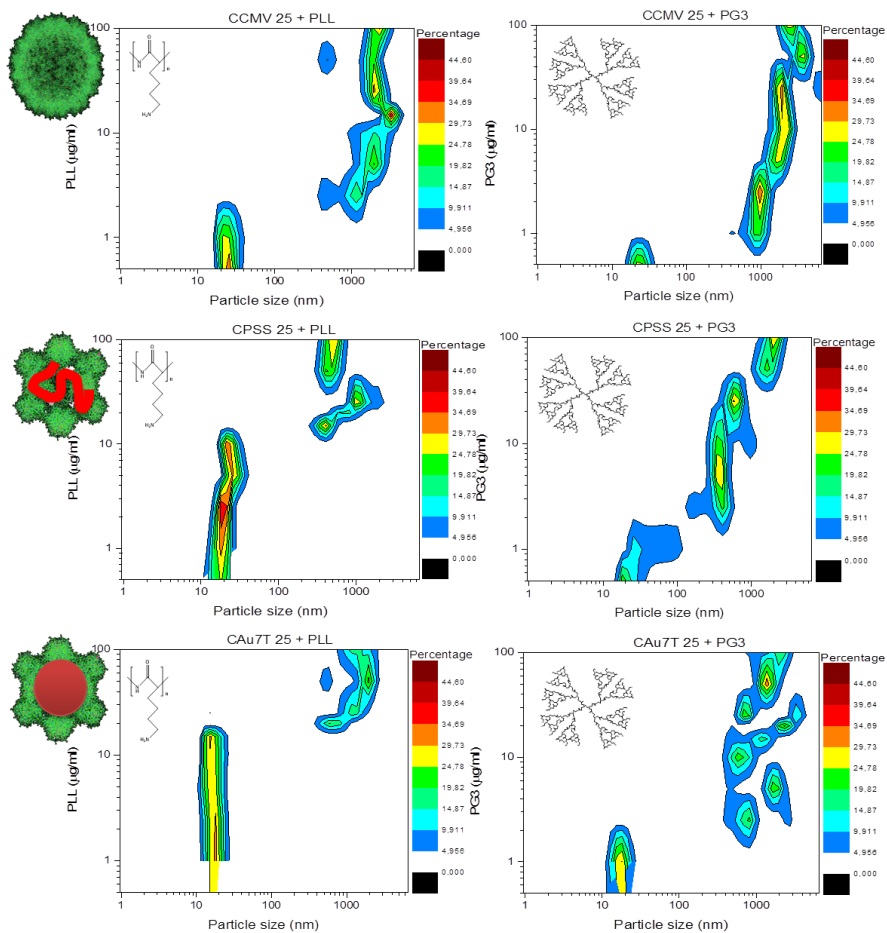


Figure 10: *Dynamic light scattering intensity plots at 50mM NaCl of 25 μg/ml (top) T=3 virus particles (CCMV), (middle) T=1 polymer containing virus capsids (CPSS) and (bottom) gold containing T=1 virus capsids (CAu7T) with increasing PLL concentration (left) and increasing PG3 concentration (right).*

The onset point of clustering with the dendrimer appears to be similar for both the T=1 and T=3 capsids (figure 10), at 1mg/ml of proteins for the T=3 CCMV capsid and 2mg/ml for the T=1 CPSS capsid. Surprisingly, this indicates an average of 10.4 dendrimers for every T=3 capsid or 7.0 for every T=1 capsid, suggesting that not all binding sites on the capsids are needed to form clusters. The T=3 clustering behaviour is similar to studies on cationic gold nanoparticles where only 24 out of a possible 60 electrostatic binding sites were found to be used on a T=3 CCMV capsid, and generally 16 were used in a crystalline assembly. [11] Kostianen et al. speculate that steric hindrance and electrostatic repulsion could play an important role in preventing neighbouring binding sites from being used.. Considering the size

of the dendrimer, $R_{SASA} = 1.6 \text{ nm}$, [20] and the distance between two binding sites, $\sim 6 \text{ nm}$ from the model, two adjacent dendrimers should be separated by $\sim 3 \text{ nm}$. This is more than the Debye length, $\kappa \approx 1.2 \text{ nm}$ for $[\text{NaCl}] = 50 \text{ mM}$, thus limiting the potential effects of steric hindrance and electrostatic repulsion. Instead, we believe that the clustering is more efficient due to strong dendrimer-binding site interaction deriving from the PG3 structure.

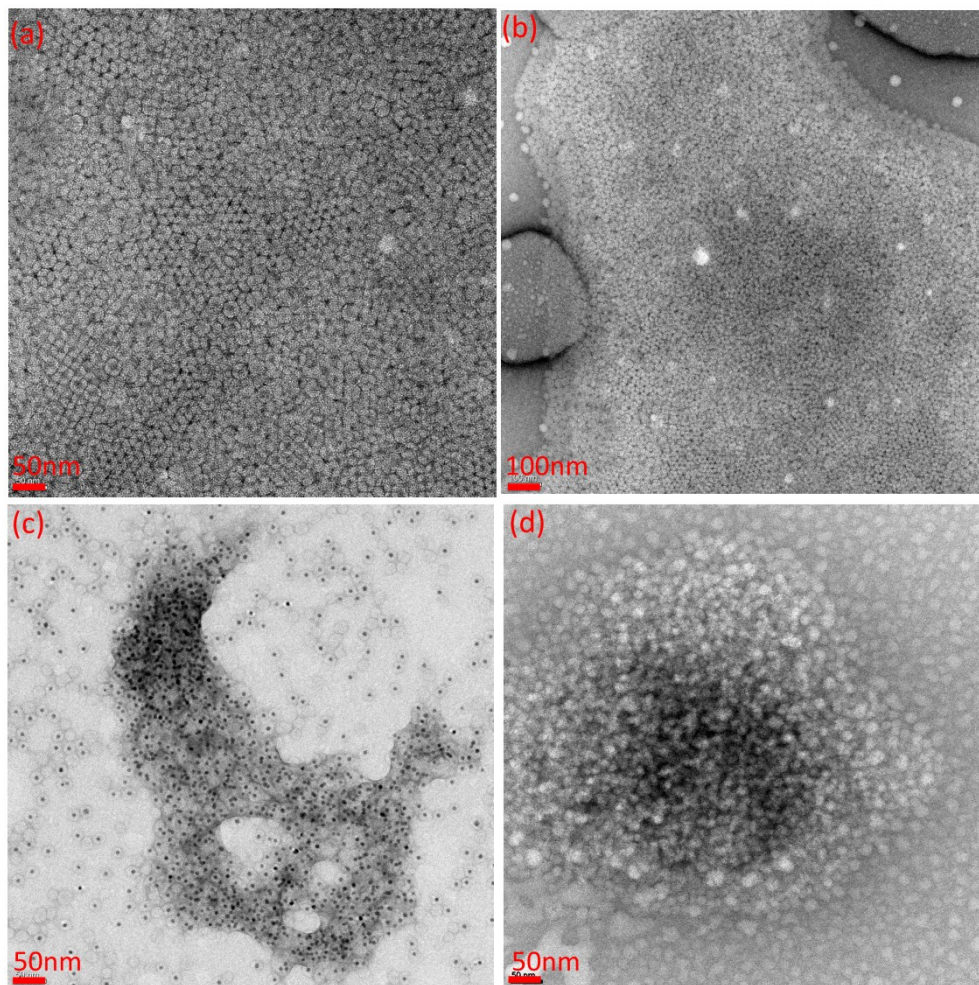


Figure 11: TEM images of 25 $\mu\text{g/ml}$ VLPs clustered with 10 $\mu\text{g/ml}$ of PG3 at 50mM NaCl (a,b) virus particles (CCMV), (c) T=1 polymer cored virus capsids (CPSS) and (d) gold cored T=1 virus capsids (CAu7T).

Interestingly, the electron microscopy images of T=3 CCMV-PG3 clusters (figure 11) show a clear multi-layered structure, with different domains within the crystals having either face centred cubic (fcc) or hexagonal close packing (hcp) structure.

This is unlike the images of PLL based clusters, that, though organized, do not show more than two organised layers and no evidence of organization in the third dimension. Similarly, images of T=1 CPSS-PAMAM G3 show a denser structure compared to those clusters formed with PLL. These findings further point to the important role of the molecular structure of PG3, that apparently prevents the collapse of the structure upon drying. Furthermore, these results can be explained by the symmetrical rotations found in the two different VLPs, with the T=3 having a six-fold, threefold and twofold rotational axis and the T=1 being limited to a fivefold and threefold rotational axis. As the binding sites are arranged according to this symmetry, a T=3 capsid could easily offer a similar binding environment on six symmetrical positions, allowing for hexagonal close packing. The T=1 capsid could only offer a similar binding site on five symmetrical positions thereby limiting it at best to quasi-crystalline arrangement or topologically close packed (tcp) structure. Such structures are not found and we believe they would require a specifically designed macromolecule, to fine-tune the binding site interaction, combined with carefully control over the clustering conditions, like pH and ionic strength.

Cargo independence of clustering

Ultimately, the goal of this research is to find pathways to organise nanoparticles and other materials contained in the virus capsids through a uniform method. As such, it is important to show that the clustering depends on the capsid, and thus the symmetry, and not the cargo. To investigate this T=1 CAu7T VLPs filled with hard material 7 nm AuNPs, rather than soft PSS or RNA, can be clustered with both PLL and PG3. These particles have been shown to be similar in size and behaviour to the T=1 VLP, as detailed previously, while the gold plasmon absorption seen in the UV-Vis spectrum (figure 2), the reduced electrophoretic mobility (figure 7) and TEM images (figure 10) of these particles all point to of a dense metallic core.

As expected, the T=1 CAu7T VLPs clusters in a similar manner to the T=1 CPSS VLPs for both the linear PLL and the spherical PG3 (figures 10 and 11). The onset point for clustering observed in DLS requires starts at 25 $\mu\text{g}/\text{ml}$ of PLL or 2 $\mu\text{g}/\text{ml}$ of PG3 for the T=1 CAu7T clusters, which is comparable to the results obtained for T=1 CPSS, rather than the T=3 CCMV. Furthermore, like their soft T=1 CPSS counterparts the T=1 CAu7T VLPs show little to no organisation upon clustering. Investigations on T=3 gold and/or CPSS cored VLPs are, however, desired to confirm if this is due to the capsid symmetry as discussed above or imperfections in the VLP shell formation as is suggested by theoretical work by Nguyen.[21]

Conclusion

The size and related symmetry structure, of CCMV based VLPs significantly impacts the electrostatic clustering with soft macromolecules. The nature of the core, whether it is a hard nanoparticle or soft polymer, does not seem to affect cluster formation beyond providing a template for the protein shell. Experimental data, supported by a model of the binding site, suggests that the smaller T=1 VLPs will trap linear PLL in a surface groove. This will prevent clustering until the T=1 VLP surface is saturated, unlike the T=3 VLPs that readily forms clusters with PLL. Clustering with spherical PG3 is, however, similarly efficient for both T=1 and T=3 VLPs. TEM images show evidence for organised fcc or hcp structures for the T=3 CCMV VLP clusters, whilst the T=1 VLP clusters show no evidence for organisation, which we attribute to the T=3 VLPs' six-fold symmetry axis.

Understanding the differences in clustering between the T=1 and T=3 VLPs enables a more careful control over the desired material properties and structure. As such, the limitations in structural order could be addressed by careful control over both the binding site interaction and conditions, e.g. pH and ionic strength. In fact we believe that by careful tuning of the clustering macromolecules' interaction with the T=1 VLP binding site, quasi-crystalline or tpc structures might be achievable. Furthermore, the core independence for T=1 VLP cluster behaviour shows the potential universality in forming clusters using the same protein scaffold. Collectively, this opens up opportunities for using VLPs as uniform building blocks in new nanomaterials with tuneable optical, electronic and structural properties.

Experimental

The following equipment and methods were used to obtain the data in this chapter.

Virus and Coat Protein Isolation

CCMV is isolated from infected plant material according to methods adapted from Verduin et al. The CCMV CP is also isolated according to methods developed by Verduin et al. and will be described in brief. CCMV is disassembled into 90 protein dimers by precipitating the RNA using Ca^{2+} , through dialysis against a pH7.5 aqueous buffered solution (500mM CaCl_2 , 50mM Tris). The RNA- Ca^{2+} precipitate can be pelleted by ultracentrifugation (2h at 40000 rpm in Fiberlite F50L-24x1.5 rotor) and the remaining Ca^{2+} is subsequently removed by dialysis against the pH7.5 aqueous buffered solution (50mM Tris; 500mM NaCl) yielding a CCMV protein dimer solution.[16]

CPSS VLP formation

The efficient formation of T=1 capsids using PSS, as described by Sikkema et al., requires a precise ratio between polymer and protein, such that for each protein monomer 40 sulphonate groups are available. In a typical experiment 70kDa PSS is encapsulated by adding a solution of PSS (milliQ, 2.75mg/ml, 200ul) to a room temperature solution of the protein dimers (6mg/ml, 300ul). After incubating it on a roller bank for 30 minutes the resulting VLPs were purified using preparative FPLC using a 0.3 M aqueous buffered solution as the eluent (50mM Tris; 300mM NaCl).[15]

CAu7T VLP formation

Encapsulation of AuNPs, as described in chapter 4, requires a large excess of protein and precise control over salt concentration to prevent particle aggregation from charge screening whilst maintaining the proteins structure. 7nm AuNP are encapsulated by adding a room temperature solution of the protein dimers (6mg/ml, 120ul) to a solution of AuNPs (milliQ, 0.5mg/ml, 480ul) and mixed by vigorous shaking for 15s. The resulting VLPs were dialysed overnight against a pH7.5 aqueous buffered solution (50mM Tris; 500mM NaCl) and purified using preparative fast protein liquid chromatography (FPLC).

Clustering procedure

Sample solutions are prepared fresh from 1 mg/ml VLP stock solutions in 0 mM or 50 mM NaCl cluster buffer solution (10mM sodium acetate, 1 mM EDTA, 1mM NaN₃, pH5.0) and 1 mg/ml of polymer stock solution in milliQ, either PLL or PG3. First, an aliquot of the VLP stock solution is diluted by addition of further cluster buffer solution. Then, the ionic strength is adjusted by addition of 1 M NaCl cluster buffer. Finally a small volume of the polymer is added such that the final concentrations are as desired.

Agarose

A 1.2% w/v agarose gel is cast in a low salt buffered solution (50mM NaCl, 10mM sodium acetate, 1 mM EDTA, 1mM NaN₃) and allowed to solidify for 30 minutes and subsequently immersed in a similar buffer. Samples are taken from 50µl of freshly made sample solution allowed that are left to equilibrate into clustered or unclustered states for 10 minutes on a shaking platform or roller bank after mixing. The samples are injected into 50ul sample wells and left to run for 2 hours at a potential difference of 100V. Afterwards samples are stained for 2 hours using bio safe commassie bleu and washed three times for at least 2 hours using milliQ to remove excess staining.

Transmission electron microscopy

Samples are taken from 100µl of freshly made sample solution allowed that are left to equilibrate into clustered or unclustered states for 10 minutes on a shaking platform or roller bank after mixing. The TEM samples are prepared by leaving 5µl of this sample solution on a formvar carbon coated copper grid for 5 minutes and subsequently removing it by tipping the grid onto low lint paper (Kimtech science precision wipes). Stained samples use 5ul of a 1% Uranyl Acetate solution which is removed after 30 seconds to provide optimal contrast. Samples are imaged using a Philips CM300ST-FEG TEM.

DLS

Dynamic light scattering samples are prepared from 500 µl fresh sample solutions and allowed to equilibrate for 2 minutes on a roller bank after mixing. Salt concentrations were controlled by using stock solutions of 0M and 1M NaCl containing buffers and in all cases the cationic polymer was the final addition. Each sample was measured five times for 120 seconds using an Anaspec nanotrack wave dynamic light scattering instrument with the best of these five measurements selected.

UV-Visible

UV-Visible samples are prepared from 500 µl fresh sample solutions and allowed to equilibrate for 2 minutes on a roller bank after mixing. They were measured in a 1cm quartz cuvette in a PerkinElmer Lambda 850 UV/VIS Spectrometer.

FPLC

FPLC size exclusion chromatography samples, ranging from 100µl up to 500µl were measured on a 24ml column stacked with superose-6 and collected by fractionation.

Bibliography

1. Xu, L., et al., *Nanoparticle assemblies: dimensional transformation of nanomaterials and scalability*. Chemical Society Reviews, 2013. 42(7): p. 3114-3126.
2. Speir, J.A., et al., *Structures of the native and swollen forms of cowpea chlorotic mottle virus determined by X-ray crystallography and cryo-electron microscopy*. Structure, 1995. 3(1): p. 63-78.
3. Loo, L., et al., *Controlled Encapsidation of Gold Nanoparticles by a Viral Protein Shell*. Journal of the American Chemical Society, 2006. 128(14): p. 4502-4503.
4. Steinmetz, N.F., et al., *Plant viral capsids as nanobuilding blocks:*

- Construction of arrays on solid supports.* Langmuir, 2006. 22(24): p. 10032-10037.
5. Steinmetz, N.F., et al., *Assembly of Multilayer Arrays of Viral Nanoparticles via Biospecific Recognition: A Quartz Crystal Microbalance with Dissipation Monitoring Study.* Biomacromolecules, 2008. 9(2): p. 456-462.
 6. Yoo, P.J., et al., *Spontaneous assembly of viruses on multilayered polymer surfaces.* Nature Materials, 2006. 5(3): p. 234-240.
 7. Suci, P.A., et al., *Influence of Electrostatic Interactions on the Surface Adsorption of a Viral Protein Cage.* Langmuir, 2005. 21(19): p. 8686-8693.
 8. Steinmetz, N.F., et al., *Layer-by-layer assembly of viral nanoparticles and polyelectrolytes: The film architecture is different for spheres versus rods.* ChemBioChem, 2008. 9(10): p. 1662-1670.
 9. Kostiainen, M.A., et al., *Self-assembly and optically triggered disassembly of hierarchical dendron-virus complexes.* Nature Chemistry, 2010. 2(5): p. 394-399.
 10. Kostiainen, M.A., et al., *Electrostatic self-assembly of virus-polymer complexes.* Journal of Materials Chemistry, 2011. 21(7): p. 2112-2117.
 11. Kostiainen, M.A., et al., *Electrostatic assembly of binary nanoparticle superlattices using protein cages.* Nat Nano, 2013. 8(1): p. 52-56.
 12. Bozic, A.L. and R. Podgornik, *Symmetry effects in electrostatic interactions between two arbitrarily charged spherical shells in the Debye-Huckel approximation.* Journal of Chemical Physics, 2013. 138(7).
 13. Caspar, D.L.D. and A. Klug, *Physical principles in the construction of regular viruses.* Cold Spring Harbor Symp. Quant. Biol, 1962: p. 27,1-24.
 14. Kostiainen, M.A., et al., *Temperature-Switchable Assembly of Supramolecular Virus-Polymer Complexes.* Advanced Functional Materials, 2011. 21(11): p. 2012-2019.
 15. Sikkema, F.D., et al., *Monodisperse polymer-virus hybrid nanoparticles.* Organic & Biomolecular Chemistry, 2007. 5(1): p. 54-57.
 16. Verduin, B., *The preparation of CCMV-protein in connection with its association into a spherical particle.* FEBS letters, 1974. 45(1): p. 50-54.
 17. Aragonés, C., *The Cowpea Chlorotic Mottle Virus as a Building Block in Nanotechnology.* 2009: UB Nijmegen [Host].
 18. Liu, X., et al., *Extinction coefficient of gold nanoparticles with different sizes and different capping ligands.* Colloids and Surfaces B: Biointerfaces, 2007. 58(1): p. 3-7.
 19. Lyklema, J., *Fundamentals Of Interface And Colloid Science, Volume 5: Soft Colloids.* Vol. 5. 2005: Academic Press.
 20. Maiti, P.K., et al., *Structure of PAMAM Dendrimers: Generations 1 through 11.* Macromolecules, 2004. 37(16): p. 6236-6254.
 21. Nguyen, H.D. and C.L. Brooks, *Generalized Structural Polymorphism in Self-Assembled Viral Particles.* Nano Letters, 2008. 8(12): p. 4574-4581.

Chapter 5: Clustering with hard nanoparticles

Cargo independent clustering of virus-like particles

The organisation of multiple different hard nanoparticles into ordered structures is affected by a multitude of forces which limit a universal approach towards building programmable nanomaterials. Virus-like particles (VLPs) hold the key towards overcoming this challenge by acting as a scaffold for the formation of organised clusters of nanoparticles. This chapter investigates the clustering of CCMV based VLPs using hard metallic gold nanoparticles, showing that the clustering of these binary particle systems have assembly dynamics and stoichiometry based on the VLP size, not core composition. Furthermore, both hard cored and soft cored T=3 VLPs show evidence of plastic crystalline AB_8^{FCC} packing, whilst the hard cored T=1 VLPs only show limited evidence of crystalline packing. These results suggest that VLP based nanomaterials are candidates for the next generation of nanostructures with potential applications in optics, electronics and functional devices.

Introduction

Scientific scope

Self-assembled metamaterials that have unique electronic, optical, structural or combined properties can be made from the controlled combination of nanoparticles into a larger structure. These nanoparticles come in two principal varieties: hard nanoparticles that possess an impressive variety of physical properties, ranging from magnetic to optical, catalytic or electronic, and soft nanoparticles that afford a great range of structural flexibility, relying on the arsenals of organic chemistry and biology. Effective combination of the two types, to obtain control over the organisation and scalability and thereby properties of nanoparticle based materials, remains a challenge.[1]

As discussed in previous chapters, VLPs offer a range of options for the encapsulation of nanoparticles and subsequent assembly of materials. However, a core challenge of nanotechnology lies in miniaturisation, ensuring the highest possible density of desired physical interactions, usually those found in hard transition metal or semiconducting materials. Therefore, by making use of a functional hard nanoparticle to induce VLP assembly, a greater density or variation of the desired physical properties can be introduced into the material. Additionally, these particles could promote interactions with the particles contained inside the virus as they are of a similar nature, thus allowing for further programming of the final material properties.

Binary nanoparticle assemblies offer structural and functional options

A multitude of forces can be used to induce self-assembly of nanoparticles and though generally a single force, like electrostatics, is dominant, the composition and structure of the formed material also takes into account entropic, van der Waals, steric and dipole interactions.[1, 2] Slight variations to the surface and shape of hard nanoparticle can lead to a wide variety of structural diversity and, as such, variations can be obtained by relative minor alterations in the synthetic conditions. This ensures that each nanoparticle has its own identity when it comes to forming particle assemblies.[3, 4] Still, when careful control over the synthesis does lead to uniform particles, these nanoparticles can lead to macroscopic crystalline structures.[5] On the other hand soft nanoparticle building blocks, like dendrimers or virus capsids, offer a great deal of modulation, size control and easy chemical modification within a single building block .[6-9] Unfortunately, truly large scale assembly of such materials is often limited by their lack of rigidity and need for fine-tuning, and, compared to hard particles, they are limited in their physical properties.

A different approach comes from combining the best of both worlds, using soft biomolecules such as DNA, micelles or viruses as a scaffold for the organisation for hard nanoparticles, thereby making the final structure independent of the nanoparticle used.[10-12] Recent work shows that viruses can also be used for the fabrication of binary nanoparticle superlattices, where electrostatics provide the driving force for assembly, whilst steric and electrostatic hindrance due to the virus capsid morphology determines the observed final structure. [12] Combined with the manifold techniques to grow, encapsulate or synthesize functional materials inside virus capsids, as well as their ability to function as nanoreactor vessels, make these binary structures of virus-like particles and hard nanoparticles a versatile tool for constructing new materials.

Virus symmetry will determine the material structure

Virus capsids can adopt a limited number of well-defined symmetrical structures, described by Caspar-Klug symmetry structures. These symmetry structures are always formed by 12 protein pentamers and increasing number of protein hexamers, increasing in regular intervals, as described in detail in chapter 2.[13] This structural symmetry also translates to a number symmetrically placed electrostatic patches on the surface, and recent work shows these to play an important factor in virus clustering.[12] Such electrostatic clustering is first described by Kostianen et al. for the native CCMV T=3 capsid, showing the potential for virus capsids to be used in growing controllable electrostatic clusters.[14-16] However, the number, shape and orientation of these electrostatic patches will change for different symmetries. This could lead to different interactions between neighbouring shells, based on the nature and placement of these patches.[17]

The CCMV based VLPs can be reassembled into a number of different structures, both spherical and rod-like, but the two most common structures are the T=1 and T=3 symmetry. These symmetries are often referred to as an icosahedron (T=3) and dodecahedron (T=1), which is conserved in the localisation of the electrostatic binding sites on the surface. According to simulations by Damasceno et al., these should both form plastic crystals upon simple condensation with either an face centred cubic (fcc), for the T=3 icosahedron, or topologically close packed (tcp), for the T=1 dodecahedron, particle packing.[18] Though the simulations did not take into account a binary system, it is reasonable to assume that with a small enough binding nanoparticle the capsid symmetry will be dominant in determining the final morphology.

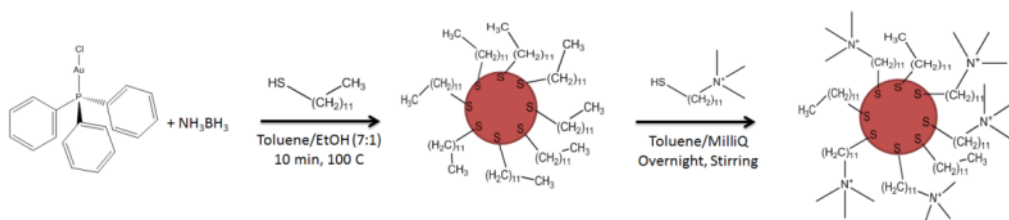
Chapter Content

In this chapter the clustering of CCMV based VLPs using cationic gold nanoparticles (AuNP+) is studied and analysed to understand the effect of capsid symmetry and cargo on the clustering with hard nanoparticles. Firstly, the synthesis of the AuNP+ is detailed to provide insight in the materials used, though the synthesis of the VLPs can be found in the previous chapter. Secondly, the clustering of well-studied CCMV T=3 capsids and CPSS T=1 capsids is examined in detail as model systems for VLP-AuNP+ clusters. Thirdly, studies on the clustering dynamics and hard nanoparticle containing capsids are discussed to show the broader functionality of this system.

Results and Discussion

Synthesis and modification of cationic gold nanoparticles

Investigating the clustering of VLPs with hard nanoparticles requires a model particle with well understood properties, synthetic control over size, shape and surface and measurable changes upon clustering. Gold nanoparticles (AuNP) fit all of these requirements in being well studied, allowing a wide variation in known synthetic procedures, and through plasmon coupling enabling a physical response upon clustering. Ideally these particles would be designed with a cationic surface and of a size comparable to the electrostatic binding pocket of the T=1 VLPs, which is described in the previous chapter.



Scheme 1: The synthesis of thiol stabilised cationic gold nanoparticles using MUTAB (11-mercapto undecyl trimethylammonium bromide) as a cationic ligand.

Thiol stabilized particles are used and prepared using a variation of the classical Brust-Schiffrin method as described by Goubet et al.[19] This method, as seen in scheme 1, yields dodecanethiol stabilised AuNP and provides for size control within the desired 3 to 5 nm size range. Ligand exchange in a vigorously stirred two phase system is used to introduce quaternary ammonia groups, from 11-mercapto undecyl trimethylammonium bromide, onto the AuNP surface. These groups provide a stable cationic charge in a wide variety of pH and ionic conditions as well

as solubility in aqueous solvents, allowing for cluster formation under conditions optimal for the VLPs.

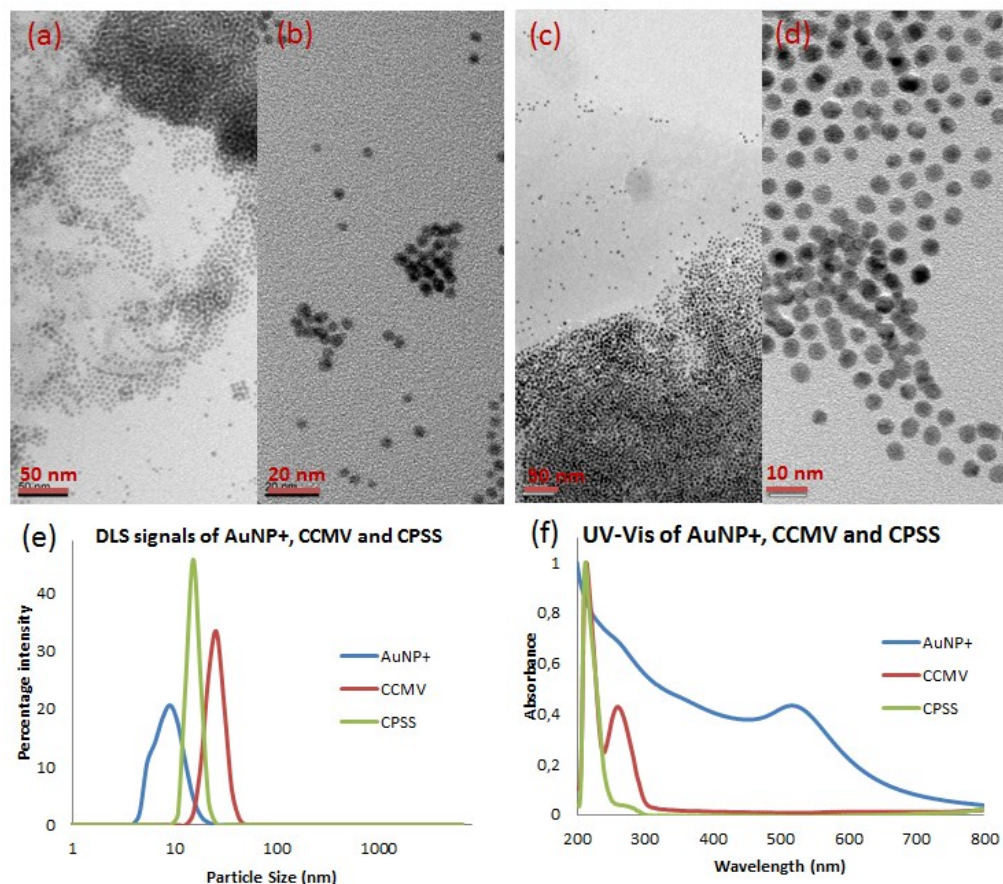


Figure 2: (a-d) TEM micrographs of; (a,b) as synthesised AuNP+ in toluene, (c,d) MUTAB modified AuNP+. (e) DLS signals of AuNP+, CCMV T=3 capsid and CPSS T=1 capsid. (f) Normalised UV signals of AuNP+, CCMV T=3 capsid and CPSS T=1 capsid.

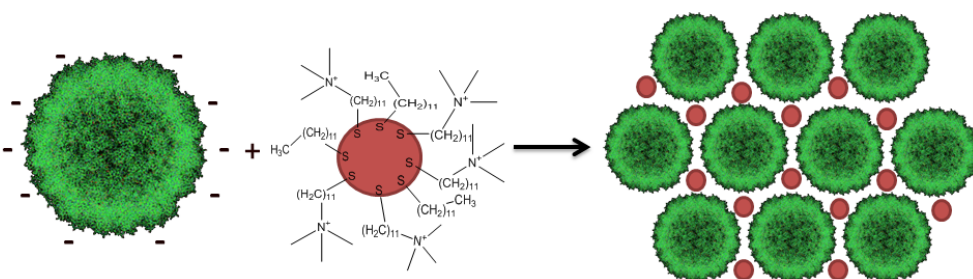
Analysis of the particles, seen in figure 2, reveals monodisperse particles of around $d = 4.7$ nm in diameter in TEM both before and after the ligand exchange, with a measured hydrodynamic diameter of $d = 9$ nm in DLS for the AuNP+. UV-Vis shows a gold plasmon absorption at $\lambda = 518$ nm, typical for small, monodisperse gold nanoparticles, far removed from the CCMV and CPSS²⁴ absorbance at $\lambda = 260$ nm and $\lambda = 280$ nm. Due to the small size no zeta potential measurements could be successfully completed, however the quaternary ammonia groups are the only

²⁴ i.e. the T=1 VLP containing polystyrene sulphonate (PSS)

groups that could promote water solubility, thus we can safely assume an overall positive surface charge.

T=3 clustering with AuNP+

Control over the clustering dynamics and structure is the first priority in making materials from VLPs and studying their properties. As such, recognising the importance of the ionic strength dependence of clustering, as detailed in the previous chapter, it is vital to study the effect of the NaCl concentration on the clustering of the native T=3 CCMV and AuNP+. Due to the spherical nature of the AuNP+ they should behave in a manner similar to the PAMAM-G3 dendrimers of the previous chapter, however their increased rigidity should also allow for greater structural uniformity.



Scheme 3: The clustering of CCMV based VLPs using cationic gold nanoparticles.

To investigate this clustering (scheme 3), assembly is studied at [NaCl] = 0mM, 50mM, 150mM and 500mM, by increasing the AuNP+ to VLP ratio at a constant VLP concentration of 25 μ g/ml of protein. Unlike the polymers, for which a mass ratio was the most accurate representation, the direct particle ratio of AuNP+ and VLPs is used for these studies. A well-defined onset point is desired, which is an indication of structural and thermodynamic control, indicating that no kinetic traps, intermediates or mixed systems are formed. Larger particles and assemblies are known to show a disproportionately strong DLS signal, as in Mie theory the scattering the signal strength is proportional to the square of the particle diameter. Therefore, the DLS data will directly reveal an onset of clustering as large particles are formed.

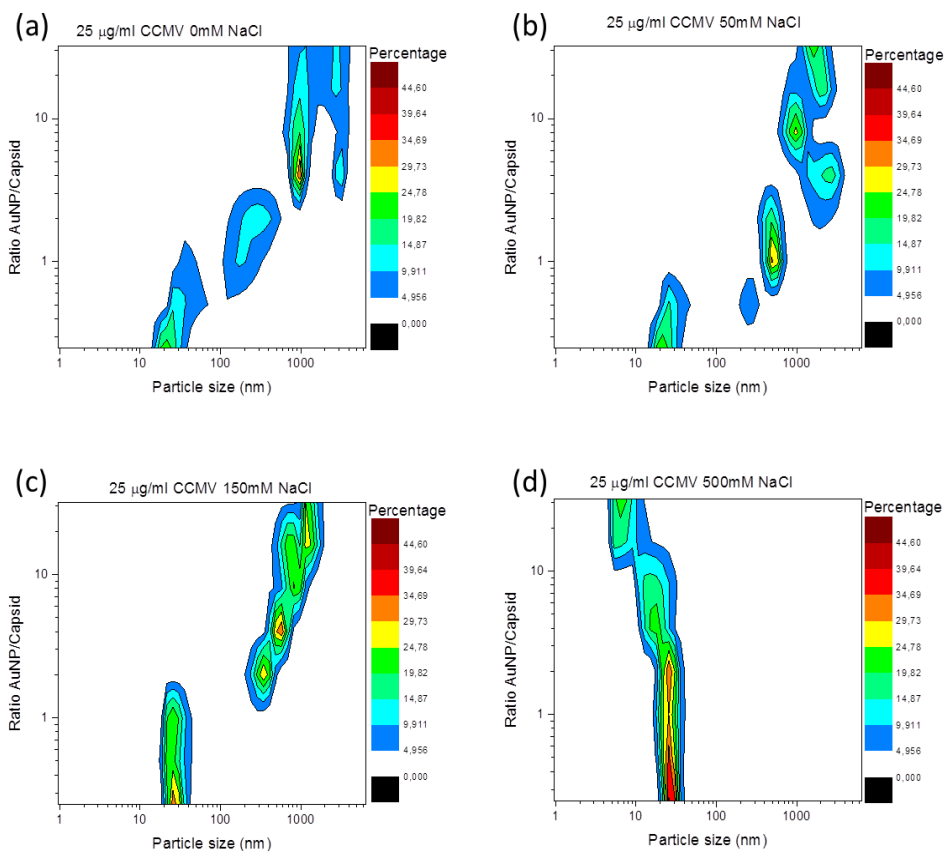


Figure 4: Contour plot of DLS (dynamic light scattering) intensities of T=3 CCMV at 25 $\mu\text{g/ml}$ of protein and increasing AuNP+ concentration at (a) $[\text{NaCl}] = 0 \text{ mM}$, (b) $[\text{NaCl}] = 50 \text{ mM}$, (c) $[\text{NaCl}] = 150 \text{ mM}$, (d) $[\text{NaCl}] = 500 \text{ mM}$.

Ultimately, the NaCl concentration enables control over the rate and degree of clustering, with more control or even a complete stop at higher concentrations of NaCl, as seen in figure 4. At $[\text{NaCl}] = 0 \text{ mM}$ and 50 mM clustering is initiated at a 1:1 ratio of AuNP+ to CCMV T=3 capsid, which rises to a 2:1 ratio at $[\text{NaCl}] = 150 \text{ mM}$ and cannot be determined for $[\text{NaCl}] = 500 \text{ mM}$, as no clustering was ever observed in assembly studies at $[\text{NaCl}] > 150 \text{ mM}$. In fact, as concentrations of AuNP+ are raised in the 500mM NaCl samples, the average size decreases due to the increased presence of more of the free AuNP+. The prevailing trend is an increasing initiation point and ultimate lack of clustering as the NaCl concentration increases. This is evidence that the binding interaction is reduced by electrostatic shielding, slowing down cluster formation. Slow formation should enable the growth of well-defined materials, thus an optimal control over the clustering exists at $[\text{NaCl}] = 150 \text{ mM}$, the highest concentration at which clustering is still readily observed in our studies. Additionally, at $[\text{NaCl}] = 150 \text{ mM}$ a well-defined onset point

is observed, with no intermediate sized or mixed states, further supporting the optimal control at this concentration.

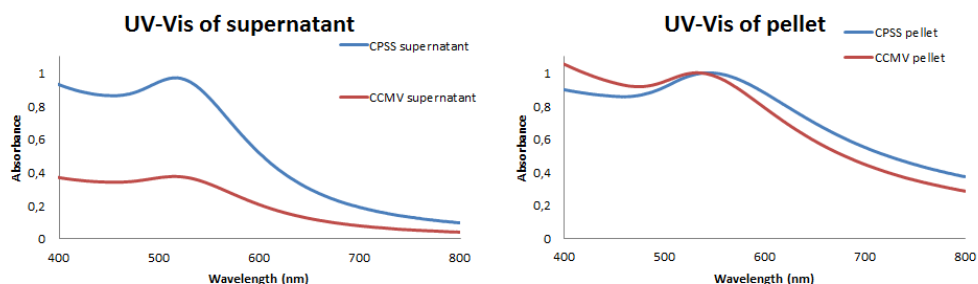


Figure 5: (left) UV-Vis spectrums of supernatant of AuNP+ and capsid assembling at $[NaCl] = 150$ mM at 16:1 particle ratio left for >48 hrs., with the gold plasmon peaks at $\lambda = 518$ nm. (right) UV-Vis spectrums of the pellet of AuNP+ and capsid assembling at $[NaCl] = 150$ mM and 16:1 particle ratio left for >48 hrs. with a plasmon peak of $\lambda = 532$ nm for saturated CCMV-AuNP+ clusters and $\lambda = 544$ nm for saturated CPSS-AuNP+ clusters.

At the onset point of 2 AuNP+ per capsid not all of the 60 binding sites are in use and potentially a greater density of AuNP+ could be achieved in the material. Indeed, to form a well-defined material the AuNP+ need to arrange themselves on the available electrostatic binding sites on the CCMV T=3 capsid in a symmetrical manner. Work by Kostianen et al. indicates that up to 24 nanoparticles could be theoretically packaged around a CCMV T=3 capsids. Each of the particles could potentially connect to one other capsid, allowing for a total of 12 bound AuNP+ per capsid. Still, only 8 bound AuNP+ per CCMV were found in their experimental results in clusters that have a crystalline AB_8^{fcc} structure.[12] Still this is far removed from the onset point at 2 AuNP+ per capsid observed in our investigations.

The structural ordering of the clusters could thus be further improved by additional AuNP+, which will help form a crystalline packing. In fact, all clustered samples show the formation of a soft pellet of precipitated material in the reaction tube after several hours as the clusters settle to the bottom. However, upon addition of 16 or more AuNP+ per CCMV T=3 capsid a pink supernatant remains, indicating the presence of free gold particles and the desired saturation of the T=3 binding sites. UV-Vis spectroscopy on the pink supernatant, see figure 5, reveals that 6 AuNP+ out of the initial 16 are left in the solution, using the $\lambda = 506$ nm absorbance of AuNP+.[20] 10 bound AuNP+ are thus included in the saturated pellets per CCMV T=3 capsid, close to the previous results on similar systems.[12] Essentially, despite saturation of the mixture, not all available binding sites are used.

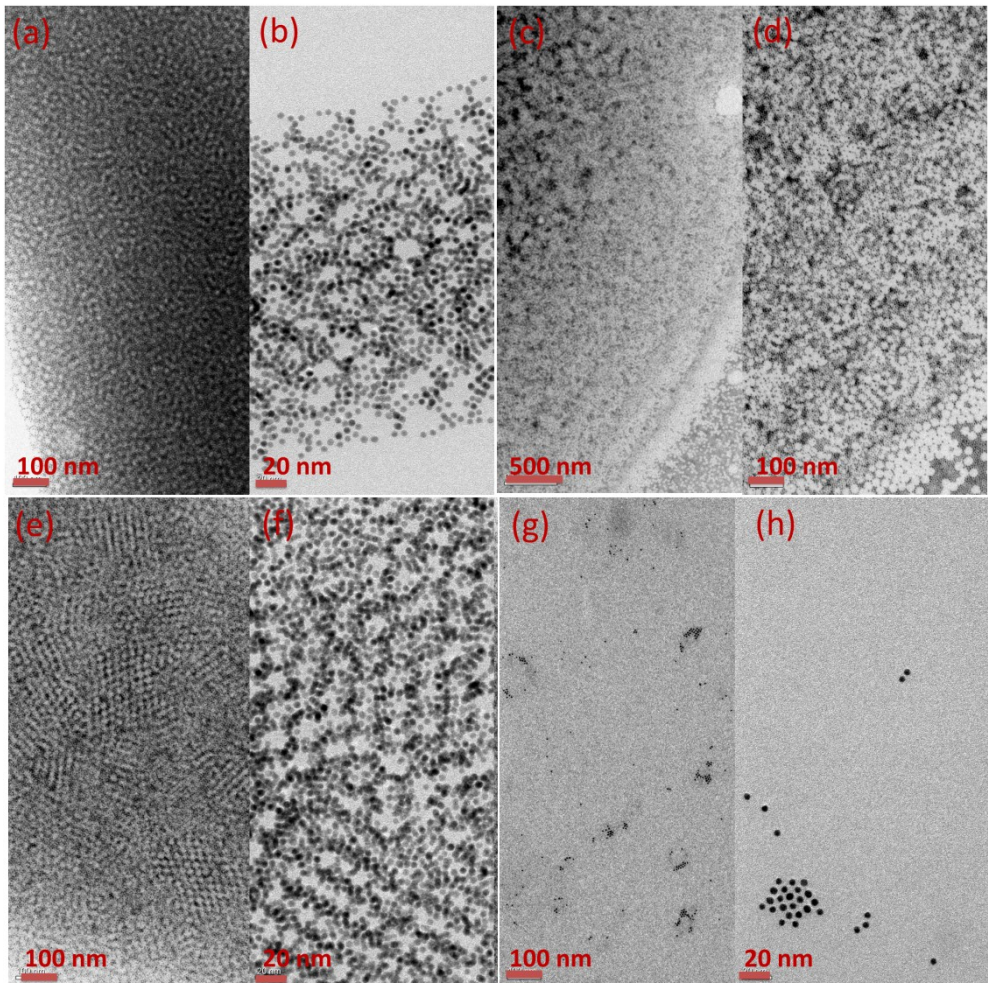


Figure 6: TEM images of: (a-f) Pelleted clusters containing 10 AuNP+ per capsid from an initial solution of T=3 CCMV at 25 μ g/ml of protein concentration and 16 AuNP+ per capsid at (a,b) [NaCl] = 0 mM, (c,d) [NaCl] = 50 mM, (e,f) [NaCl] = 150 mM, (g,h). Unclustered material from an initial solution of T=3 CCMV at 25 μ g/ml of protein concentration and 16 AuNP+ per capsid at [NaCl] = 500 mM.

Saturation does not necessarily promote an ordered structure, the effect of the ionic strength also needs to be taken into account. As such, the precipitated clusters, if any, formed from a saturated solution of 16 AuNP+ to 1 CCMV, were pelleted and separated from the supernatant containing free AuNP+. The redispersed pellets can subsequently be imaged in TEM and studied using SAXS. The resulting TEM images of the redispersed pellets, see figure 6, confirm the formation of clusters in [NaCl] = 0mM, 50mM and 150mM and the lack of

clustering in [NaCl] = 500mM samples. Furthermore, they show a trend of increasing organisation from random clustering at 0mM NaCl, to showing semi-crystalline steps at 50mM NaCl, and large multi-domain crystals at [NaCl] = 150 mM. All of this is in stark contrast to the [NaCl] = 500mM sample, where no pellet was formed, and as such no areas of clustering or even particle aggregation were observed.

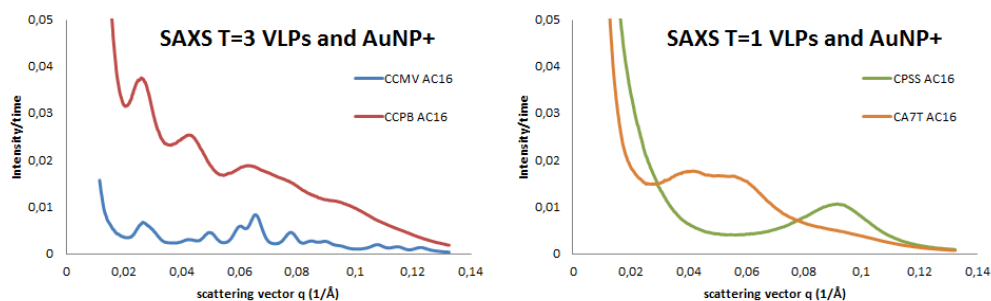


Figure 7: SAXS scattering profiles for (left) T=3 VLPs and (right) T=1 VLPs at [NaCl] = 150 mM. The native CCMV T=3 capsid shows clear (hkl)-reflections for (111), (220), (331), (333), (440), (600), (620), (640), (731) and (733), and the CCPB25 T=3 capsids follows this pattern, though with less ordering. The soft cored CPSS T=1 capsid shows only a single scattering peak, corresponding to an amorphous structure, though the hard core CA7T shows limited evidence of small crystalline domains of undetermined structure.

SAXS measurements (figure 7) on clusters on the CCMV T=3 Capsids also confirm the high degree of crystallinity observed in the [NaCl] = 150mM samples. The diffraction maxima shown are analogues to the AB_8^{fcc} structure reported by Kostianin et al. for similar systems.[8] Assuming this structure, the (hkl)-reflections for (111), (220), (331), (333), (440), (600), (620), (640), (731) and (733) can be readily identified. The high degree of crystallinity is likely due to the monodispersity of the native CCMV, with the final AB_8^{fcc} structure being derived from the symmetry of the capsid. These highly organised structures found in both the TEM and SAXS results were effectively predicted by DLS and UV/Vis data. Based on the combined DLS and UV/Vis measurements, the ideal ionic strength and particle saturation for cluster formation was determined. As both DLS and U/Vis for a single sample are considerably faster than either SAXS or TEM, this allows for fast screening of the ideal conditions for other VLPs.

²⁵ i.e. the T=3 VLP containing Prussian blue (PB)

Clusters in 3D

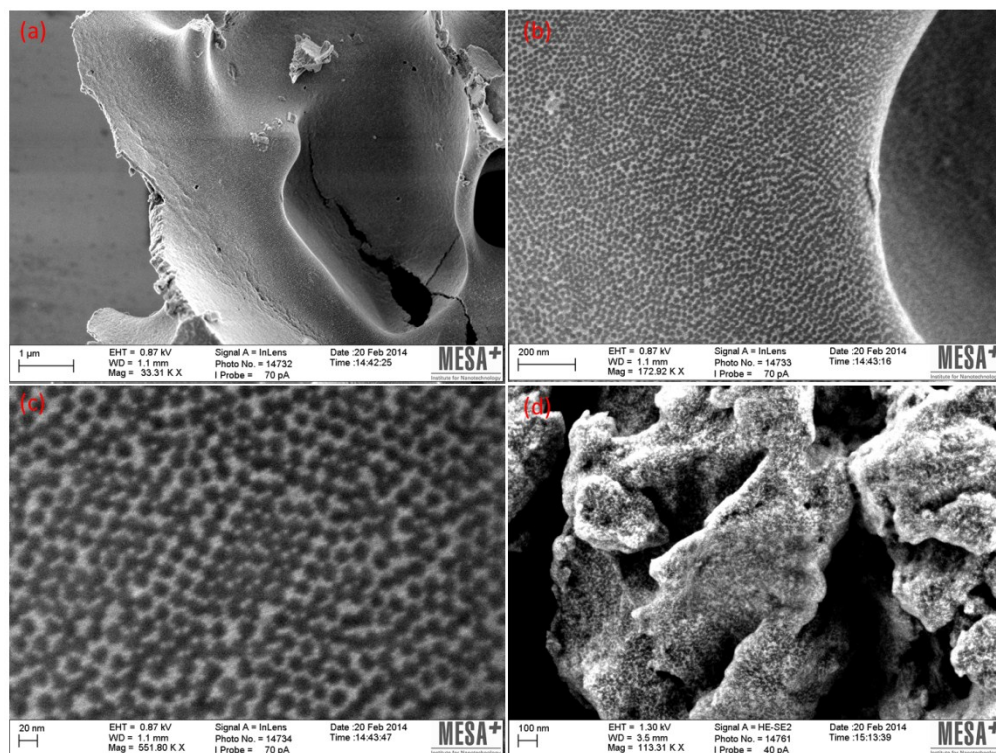


Figure 8: SEM images of freeze dried clusters for; (a,b,c) saturated CCMV T=3 capsid-AuNP+ clusters at $[\text{NaCl}] = 150 \text{ mM}$ at increasing magnification showing the contrast is given by the AuNP+, (d) saturated CCMV T=3 capsid-AuNP+ clusters at $[\text{NaCl}] = 150 \text{ mM}$ washed with milliQ after formation.

The DLS results indicate three dimensional clusters in the micron regime; however, the TEM images are from redispersed samples and allow only thin layers to be imaged. By freeze drying the clusters and imaging them using scanning electron microscopy (SEM) (figure 8a,b,c) the micron scale size of these clusters can be appreciated. The degree of organisation of the virus capsids quickly becomes evident from these images as crystalline domains can be seen on every part of the surface of CCMV T=3 capsid-AuNP+ clusters studied. Washing with milliQ water after cluster formation and precipitation disrupts these domains, see figure 10d, even without redispersion, showing the important role of ionic strength even after cluster formation.

T=1 clustering with AuNP+

Many VLPs do not conform to the native T=3 symmetry structure of CCMV and vary in size, and thus symmetry structure, which will affect the assemblies they can form. To study this 70kDa polystyrene sulphonate can be encapsulated to form the

CPSS T=1 capsid²⁶ and subsequently clustered, again allowing the optimal conditions for an organised structure to be determined by DLS and UV. The previous chapter reveals the interplay between VLP size and the binding of soft cationic macromolecules and as stated the AuNP+ are most similar to the PAMAM G3 dendrimers. Therefore, as is the case for PAMAM-G3, both T=3 and T=1 VLPs are expected to form clusters in a similar manner with AuNP+, with regards to clustering dynamics. A key difference is expected in the final organisation, with the 5 fold T=1 axis allowing no fcc organisation as described above.

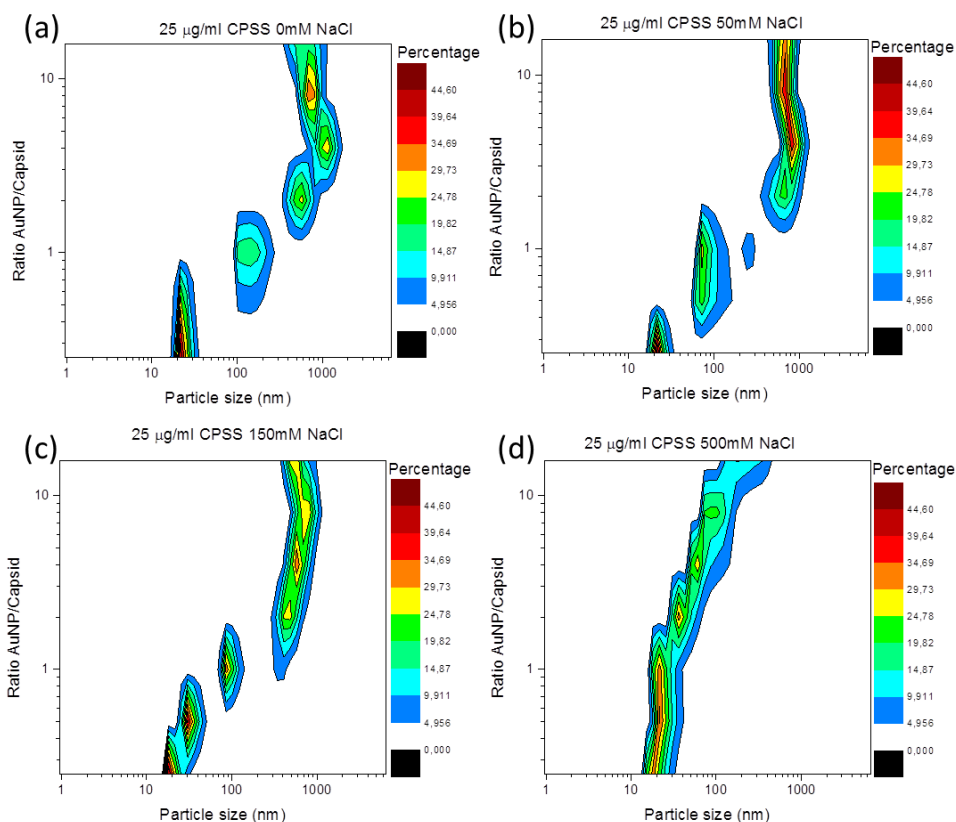


Figure 9: Contour plot of DLS intensities of T=1 CPSS at 25µg/ml of protein and increasing AuNP+ concentration at (a) [NaCl] = 0 mM, (b) [NaCl] = 50 mM, (c) [NaCl] = 150 mM, (d) [NaCl] = 500 mM.

DLS data (figure 9) at [NaCl] = 0 mM, 50 mM and 150 mM for the CPSS T=1 capsid confirm a similar trend of the T=1 VLPs compared to the CCMV T=3 capsid, with clustering being initiated at a 1:1 or 2:1 AuNP+ to capsid ratio. However, the results at [NaCl] = 500 mM are different, showing a slow growth of particle size as the

²⁶ For details on the encapsulation and characterisation, see chapter 4.

AuNP+ concentration increases, though not as dramatically as is the case for lower NaCl concentrations. Furthermore, unlike the T=3 capsids no clear onset point for clustering is observed at any concentration of NaCl, indicating little to no organised structures will be formed, with (kinetic) intermediate assemblies dominating instead.

Like for the T=3 VLPs, the T=1 binding sites are found on the threefold axis positions, i.e. 20 for the T=1 size symmetry structure. For the T=3 VLP, based on steric hindrance and electrostatic repulsion, one binding site is unused between the AuNP+.[12] Thus, if a clustered material based on a T=1 VLP follows the same limitations, only 8 binding sites for AuNP+ would be available per VLP, rather than 20. Each AuNP+ will be bound to one binding site on two different capsids, pointing to 4 bound AuNP+ for each T=1 VLP. Like the CCMV T=3 capsid, the CPSS T=1 capsid samples show precipitation for [NaCl] = 0 mM, 50 mM and 150 mM but also for [NaCl] = 500 mM. However, a pink supernatant, that indicates free gold nanoparticles and thus a saturated cluster, is only observed for samples with an AuNP+:capsid ratio of 16:1 or greater. Furthermore, the UV-Vis data (figure 5), for the [NaCl] = 150 mM clusters reveals that 10 AuNP+ per CPSS T=1 capsid are included in the saturated clusters, calculated from the AuNP+ absorption at $\lambda = 506$ nm.[20] As the T=1 binding sites are limited to 20 per capsid this indicates that all binding sites are used by the AuNP+ in a saturated sample if every gold nanoparticle is assumed to be shared by two capsids. This suggests that steric hindrance and electrostatic repulsion do not play such a significant role in the binding of AuNP+ to the T=1 VLPs, allowing for denser packing of particles.

The plasmon absorption band in gold nanoparticles is subject to shift upon the proximity of other gold nanoparticles and dependent on the inter-particle distance.[21] The difference in packaging density between the CCMV T=3 capsids and CPSS T=1 capsid can therefore be monitored by the plasmon wavelength shift of the AuNP+ peak absorption at $\lambda = 516$ nm. The redispersed pellets of a saturated CCMV T=3 Capsid-AuNP+ clusters (figure 5b) show a blueshift of the plasmon absorption band of $\Delta\lambda = 14$ nm. However, the redispersed CPSS T=1 Capsid-AuNP+ clusters (figure 5b) show a blueshift of the plasmon absorption band of $\Delta\lambda = 26$ nm, indicating a smaller inter-particle distance for the AuNP+ in the T=1 VLP clusters compared to that in the T=3 VLP, in support of the above hypothesis.

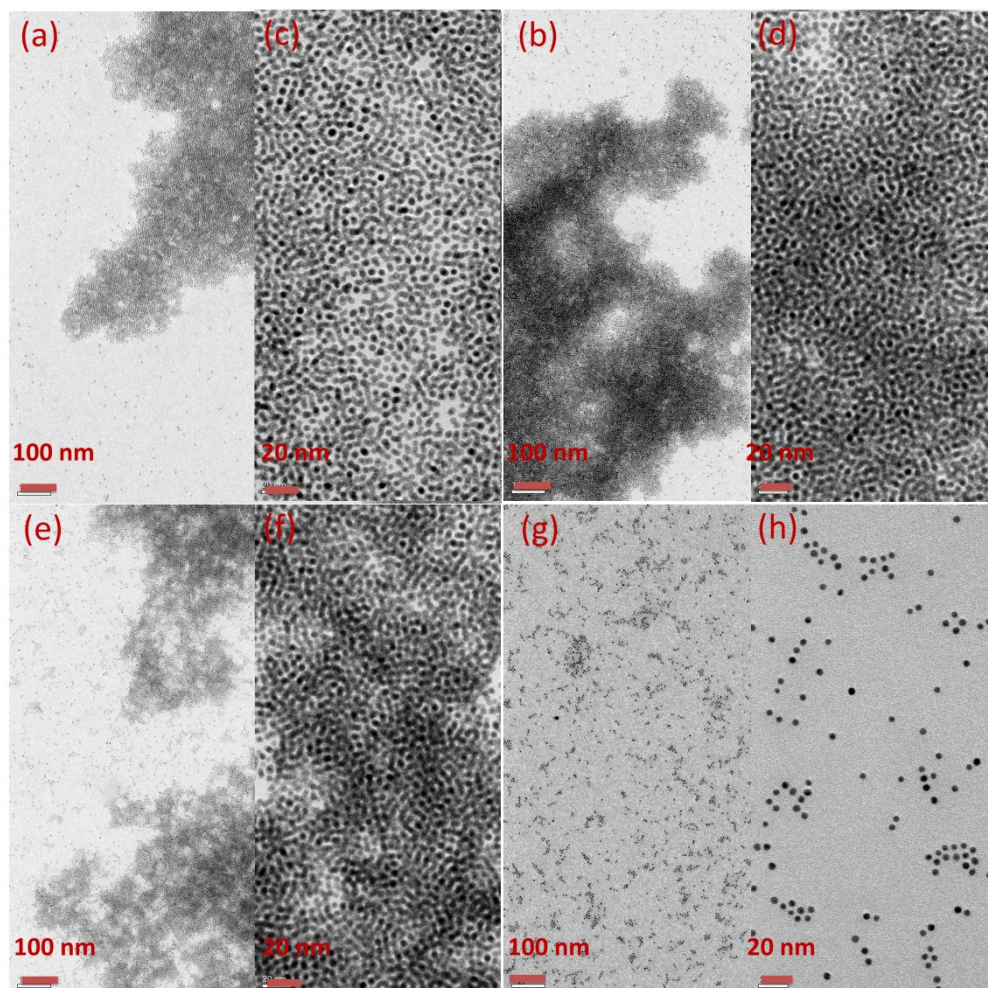


Figure 10: TEM images of pelleted clusters containing 10 AuNP+ per capsid from an initial solution of T=1 CPSS at 25 $\mu\text{g}/\text{ml}$ of protein concentration and 16 AuNP+ per capsid at (a,b) $[\text{NaCl}] = 0 \text{ mM}$, (c,d) $[\text{NaCl}] = 50 \text{ mM}$, (e,f) $[\text{NaCl}] = 150 \text{ mM}$, (g,h) $[\text{NaCl}] = 500 \text{ mM}$.

The unexpected dense packing of AuNP+ around the CPSS T=1 capsid should be reflected in the organisation of the capsid. As stated, to organise 10 AuNP+ per VLP around a T=1 capsid in a cluster, with each AuNP+ being bound by two binding sites from two different capsids, requires the use of all 20 binding sites. The only way to then symmetrically arrange other capsids around the CPSS T=1 capsid is to make use of the inherent 5-fold symmetry in the T=1 capsid. This suggests that no crystalline packaging of material can take place and at best a pseudo crystalline 5-fold symmetry crystal can be expected. To confirm this, the precipitated material of the AuNP+ saturated CPSS T=1 capsid samples can be redispersed and imaged using

TEM (figure 10) in a similar manner to the AuNP+ saturated CCMV T=3 samples described above. The resulting images show no evidence of crystalline packaging for [NaCl] = 0 mM, 50 mM and 150 mM. They do seem to show a locally organised mosaic of dark AuNP+ on 10 to 20 nm length scales, comparable to the T=1 VLPs 18 nm diameter. Surprisingly, despite DLS evidence suggesting assembly, the [NaCl] = 500 mM samples show no evidence of clustered material in TEM.

The lack of crystallinity is confirmed by SAXS measurements (figure 7) on clusters of the CPSS T=1 VLPs. Due to the relative electron density of the materials, the scattering of the AuNP+ will dominate, as such revealing their lack of large scale organisation. The single scattering maximum at $q_{\max} = 0.091 \text{ \AA}^{-1}$ corresponds to an average centre-to-centre distance of 6.9 nm, supporting the idea of a close packing of AuNP+ around these VLPs with no large scale order. Most likely, the local mosaic pattern of the AuNP+ seen in TEM is the result of the symmetrical distribution of AuNP+ around a single capsid, but no evidence for quasi crystalline packing was found.

Cluster dynamics

The differences in the AuNP+ density in saturated clusters of CPSS T=1 and CCMV T=3 VLPs suggest a different affinity for AuNP+ between the two VLPs, pointing to different formation dynamics, with faster assembly for the more densely packed T=1 VLPs. To study this, the cluster formation in saturated clusters of CPSS T=1 and CCMV T=3 VLPs can be monitored over time using DLS and UV-Vis.

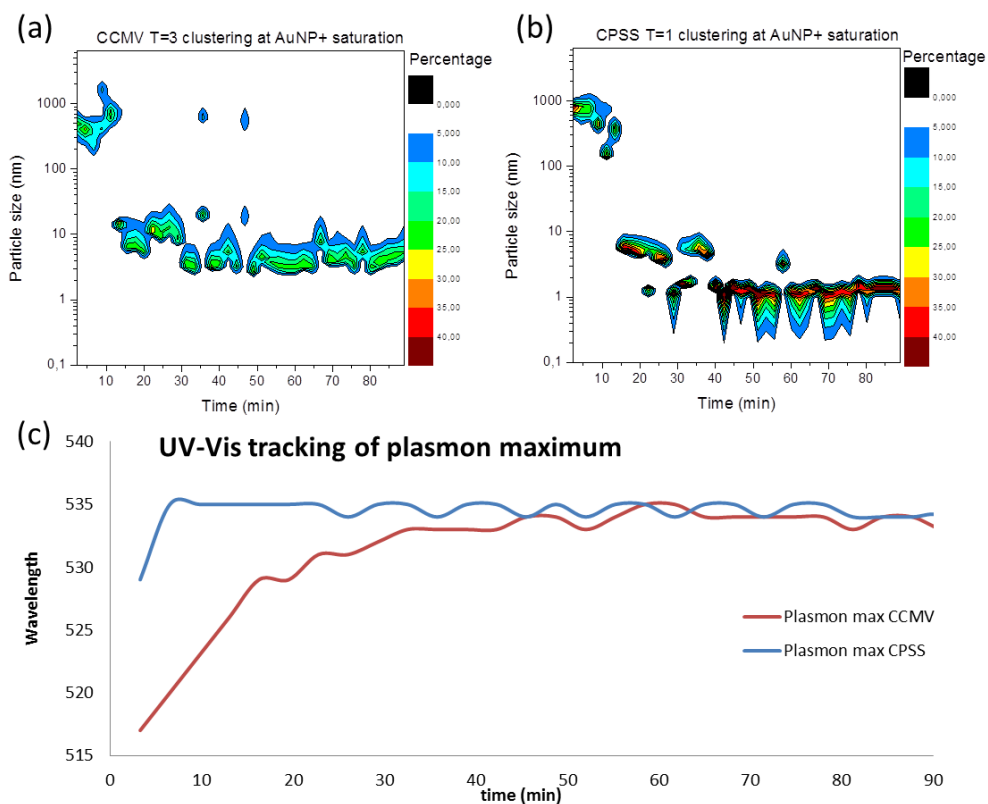


Figure 11: (a) Contour plot of DLS intensities of clusters assembly over time, formed by CCMV T=3 capsid and AuNP+ at $[NaCl] = 150$ mM, at a starting concentration at time=0 of $25\mu\text{g/ml}$ of protein and 10:1 AuNP+ to capsid ratio. (b) Contour plot of DLS intensities of clusters assembly over time, formed by CPSS T=1 capsid and AuNP+ at $[NaCl] = 150$ mM, at a starting concentration at time=0 of $25\mu\text{g/ml}$ of protein and 10:1 AuNP+ to capsid ratio. (c) Plasmon maximum over time for the CPSS and CCMV clusters in (a) and (b). The precipitation in the DLS indicates the formation of large clusters, although only the remaining (small) particles in solution are detected.

The dynamics (figure 11) of both the T=1 and T=3 clusters is studied using solutions at the saturation point of 10 AuNP+ per T=3 VLP and 10 AuNP+ per T=1 VLP. The CCMV T=3 capsid shows some initial growth from 500nm to 1000nm clusters and drops back down to the AuNP+ level after 20 minutes. The CPSS T=1 capsid shows no growth over the timescale measured and drops to AuNP+ levels within 15 minutes before dropping to noise levels after 30 minutes. The loss of large size clusters in the solution is attributed to a loss of signal from material visibly precipitating, with the DLS probe measuring only the top layers of the solution.

More importantly, as expected, the T=3 particles seem to have slightly slower dynamics, allowing more time for cluster formation before precipitation thereof.

This difference in dynamics is more apparent for changes in the plasmon maximum measured by UV-Vis absorption, caused by AuNP-AuNP proximity and the resulting plasmon coupling upon clustering. The plasmon wavelength shifts slowly to the blue for the CCMV T=3 VLP and starts near the maximum for the CPSS T=1 VLP, with both reaching a final shift of $\Delta\lambda=18$ nm in this timeframe. This again confirms the faster dynamics for the T=1 VLP compared to the T=3 VLP. Additionally, the measured blueshift of the T=1 VLP clusters for the first 90 minutes is less than the $\Delta\lambda=26$ nm blueshift for the suspended clusters (figure 5b). This could result from the rapid precipitation of material, with kinetically trapped states that do not yet have the dense VLP packaging, but will mature over time.

The combined DLS and UV-Vis data confirms the faster assembly of the T=1 VLP compared to the T=3 VLP. This suggests stronger interaction, i.e. less reversible, between AuNP+ for the T=1 VLP compared to the T=3 VLP. As seen for soft macromolecules in the previous chapter, these differences might result from the changing nature of the binding site, with the AuNP+ being trapped and locked in the grooves on the T=1 surface.

Competition for AuNP+ with T=1 and T=3

The time dependent data shows faster clustering for the T=1 VLPs compared to the T=3 VLPs, however, the T=1 does not show immediate formation of the densest packing. This suggests that whilst the initial binding might be stronger, the T=1 VLP bound AuNP+ are still dynamic and rearrangements are possible until the system is matured. A competition experiment between the CCMV T=3 and CPSS T=1 VLPs, mixing equal molar amounts of VLP will show if the AuNP+ have any initial preference for either VLP, and indicate differences in binding affinity.

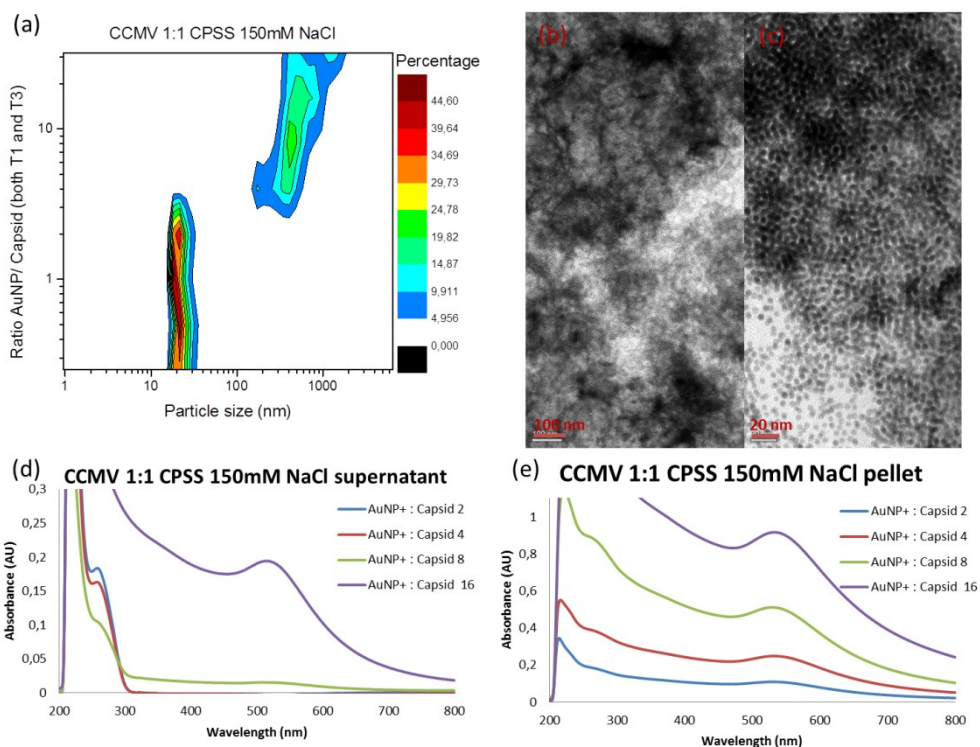


Figure 12: (a) DLS for a 1:1 molar ratio mixture of CPSS T=1 VLPs and CCMV T=3 VLPs at 25 μ g/ml of CCMV with increasing AuNP+. (b,c) TEM images of the redispersed pellet for 1:1 CPSS T=1 capsids and CCMV T=3 capsids at 25 μ g/ml of CCMV and AuNP+; (d) UV-Vis spectrum of the supernatant of mixed clusters at given AuNP+ ratio, showing a steadily decreasing $\lambda = 260$ nm absorption until the sample is saturated (at 16 AuNP+); (e) UV-Vis spectrum of the supernatant of mixed clusters at given AuNP+ ratio, showing a plasmon max of $\lambda = 531$ nm (AuNP+: capsid 2), $\lambda = 532$ nm (AuNP+: capsid 4), $\lambda = 531$ nm (AuNP+: capsid 8) and $\lambda = 532$ nm (AuNP+: capsid 16).

DLS shows that, at 150mM and a 1:1 molar ratio between the CCMV T=3 and CPSS T=1 VLPs, clusters are formed at a similar point compared to pure VLPs, with a sharp onset point. Over time precipitates form in these samples, so both the pellet and supernatant can be characterised using UV-Vis spectroscopy. The UV-Vis spectrum of the supernatant of these samples (figure 12d) shows a steady decrease in the 260nm concentration. This can be contributed to a reduction in the RNA absorption of the CCMV T=3 VLPs (figure 2f), which has a far greater extinction coefficient than the CPSS T=1 VLPs ($\epsilon_{260,ccmv} = 2.78 \cdot 10^7 \text{ M}^{-1}\text{cm}^{-1} > \epsilon_{260,cpss} = 1.29 \cdot 10^6 \text{ M}^{-1}\text{cm}^{-1}$). In fact, the proportional decrease suggests that around half of the clustered capsids would be from either VLP, thereby ruling out any selectivity by

the AuNP+. This finding is also reflected in the UV-Vis spectrum of the pellet (figure 12d) which shows a plasmon shift of around $\Delta\lambda = 14$ nm for all samples, similar to CCMV T=3 clusters, indicating the densely packed structure of the CPSS T=1 VLP clusters is not formed. To elucidate the exact structure of the clusters, more experiments are needed.

Electrostatic release of AuNP+ from cluster

An advantage of using biological systems is often seen in the dynamic interactions that allow materials to form, break down and reform differently. If VLP based materials, being potentially highly modular, could benefit from such dynamic rearrangement, it allows the formation of many structures with only a limited set of re-usable building blocks. The first step in this is reversibility, and, fortunately, electrostatic interactions are generally reversible, as by altering the pH or ionic strength the charges can be screened or altered.

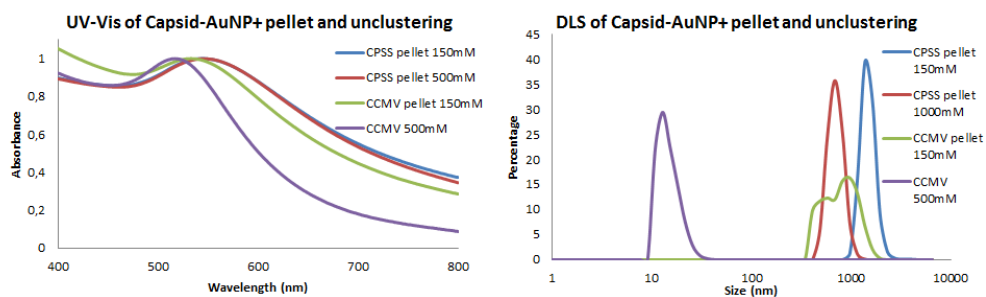


Figure 13: (left) UV-Vis spectra, and (right) DLS data of pellets from CCMV T=3 and CPSS T=1 capsid-AuNP+ clusters at [NaCl] = 150 mM and subsequent redispersion at [NaCl] = 500 mM or 1000 mM.

To study this electrostatic reversibility CCMV T=3 and CPSS T=1 capsid-AuNP+ clusters are formed at 150mM and subsequently redispersed at [NaCl] = 500 mM or 1000 mM. As seen in figure 4d, the CCMV T=3 capsid has no ability to cluster at [NaCl] = 500 mM, therefore, the formed clusters could be disassembled. DLS measurements (figure 13) on the CCMV T=3 capsid show the loss of the large aggregates upon redispersion in a 500mM NaCl buffered solution. This is confirmed by UV-Vis spectroscopy (figure 13) in which the $\Delta\lambda = 14$ nm plasmon shift of the pellet disappears. This electrostatic release makes the CCMV T=3 capsid of interest for the creation of dynamic materials, that are responsive to ionic strength.

Conversely, CPSS T=1 VLP-AuNP+ clusters shows no disassembly even if the NaCl concentration is increased to 1000 mM, which is confirmed by a conservation of the $\Delta\lambda = 26$ nm blueshift of the plasmon band. These observations also point to stronger binding of the AuNP+ to the CPSS T=1 capsid.

Clustering of hard materials inside the capsid

The core of a virus like particle has a well-studied effect on the size and thus symmetry structure; however, these still obey the Caspar-Klug symmetry laws for spherical viruses. As seen in the previous chapter, for soft polymer clustering agents the symmetry structure seems dominant in the clustering behaviour with the core merely dictating the size, and thus symmetry structure, of the VLP. For hard metal nanoparticles a similar effect is expected. To test this, clusters of T=3 CCPB, formed by biomineralisation of Prussian blue in an empty CCMV capsid, and CA7T T=1 VLPs, containing a 7 nm gold particle core, were formed and analysed by DLS, UV-Vis and SAXS.

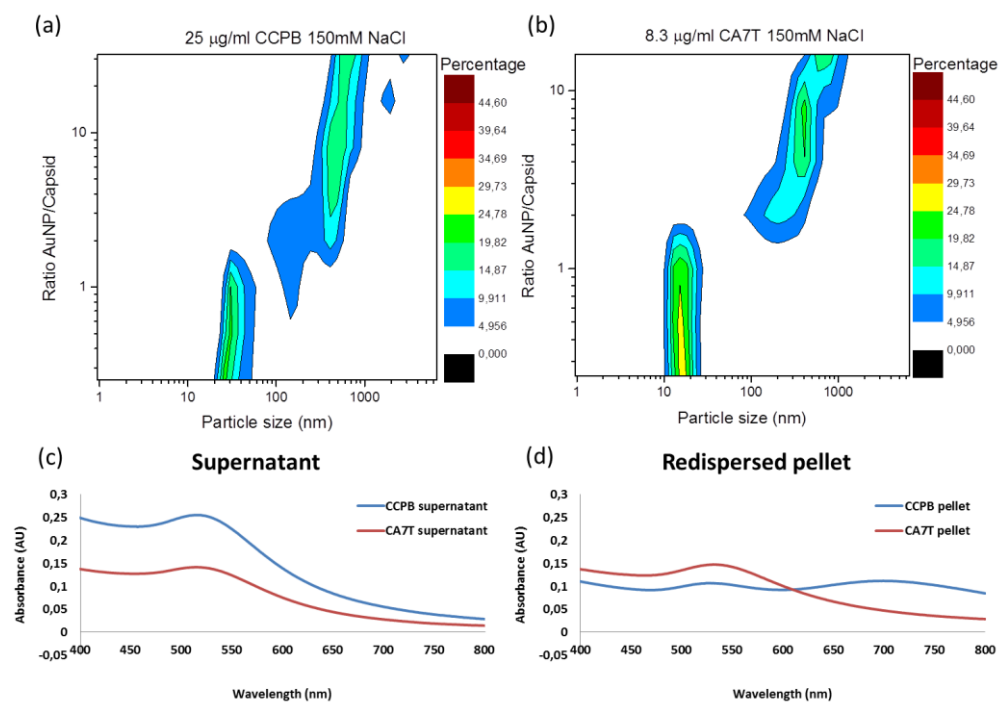


Figure 14: (a) DLS for an estimate of 25 $\mu\text{g/ml}$ CCPB T=3 capsids with increasing AuNP+; (b) DLS for 8.3 $\mu\text{g/ml}$ CA7T T=1 capsids with increasing AuNP+ (c) UV-Vis spectra of supernatant of AuNP+ and capsid clustering at [NaCl] = 150 mM and 16:1 particle ratio after >48 hrs., with the gold plasmon peaks at $\lambda = 516$ nm. (d) UV-Vis spectra of pelleted VLP- AuNP+ clusters at [NaCl] = 150 mM, after >48 hrs., with a plasmon peak of $\lambda = 531$ nm for both the CCPB T=3 capsid and CA7T T=1 capsid.

The DLS results (figure 14 a and b) show clustering behaviour for CCPB T=3 capsids and CA7T T=1 capsids that is comparable to the CCMV T=3 and CPPS T=1 capsids,

respectively (see above). Similarly, the UV-Vis spectra of the supernatant of the samples (figure 14c) shows a spectrum dictated by the free AuNP+. As with the supernatant UV-Vis of the soft cored VLP-AuNP+ clusters, seen in figure 5, the number of AuNP+ that must be in the cluster can be determined. The CA7T T=1 capsids-AuNP+ clusters show 10 AuNP+ per capsid, just like the CPSS T=1 capsid-AuNP+ clusters did, again showing a full coverage of all possible binding sites. However, the CCPB T=3 capsid AuNP+ clusters show only 7 AuNP+ per capsid. This decrease, however, is most likely due to the inability to accurately determine the exact concentration of the CCPB using spectroscopy, instead relying on the capsid protein concentration present before biomineralisation of the core.

The hard cored capsid-AuNP+ clusters found in the pellet (figure 14d) should show plasmon peak shifts similar to the soft cored capsid-AuNP+ clusters as the AuNP+ particle proximity would be similar. The CCPB T=3 capsid-AuNP+ clusters indeed shows a peak for both AuNP+ ($\lambda = 531\text{nm}$) and Prussian blue ($\lambda = 700\text{ nm}$), with the AuNP+ plasmon absorption having a blueshift of $\Delta\lambda = 13\text{ nm}$ comparable to the CCMV T=3 capsid-AuNP+ clusters. Yet, the plasmon peak for the CA7T T=1 capsid-AuNP+ clusters also shows a blueshift of merely $\Delta\lambda = 13\text{ nm}$, instead of the $\Delta\lambda = 26\text{ nm}$ found for the CPSS T=1 capsids-AuNP+ clusters. This can be caused by the gold nanoparticle inside the capsid, that can alter the plasmon coupling of the surrounding gold particles due to its own inherent plasmon generated dipole. Even so, it is surprising that this leads to a reduction of the blue shift, rather than a further blue shift of the plasmon band absorption. More experiments are needed to identify the origin of this observation.

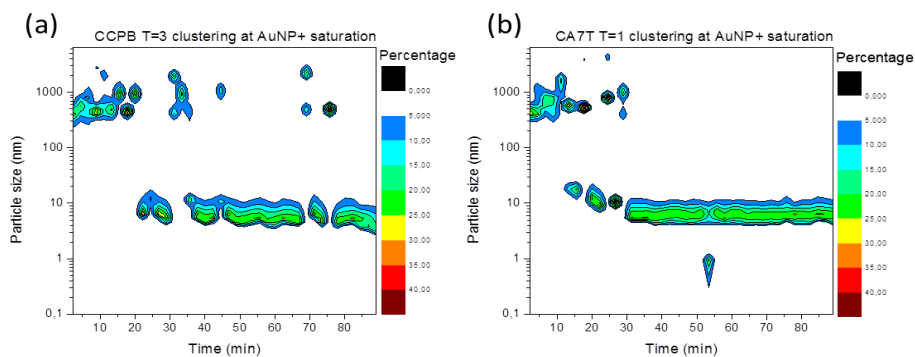


Figure 15: (a) Particle size by DLS of clusters, formed by CCPB T=3 capsid and AuNP+ at $[\text{NaCl}] = 150\text{ mM}$, over time at a starting concentration at time=0 of $25\text{ }\mu\text{g/ml}$ of protein and 101 AuNP+ to capsid ratio; (b) Particle size by DLS of clusters, formed by CA7T T=1 capsid and AuNP+ at $[\text{NaCl}] = 150\text{ mM}$, over time at a starting concentration at time=0 of $8.3\text{ }\mu\text{g/ml}$ of protein and 10:1 AuNP+ to capsid ratio.

Furthermore, DLS studies on the formation of clusters over time (figure 15c,d) show the same clustering dynamics for CCPB T=3 and CA7T T=1 capsids as the CCMV T=3 and CA7T T=1 capsids respectively, using the same particle ratio's. Like their soft cored equivalents, the hard cored particles reveal a slightly faster clustering for the T=1 capsid. Tracking of the plasmon shift by UV-Vis spectroscopy for these clusters is however not possible, as no accurate correction for the absorption of the encapsulated 7nm AuNP or Prussian blue can be applied.

SAXS measurements (figure 7) on clusters on the CCPB T=3 hard cored capsids show results comparable to the native CCMV T=3 capsid. Though the peaks are heavily broadened compared to the CCMV T=3 capsid, the CCPB T=3 capsids scattering profile still suggests the AB_8^{fcc} structure. Unlike the CPSS T=1 capsid, the hard cored CA7T T=1 capsid does show evidence for a limited crystalline structure in its scattering profile. The domain size for these clusters is, however, likely less than 100nm, each domain consisting of only a few dozen VLPs at most. Still, it is likely that, with more careful control over the clustering conditions, predominantly ionic strength and particle concentration, a more pronounced crystallinity is possible for both hard cored particles. This can be attributed to the strong stabilising effect these particles have upon the VLP structure (see chapter 3) resulting in capsids that are more rigid, monodisperse, and show little to no dynamic rearrangement of pentameric or hexameric capsomer subunits. Furthermore, these results suggest that hard cored non-native VLPs are in principle capable of forming crystalline structures. This opens up many opportunities in making biohybrid systems by variation of the core composition, or indeed variation in the cationic clustering inducing particle.

Conclusion

The clustering of CCMV based VLPs using cationic gold nanoparticles is studied in this chapter. Both the CCMV T=3 and CPSS T=1 capsids form clusters at $[NaCl] \leq 150mM$, with the CCMV T=3 clusters being reversible at $[NaCl] > 500 mM$. This effect is likely due to a denser packing of the AuNP+ in the CPSS T=1 cluster-AuNP+ that shows full coverage of AuNP+ on all potential electrostatic binding sites as shown by UV-Vis absorbance. While the larger blueshift of the plasmon absorbance band of $\Delta\lambda = 26 nm$ points to small AuNP-AuNP distances. This is in contrast to the CCMV T=3 capsid-AuNP+ clusters that showed a only 10 AuNP+ per capsid, filling only a third of the potential binding sites and having a blueshift of the plasmon absorbance band of only $\Delta\lambda = 14 nm$. Additionally, known VLPs with a hard nanoparticle or crystalline interior were also shown to behave similarly to their soft cored counterparts of similar size and symmetry structure with regards to

clustering dynamics and stoichiometry. Furthermore, the CCPB T=3 capsid is found to form the same AB_8^{fcc} crystalline structure as the native CCMV T=3 capsid. The hard cored CA7T T=1 capsid also shows evidence of limited crystallinity, unlike its soft cored CPSS T=1 counterpart. This is attributed to the strong templating effect that the hard cores have upon the VLP structure. It should be noted, however, that optimization of these systems is still required.

These results offer the framework for creating binary nanoparticle systems with tuneable properties by altering the core content of the capsid, mixing different cored VLPs or changing the cluster inducing cationic nanoparticle. Such structures would form predictable structures depending only on the virus symmetry, provided the core provides a sufficiently rigid template, which will in turn allow a detailed study on the physical properties of such systems. Though each of these biohybrid structures would require fine tuning of the exact stoichiometric ratios and ionic strength, overall the same general design principles will apply. As a wide range of different core options are already available for CCMV based VLPs future work will thus allow for the creation of complex biohybrid architectures, with potential application in the next generation optical, electronic and other functional nanodevices.

Experimental

Most experimental techniques are similar to those found in chapter 4, however, due to differences in sample nature, slight variations were made on occasion and as such these altered techniques are again detailed below in a similar manner to chapter 4.

Cationic gold nanoparticle synthesis and ligand exchange

Thiol-stabilised AuNP were synthesised using a variation of the classical Brust-Schiffrin method as described by Goubet et al, as seen in figure 1.[19] In short, 0,25mmol of Chloro (triphenylphosphine) Gold ($Cl(Phen)_3Au(I)$, $m_w=494.71$, 123.93mg) and 500 μ l of dodecanethiol ($CH_3(C_{10}H_{20})CH_2SH$, $m_w=202.40$) were dissolved in 25ml of toluene and heated to 100°C. A separate solution of ammonia-borane (NH_3BH_3 , $m_w=37,83$, 9.45 mg) in 5ml of ethanol and 10ml of toluene was prepared and also heated to 100°C before addition to the gold containing solution. The mixture was stirred at 100°C for 10 minutes and turned dark red in colour, that indicated successful formation of the gold nanoparticle, before being allowed to cool to room temperature. Solvents were removed by rotary evaporation and the resulting dark powder was washed twice with 20ml of ethanol and precipitated using light centrifugation (5 minutes, 5krpm in an eppendorf 5804 centrifuge). The purified powder was resuspended in 10ml of toluene and ultrasonicated for 30

minutes before being again centrifuged (5 minutes, 5krpm in an eppendorf 5804 centrifuge) to remove larger particles and impurities. The resulting particles showed good monodispersity and long term stability.

Modification on these particles was achieved by a ligand exchange process to introduce quaternary ammonia groups on the surface of the particles. To this end, 0.1mmol of 11-mercapto undecyl trimethylammonium bromide ($\text{HSCH}_2(\text{C}_{11}\text{H}_{20})\text{N}(\text{CH}_3)_3\text{Br}$, $m_w=326.38$, 34.065mg) in 1ml of milliQ (H_2O , 18.2M Ω) was added to 1ml of the AuNP solution in toluene and left stirring overnight. To aid phase separation a few drops of diluted hydrochloric acid (HCl, 1M in milliQ) can be added after which the aqueous layer now containing the modified AuNPs was collected and stored. The resulting particles retain their monodispersity around 4.7nm in TEM and a hydrodynamic radius around 9nm in DLS with a plasmon absorbance maximum at 518nm in milliQ.

VLP synthesis

CCMV was isolated from infected plant material according to methods adapted from Verduin et al and described in the previous chapters.[22] The CPSS and CA7T T=1 VLPs were synthesised as described in the previous chapter. CCPB T=3 VLPs were synthesised using biomineralisation of Prussian blue according to a previously developed procedure, with a brief description given below.[23]

To synthesize Prussian blue in the CCMV capsid a precursor solution of $\text{Fe}^{\text{III}}(\text{C}_2\text{O}_4)_3^{3-}$ and $\text{Fe}^{\text{III}}(\text{CN})_6^{3-}$ is prepared from ammonium iron(III) oxalate ($(\text{NH}_4)_3[\text{Fe}^{\text{III}}(\text{C}_2\text{O}_4)_3]$) and potassium ferricyanide ($\text{K}_3\text{Fe}^{\text{III}}(\text{CN})_6$). 1.0 gram of $\text{K}_3\text{Fe}^{\text{III}}(\text{CN})_6$ (6mmol) was added to 2.6g of $(\text{NH}_4)_3[\text{Fe}^{\text{III}}(\text{C}_2\text{O}_4)_3]$ (3mmol) and dissolved in 3ml of milliQ. The solution was heated to 40°C and stirred for 40 minutes, allowing a precipitate to form. The solution was cooled to room temperature and left in the dark for 2 hours, after which the precipitate was filtered, yielding a 1M precursor stock solution of $\text{Fe}^{\text{III}}(\text{C}_2\text{O}_4)_3^{3-}$ and $\text{Fe}^{\text{III}}(\text{CN})_6^{3-}$.

Empty T=3 CCMV capsids were formed from CCMV coat protein dimers by dialysing to an aqueous pH5 buffer (0.5M NaCl, 50mM sodium acetate, 1mM NaN_3). One aliquot of the precursor solution was added to nine aliquots of this capsid solution such that the final concentration of precursors was 0.1 M. Subsequently the solution was placed in a 4°C fridge and irradiated for 2 days using a 200W lamp to photo reduce the $\text{Fe}^{\text{III}}(\text{C}_2\text{O}_4)_3^{3-}$ and form Prussian blue both inside and outside the capsid. The unencapsulated material precipitates rapidly and can be removed by low speed centrifugation (10 minutes at 5krpm on an Eppendorf 5415 R centrifuge) to yield a clear dark blue solution of CCPB.

Clustering Procedure

Sample solutions are prepared fresh from VLP stock solutions, at a known protein concentration (generally around 0.5mg/ml), in 0 mM or 50 mM NaCl cluster buffer solution (10mM sodium acetate, 1 mM EDTA, 1mM NaN₃, pH5.0) and 0.434 μ M of AuNP+ stock solution in milliQ. First, an aliquot of the VLP stock solution is diluted by addition of further cluster buffer solution. Then, the ionic strength is adjusted by addition of 1 M NaCl cluster buffer. Finally a small volume of the AuNP+ solution is added such that the final concentrations and particle ratios are as desired.

TEM microscopy

Samples were taken from a freshly made sample solution allowed that are left to equilibrate into clustered or unclustered states for 10 minutes on a shaking platform or roller bank after mixing. For clustered samples, low speed centrifugation (10 minutes at 2krpm on an Eppendorf 5415 R centrifuge) is used to precipitate the pellet after which the supernatant was removed and the pellet redispersed in a small amount (10-20 μ l) of buffer. The TEM samples were prepared by leaving 5 μ l of this sample solution on a formvar carbon coated copper grid for 5 minutes and subsequently removing it by tipping the grid onto low lint paper (Kimtech science precision wipes). Stained samples use 5 μ l of a 1% Uranyl Acetate solution which was removed after 30 seconds to provide optimal contrast. Samples were imaged using a Philips CM300ST-FEG TEM.

UV/Vis

UV-Visible samples are prepared from 500 μ l or 1000 μ l fresh sample solutions. If separation between pellet and sample is desired the 500 μ l samples are centrifuged at 5krpm (Eppendorf centrifuge 5451 R). After this 450 μ l of supernatant is removed and the pellet, if any, is redispersed by adding 950 μ l of buffer. All solutions were measured in a 1cm quartz cuvette in a PerkinElmer Lambda 850 UV/VIS Spectrometer.

DLS

Dynamic light scattering samples were prepared from 500 μ l fresh sample solutions and allowed to equilibrate for 2 minutes on a roller bank after mixing. Salt concentrations were controlled by using stock solutions of 0M and 1M NaCl containing clustering buffers (10mM sodium acetate, 1 mM EDTA, 1mM NaN₃, pH5.0) and in all cases the AuNP+ solution is added last. Each sample is measured five times for 120 seconds using an Anaspec nanotrack wave dynamic light scattering instrument with the best of these five measurements selected. For single VLPs, which are approximately spherical, the particle size can be seen to represent the diameter.

SAXS

Concentrated samples (>0,5mg/ml of protein after redispersion of pellet) of VLPs and AuNP+ at the desired stoichiometric ratio were prepared and allowed to incubate for at least 12 hours, allowing a precipitate to form. The resulting solutions were subjected to low speed centrifugation to condense the precipitate. After carefully removing the supernatant the pellet was redispersed in 20µl of buffer solution. 10µl of the redispersed pellet was sealed between two layers of capton foil so that it completely filled the cavity of a hollow stainless steel ring.

Samples were measured at the department of Applied Physics at Aalto University according to the following procedure: [24]

“The liquid samples were sealed between two capton foils during the SAXS measurements and the sample environment was evacuated to reduce scattering from air.

The SAXS was measured using a rotating anode Bruker Microstar microfocus X-ray source (Cu K_α radiation, 1.54 Å). The beam was monochromated and focused by a Montel multilayer focusing monochromator (Incoatec). The X-ray beam was further collimated by a set of four slits (JJ X-Ray) resulting in the final spot size of less than 1 mm at the sample position.

The scattered intensity was collected using a Hi-Star 2D area detector (Bruker). Sample-to-detector distance was 1.59 m and silver behenate standard sample was used for calibration of the length of the scattering vector q . One-dimensional SAXS data were obtained by azimuthally averaging the 2D scattering data. The magnitude of the scattering vector q is given by $q = 4\pi \sin \theta / \lambda q$, where 2θ is the scattering angle.” - [24]

Bibliography

1. Xu, L., et al., *Nanoparticle assemblies: dimensional transformation of nanomaterials and scalability*. Chemical Society Reviews, 2013. **42**(7): p. 3114-3126.
2. KHANNA, S.N. and D.A. TOMALIA, *IN QUEST OF A SYSTEMATIC FRAMEWORK FOR UNIFYING AND DEFINING NANOSCIENCE*. Modern Physics Letters B, 2014. **28**(03): p. 1430002.
3. Shevchenko, E.V.T.D.V.K.N.A.O.B.S.C.B., *Structural diversity in binary nanoparticle superlattices*. 2006, Nature Publishing Group. p. 55-59.
4. Glotzer, S.C. and M.J. Solomon, *Anisotropy of building blocks and their assembly into complex structures*. Nat Mater, 2007. **6**(7): p. 557-562.

5. Kalsin, A.M. and B.A. Grzybowski, *Controlling the Growth of "Ionic" Nanoparticle Supracrystals*. Nano Letters, 2007. **7**(4): p. 1018-1021.
6. van Dongen, M.A., S. Vaidyanathan, and M.M. Banaszak Holl, *PAMAM dendrimers as quantized building blocks for novel nanostructures*. Soft Matter, 2013. **9**(47): p. 11188-11196.
7. Tomalia, D.A., *Dendrons/dendrimers: quantized, nano-element like building blocks for soft-soft and soft-hard nano-compound synthesis*. Soft Matter, 2010. **6**(3): p. 456-474.
8. Kostiainen, M.A., et al., *Electrostatic self-assembly of virus-polymer complexes*. Journal of Materials Chemistry, 2011. **21**(7): p. 2112-2117.
9. Mikkilä, J., et al., *Janus-Dendrimer-Mediated Formation of Crystalline Virus Assemblies*. ACS Macro Letters, 2013. **2**(8): p. 720-724.
10. Macfarlane, R.J., et al., *Nanoparticle Superlattice Engineering with DNA*. Science, 2011. **334**(6053): p. 204-208.
11. He, J., et al., *Self-Assembly of Inorganic Nanoparticle Vesicles and Tubules Driven by Tethered Linear Block Copolymers*. Journal of the American Chemical Society, 2012. **134**(28): p. 11342-11345.
12. Kostiainen, M.A., et al., *Electrostatic assembly of binary nanoparticle superlattices using protein cages*. Nat Nano, 2013. **8**(1): p. 52-56.
13. Caspar, D.L.D. and A. Klug, *Physical principles in the construction of regular viruses*. Cold Spring Harbor Symp. Quant. Biol, 1962: p. 27,1-24.
14. Kostiainen, M.A., et al., *Self-assembly and optically triggered disassembly of hierarchical dendron-virus complexes*. Nature Chemistry, 2010. **2**(5): p. 394-399.
15. Kostiainen, M.A., et al., *Electrostatic self-assembly of virus-polymer complexes*. Journal of Materials Chemistry, 2011. **21**(7): p. 2112-2117.
16. Kostiainen, M.A., et al., *Temperature-Switchable Assembly of Supramolecular Virus-Polymer Complexes*. Advanced Functional Materials, 2011. **21**(11): p. 2012-2019.
17. Bozic, A.L. and R. Podgornik, *Symmetry effects in electrostatic interactions between two arbitrarily charged spherical shells in the Debye-Huckel approximation*. Journal of Chemical Physics, 2013. **138**(7).
18. Damasceno, P.F., M. Engel, and S.C. Glotzer, *Predictive Self-Assembly of Polyhedra into Complex Structures*. Science, 2012. **337**(6093): p. 453-457.
19. Goubet, N., et al., *Which Forces Control Supracrystal Nucleation in Organic Media?* Advanced Functional Materials, 2011. **21**(14): p. 2693-2704.
20. Liu, X., et al., *Extinction coefficient of gold nanoparticles with different sizes and different capping ligands*. Colloids and Surfaces B: Biointerfaces, 2007. **58**(1): p. 3-7.
21. Sonnichsen, C., et al., *A molecular ruler based on plasmon coupling of single gold and silver nanoparticles*. Nat Biotech, 2005. **23**(6): p. 741-745.
22. Verduin, B., *The preparation of CCMV-protein in connection with its association into a spherical particle*. FEBS letters, 1974. **45**(1): p. 50-54.

23. de la Escosura, A., et al., *Viral capsids as templates for the production of monodisperse Prussian blue nanoparticles*. *Chemical Communications*, 2008. **0**(13): p. 1542-1544.
24. Description provided by Mr. V. Liljeström, Aalto University, department of applied physics

Chapter 6: Functional virus-like particle based materials

Metal enhancement fluorescence in plasmonic virus-like particle clusters

Nanotechnology enables us to break the physical limitations of ordinary materials, such as the size limits imposed by the wavelength of light in classical near field optics. This, however, requires components that allow for precise placement and spacing of the optical materials, to not only overcome these optical limits, but also control the resulting outcome. Protein cage-based nanomaterials offer a natural scaffold that enable symmetrical modifications and show promising structural properties, enabling both this precise placement and spacing. This chapter investigates the plasmonic effects of gold nanoparticles (AuNPs) encased in virus-based protein cages upon the excitation of fluorescent dyes on the protein cage surface. These virus-like particles (VLPs) show up to a 4.4 fold increase in fluorescence, which is conserved as a 2.2 fold increase upon electrostatic clustering of these VLPs. The data shows that VLP-based architectures can be used not only to study metal enhanced fluorescence, but also suggests that complex photonic structures can be formed by mixing VLP clusters with a variety of cargo and surface modifications.

Introduction

Plasmonic nanomaterials

Plasmonic nanomaterials are rapidly evolving into the photonic equivalent of electronic circuitry for optical signal processing, sub-wavelength resolution optical sensors and other nanoscale optical devices.[1-4] In part, this is due to their ability to focus and control light to sub wavelength resolutions and generate, trap, guide and manipulate this in its structure.[5, 6] Such materials have been made in a variety of ways, such as by using metallic films, nanowires or chains of nanoparticles, with both shape geometry and spacing influencing the resulting properties. [7-9] While plasmonics allow the manipulation of visible and near field light at the nanoscale, the control over the structure ultimately dictates the final properties.[10] For instance, the effect of plasmonic structures on fluorophores is known to depend not only on the distance and orientation of the fluorophore relative to the plasmonic structure, but also on the local field strength.[11-13]

As the result of recent advances, protein cage based nanomaterials are now promising candidates in further advancing the field of plasmonic nanomaterials.[14] Their biological functionality allows for the precise incorporation of a wide variety of molecules and nanoparticles on both their surface and their interior, including quantum dots, gold nanoparticles and fluorophores.[15-18] The resulting virus like particles (VLPs) retain their symmetrical architecture, which leads to precise control over the orientation and localisation of the newly introduced functional species.[14, 18, 19] Furthermore, VLPs have been demonstrated to form highly organised structures using electrostatic controlled clustering due to their symmetrical architecture.[20, 21] Consequently, the combination of plasmonic and fluorescent VLPs in a cluster should enable the formation of modular plasmonic architectures with tuneable properties.

Plasmons and fluorescence

Studies on fluorescent molecules near plasmonic particles or structures reveal the interplay between short range emission quenching, medium range excitation enhancement and long range emission enhancement.[22-24] The short range quenching is attributed to both a decrease in the radiative rate and an increase in non-radiative rate, thus changing the fluorescence lifetime, of fluorophores in the proximity of plasmonic metal.[25-27] In contrast, the metal enhancement fluorescence is attributed to two complimentary effects. The first is an increased rate of excitation as the local light intensity is increased due to the increased local absorption cross section of the plasmonic structure, the so-called lightning rod

effect.[28] The second is an interaction between the fluorophore dipole and the scattering component of the plasmonic structure, which physically are of a similar nature, therefore enabling a radiative emission increase, thus decreasing fluorescence lifetime.[23, 29]

Chapter content

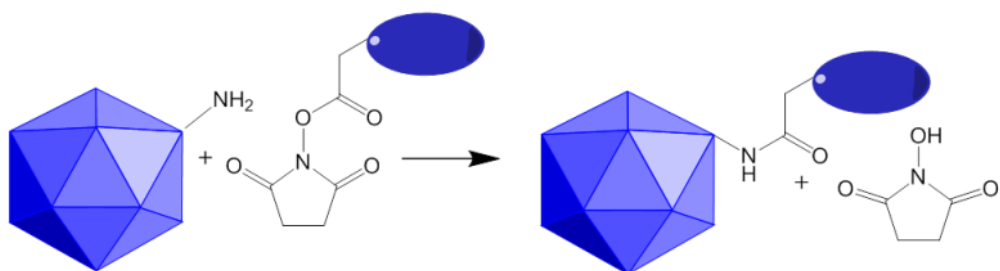
In this chapter, the interplay of gold nanoparticles (AuNP) encapsulated in Cowpea Chlorotic Mottle Virus (CCMV) based VLPs combined with fluorescent dye molecules on the VLP surface is investigated. Thus is combined with the effects of forming electrostatic clusters of these VLPs. As in the preceding chapters, the fabrication of the VLPs used is discussed, with the coupling of fluorescent dyes to these VLPs is described in more detail. Subsequently, the fluorescent properties of both T=1 and T=3 VLPs is studied to investigate the metal enhanced fluorescence. Finally clusters of these VLPs are formed to investigate if the increased density in plasmonic states has a further effect on the fluorescence.

Results and Discussion

Dye coupling to CCMV VLPs

Key parameters to study metal enhanced fluorescence are the optical and electronic properties of the metal particles, which are determined by the gold nanoparticle (AuNP). Encapsulation of different size AuNP will in turn affect the virus size and symmetry, as discussed in chapter 3. Therefore, four different CCMV-based VLPs are selected and prepared as described in the previous chapters: two T=3 sized particles, the native virus (CCMV) and CCMV with a 17nm gold core (CA17); and two T=1 sized capsids CCMV with a polystyrene sulphonate core (CPSS) and CCMV with a 7nm gold core (CA7T).

Another important factor in studying metal enhance fluorescence is the dye itself, in which both the quantum yield and spectral properties are of concern. As such, high quantum yield dyes with good photo stability and activity in a broad pH range are requirements for selection. Furthermore, spectral overlap between the gold plasmon peak and emission spectrum might affect the emission of the dyes, which needs to be studied. All this leads to the selection of two dyes; Atto390 ($\lambda_{\text{ex}} = 390\text{nm}$, $\lambda_{\text{em}} = 471\text{nm}$) which overlaps only slightly with the gold plasmon band, and Oregon Green 488 (Ore488, $\lambda_{\text{ex}} = 494\text{nm}$, $\lambda_{\text{em}} = 520\text{nm}$), which emits on the gold plasmon absorption peak. Furthermore, both dyes could potentially form a FRET pair making them of interest for future studies.



Scheme 1: Reaction scheme for the NHS-dye coupling used to modify the VLPs, each individual protein on the VLPs has 3 to 4 accessible primary amines that can be targeted with this procedure.

The fluorescent dyes were coupled to the CCMV VLPs using an NHS protein labelling technique to ensure uniform binding of the dye to each VLP, which all have a capsid based on the same CCMV proteins. This is achieved by dialysing the VLPs to a phosphate buffer (100mM PO_4^{2-} , 1mM EDTA, pH 7,5) and incubating them with the dye (in DMSO stock solution) ensuring a minimal (<5% v/v) amount of DMSO is added. To ensure a uniform coupling, the ratio of dye to protein during the reaction was kept constant for all samples at 5 dye molecules per protein and any unreacted dye was removed by chromatography or filtration.

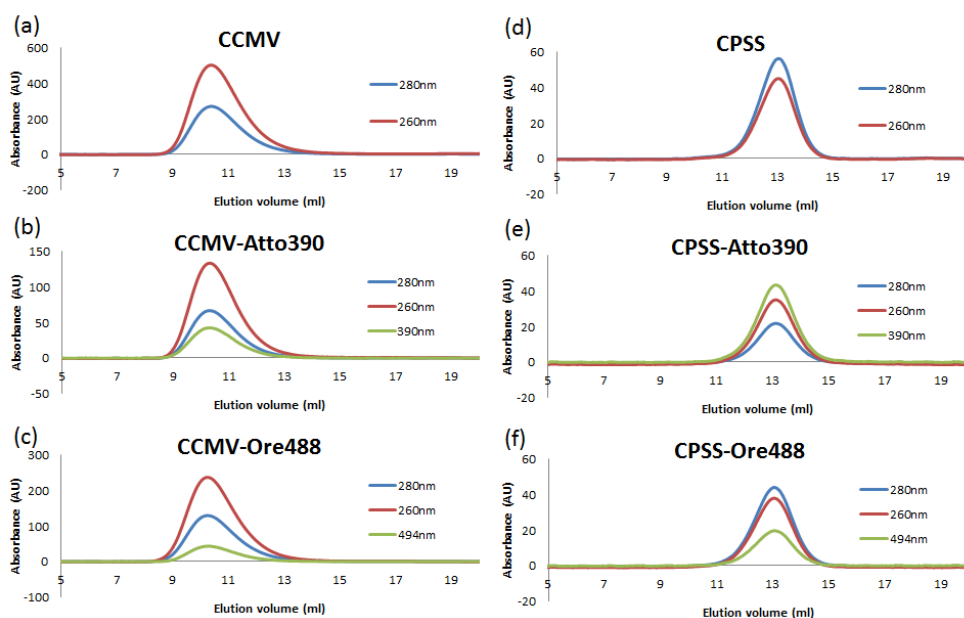


Figure 2: FPLC chromatograms for purified samples of; (a) CCMV, (b) CCMV with coupled Atto390 dye, (c) CCMV with coupled Ore488 dye, (d) CPSS, (e) CPSS with coupled Atto390 dye, (f) CPSS with coupled Ore488 dye.

Due to their ease of fabrication and lack of spectral interference from a plasmon band the CCMV T=3 and CPSS T=1 VLPs can be characterised in detail to track the dye coupling. FPLC size exclusion chromatography (figure 2) shows the dye-modified particles elute at the same volume as their native VLPs, $V = 11$ ml for T=3 and $V = 13$ ml for T=1, and show no disassembly or aggregation. This indicates that the modified particles are of comparable size to their native VLPs and possess an intact protein shell. Furthermore, a dye specific peak co-elutes at the same elution volume as the $\lambda = 260$ nm and 280 nm absorbance with no further dye specific peaks eluting. These data confirm the successful coupling of the desired dye to an intact VLP.

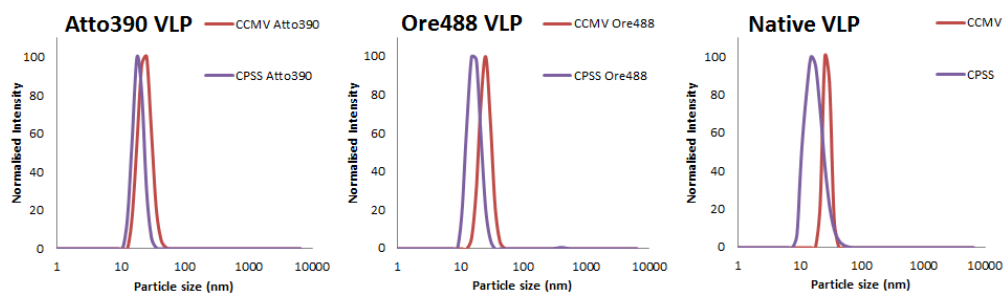


Figure 3: DLS spectra of; (left) CCMV and CPSS with coupled Atto390, (centre) CCMV and CPSS with coupled Ore488, (right) the native CCMV and CPSS particles.

The conservation of particle size that is seen in FPLC chromatography is also clear from the DLS size distribution plot (figure 3), in which the difference between the T=1, with $D = 18$ nm, and T=3 VLPs, with $D = 28$ nm, is clearly evident. Furthermore, TEM micrographs (figure 4) of the particles show single intact particles of the expected size. The particle staining, however, seems less uniform compared to native CCMV samples, likely a result of the presence of the dye molecules.

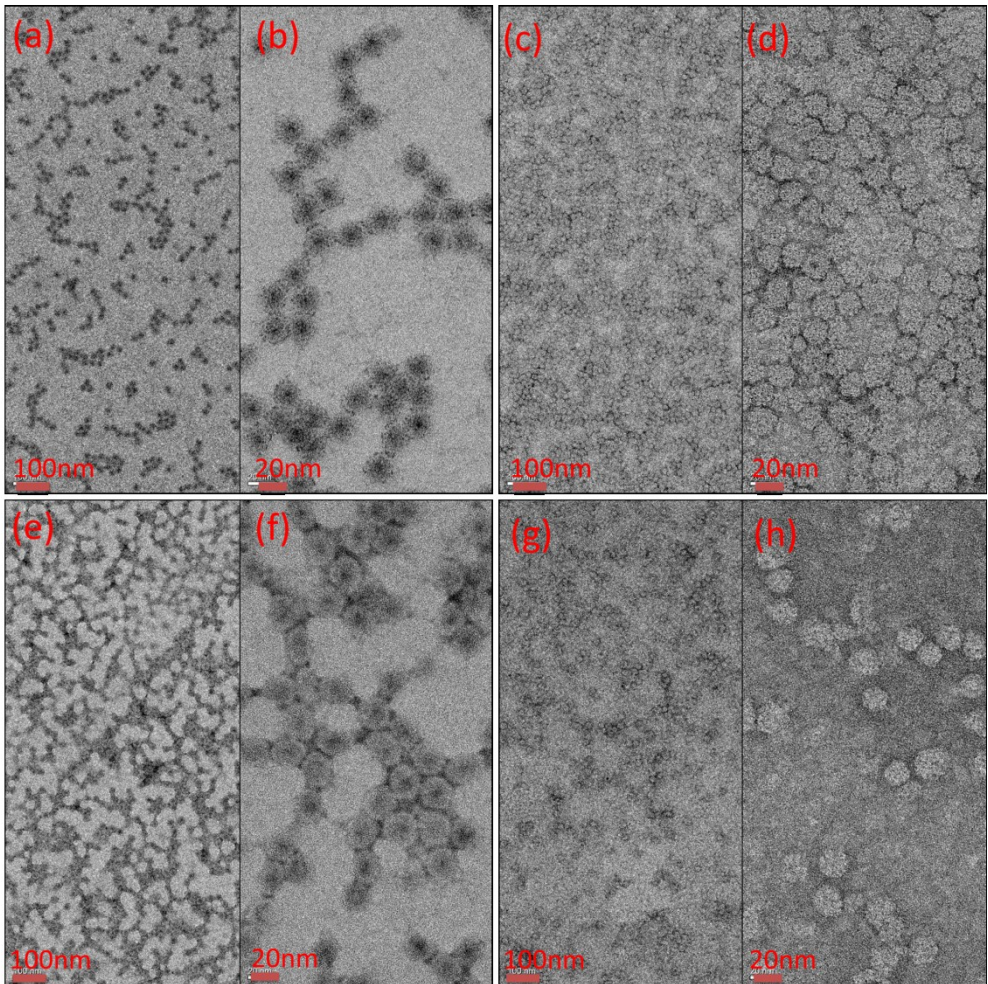


Figure 4: TEM images at two magnifications of (a,b) CCMV after Atto390 coupling, (c,d) CPSS after Atto390 coupling, (e,f) CCMV after Ore488 coupling, (g,h) CCMV after Ore488 coupling.

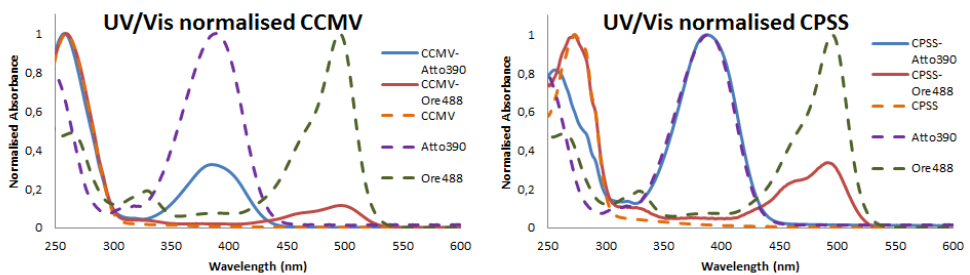


Figure 5: UV-Vis spectra of VLP and dyes, with the maximum absorbance normalised to 1, before and after dye coupling and purification; (left) the T=3 sized CCMV VLP and dyes, (right) the T=1 sized CPSS VLP and dyes.

The UV-Vis spectra (figure 5) of the purified samples can be used to determine the degree of modification by the relative intensities of the absorption signals, correcting for any overlap by assuming a linear combination of signals. For the Atto390 dye ($\epsilon_{390nm} = 24,000 \text{ M}^{-1} \text{ cm}^{-1}$) these spectra point to 380 dye molecules coupled to every T=3 CCMV capsid ($\epsilon_{260} = 2.78 * 10^7 \text{ M}^{-1} \text{ cm}^{-1}$), and that 125 dye molecules are coupled to every T=1 CPSS capsid ($\epsilon_{280,protein} = 2.41 * 10^4 \text{ M}^{-1} \text{ cm}^{-1}$, $\epsilon_{260,PSS} = 2.17 * 10^6 \text{ M}^{-1} \text{ cm}^{-1}$, $\epsilon_{280,PSS} = 4.96 * 10^5 \text{ M}^{-1} \text{ cm}^{-1}$). For a 5 fold excess of dye per protein, about 2 dye molecules per protein are attached, regardless of the capsid symmetry. Furthermore, the fluorescence spectra (figure 6 and 7) clearly show the characteristic Atto390 dye fluorescence in these purified VLP samples. For the Oregon green 488 dye, the absorption spectrum of the dye is altered, which is most pronounced by the change in the relative intensities of the $\lambda = 470 \text{ nm}$ and 494 nm peaks. As such, no quantitative analysis of the coupling can be made, though estimates range between 0.1 and 0.3 dye molecules per protein based on the $\lambda = 494 \text{ nm}$ and 470 nm absorbance respectively. Still, despite the apparent low modification, the resulting Ore488 VLPs display the characteristic Ore488 dye fluorescence (figure 6 and 7). Furthermore, they follow the same qualitative trend as the Atto390 modified VLPs with similar numbers of dye per protein attached for the T=1 and T=3 VLPs, in that way allowing for a qualitative study of the fluorescence enhancement.

The above data shows the desired modification and suggests that the degree of dye coupling is dependent on the individual proteins reactivity, and thus should be similar for any CCMV based VLP. For the CA17 T=3 VLPs and CA7T T=1 VLPs, however, the gold plasmon band makes direct spectral analysis difficult. Still, the data for the CA17 T=3 VLP and CA7T T=1 VLP before and after coupling shows a similar trend (appendix A) compared to the data of the CCMV and CPSS respectively. After all, the UV-Vis data show evidence for significant levels of dye coupling, and, despite poor uranyl acetate staining contrast due to the dense AuNP core, the TEM shows intact, non-aggregated core-shell particles. Furthermore, the fluorescence spectra (figure 6 and 7) show the characteristic dye fluorescence in these purified VLP samples. Combined with the hypothesis that dye coupling is protein, not structure, dependent we expect a similar degree of dye-modification for these AuNP cored VLP compared to their soft cored equivalents.

Metal enhanced fluorescence

As discussed, the effect of metal enhanced fluorescence strongly depends on the size of the AuNPs and the resulting electromagnetic field associated with the surface plasmons. The protein coat itself has no significant impact upon the plasmon absorbance, as is shown in this thesis. Therefore, even though both the

T=3 and T=1 symmetry capsids show an equivalent degree of modification with the dye molecules, the 7nm and 17nm sized gold cores are expected to show a different interaction with the fluorescent dyes.[22]

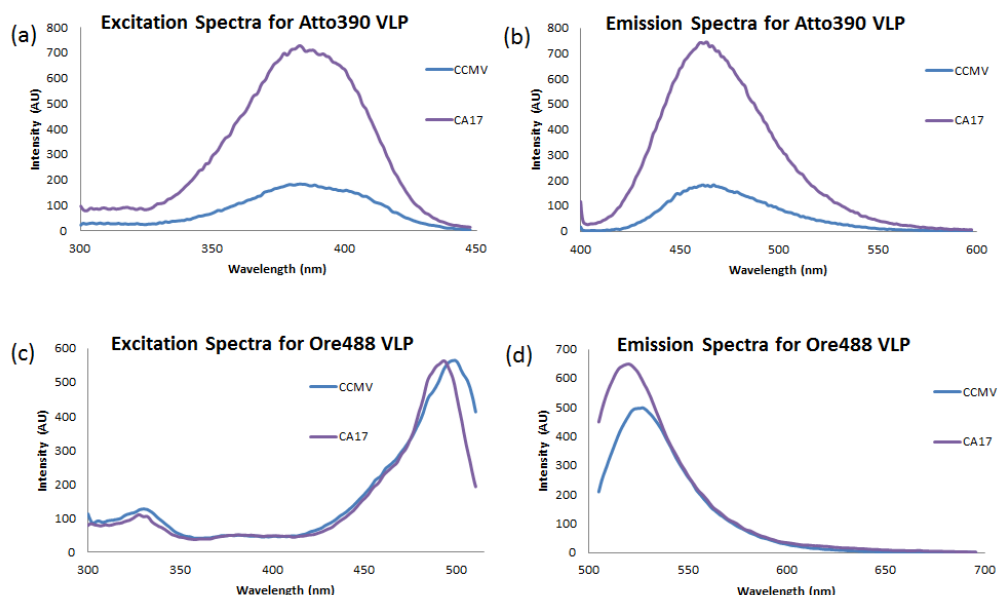


Figure 6: Fluorescence spectra of T=3 sized VLPs with (CA17) and without (CCMV) a gold core; (a) excitation for Atto390 VLPs (measured at $\lambda = 494\text{nm}$), (b) emission for Atto390 VLPs (with dye excited at $\lambda = 390\text{nm}$), (c) excitation for Ore488 VLPs (measured at $\lambda = 544\text{nm}$), (d) emission for Ore488 VLPs (with dye excited at $\lambda = 470\text{nm}$).

The effect of an AuNP core in a T=3 capsid is immediately apparent from the increased fluorescent emission for both the Atto390 and Ore488 dyes. Here, the 4.4 fold increase in fluorescence for the Atto390 dye is stronger than the 1.2 fold increase of the Ore488 dye. Furthermore, both the emission and excitation maximum of the Ore488 dye show a significant blue shift, while the excitation spectrum shows no increase. This is most likely due to the broad gold plasmon absorption peak at $\lambda = 520\text{ nm}$ absorbing part of the Ore488 emission and interfering directly with the measurement of the excitation spectrum at $\lambda = 544\text{ nm}$.

T=3 VLPs	Atto390			Ore488	
	τ (ns)	τ_{fast} (ns)	I/I_{CCMV}	τ (ns)	I/I_{CCMV}
Dye	3.7	N/A	N/A	3.5	N/A
CCMV	3.1	N/A	1	3.1	1
CA17	(4.6)	(1.5)	4.4	4.0	1.2

Table 1: Overview of the dominant fluorescent lifetimes (τ) and, where present, faster fluorescent lifetime components (τ_{fast}) for Atto390 and Ore488 and the T=3 sized VLPs along with fluorescence intensity increase of the VLPs compared to the CCMV fluorescence intensity (I/I_{CCMV}) (decay slope and fit are in appendix B).

To understand why the increase in fluorescence happens, the fluorescence lifetimes are essential, as it reveals the nature of the decay of the excited state. Both the fitted CCMV and CA17 lifetimes should give similar values, as the decay curves are similar (see appendix B). The fitted values, however, suffer from inaccuracy due to a substantial presence of uncorrelated photons, especially for the CA17 VLPs and more so for the Ore488 dye. Added to the complexity of the system, where many factors, like fluorophore orientation, distance to the metal surface as well as the size of the nanoparticle play a role, this limits the insight potential gained from the data.[22] Despite this inaccuracy, there is a difference in the lifetime of both CCMV and CA17 compared to the native dye for the Atto390 as well as the Ore488 dye. The decrease of the CCMV-dye lifetime can be tentatively attributed to concentration quenching between the densely packed fluorophores on the surface of CCMV, allowing for a faster non-radiative decay as multiple pathways are present. Furthermore, though the observed differences between the fitted VLPs-dye lifetimes are of limited use due to the inaccuracy, a fast lifetime component (τ_{fast}) seems to emerge for the CA17-Atto390 system when the data is fitted. Though being hard to observe in the decay curves, the appearance of τ_{fast} could suggest a change in the radiative and/or non-radiative rate of decay. Due to the close proximity of some fluorophores to the metal surface, an increase in non-radiative decay is likely dominant. [25-27] This would potentially lead to a limited quenching behaviour, but this is not observed. Without a clear change in the lifetimes, the increase in fluorescence intensity for the CA17 system can be attributed to an enhanced rate of excitation, stemming from the lightning rod effect caused by the greater optical cross section of the AuNP.

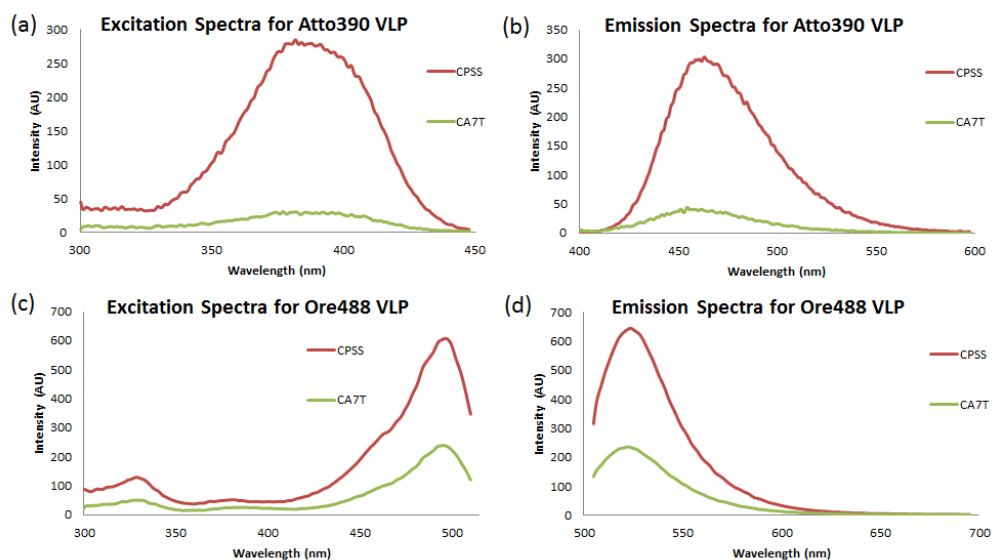


Figure 7: Fluorescence spectra of T=1 sized VLPs with (CA7T) and without (CPSS) a gold core; (a) excitation for Atto390 VLPs (measured at $\lambda = 494$ nm), (b) emission for Atto390 VLPs (with dye excited at $\lambda = 390$ nm), (c) excitation for Ore488 VLPs (measured at $\lambda = 544$ nm), (d) emission for Ore488 VLPs (with dye excited at $\lambda = 470$ nm).

The PSS cored T=1 VLPs shows a slightly stronger fluorescence intensity at similar dye concentrations compared to the native CCMV T=3 VLPs. This can be attributed to a larger number of free VLPs over which the dye molecules are spread, in that way slightly limiting the potential concentration quenching. Furthermore, the Ore488 modified T=1 CA7T VLPs lack the blueshift observed for their T=3 counterparts, which indicates the remaining dye emission is not affected by the absorption of the AuNPs $\lambda = 520$ nm plasmon absorption band.

<u>T=1 VLPs</u>	Atto390			Ore488	
	τ (ns)	τ_{fast} (ns)	I/I_{CPSS}	τ (ns)	I/I_{CPSS}
Dye	3.7	N/A	N/A	3.5	N/A
CPSS	3.1	N/A	1	3.8	1
CA7T	(4.1)	0.9	0.14	(3.5)	0.36

Table 2: Overview of the dominant fluorescent lifetimes (τ) and, where present, faster fluorescent lifetime components (τ_{fast}) for Atto390 and Ore488 and the T=1 sized VLPs along with fluorescence intensity increase of the VLPs compared to the CPSS fluorescence intensity (I/I_{CPSS}) (decay slope and fit are in appendix B).

The obtained lifetimes for the T=1 VLPs are similar in nature to those of the T=3 VLPs, again being somewhat inaccurate due to uncorrelated photons, especially for the AuNP containing VLPs and more so for the Ore488 dye. Regardless, the clear appearance of a fast fluorescence lifetime component for the Atto390 AuNP containing VLPs shows, as expected, that the emission of these particles is indeed quenched by the presence of an AuNP, with an increase in non-radiative decay being dominant over any potential decrease in radiative decay. For the Ore488 dye, however, the lifetime of AuNP containing T=1 VLPs was difficult to obtain and we were unable to distinguish between scattering and a potential fast lifetime component. Ultimately, CA7T only shows evidence of fluorescence quenching from the AuNPs and no evidence for an increased rate of excitation. This quenching could thus be attributed to an increase of the non-radiative rate and not the absorption of the emission by the AuNP plasmon band, as no blueshift was observed.

These results effectively give us two different components for use in plasmonic materials, i.e. fluorescence quenching T=1 VLPs and fluorescence enhancing T=3 VLPs. Still, these types of particles are known to interact through plasmon coupling when placed close together. Further studies of clusters of these particles are carried out to see if the optical properties of these virus-based materials can be further altered.

Cluster-enhanced fluorescence

A single AuNP is known to affect the fluorescence in its direct environment, a property conserved for AuNPs encapsulated in VLPs. This offers an advantage; as these VLPs can be used to construct a material, such that, by combining the individual VLP properties, collective material properties might emerge. The assembly techniques discussed in previous chapters provide an excellent basis for this clustering, as it allows for the creation of structured materials with a dense packing of individual particles inside. This organization of particles could influence the properties of the individual particles either constructively, by further fluorescence enhancement, or destructively by promoting additional quenching. As such, we wish to study if the VLPs retain their properties after clustering or if fluorescence is further enhanced by the interacting electric fields of the AuNP plasmons.

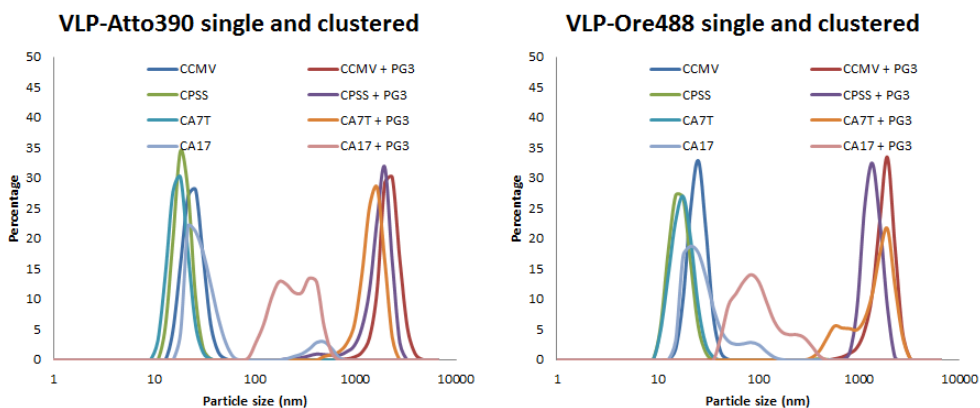


Figure 8: DLS spectra of free particles versus clusters; (left) VLPs with coupled Atto390 dye, (right) VLPs with coupled Ore488 dye. The CA17 particles clustered at $5\mu\text{g/ml}$ of protein with $2\mu\text{g/ml}$ of PAMAM G3 (PG3) (a 25:10 mass ratio, similar to chapter 4); therefore the resulting clusters are smaller than those of the other VLPs clustered at $25\mu\text{g/ml}$ of protein with $10\mu\text{g/ml}$ of PAMAM G3 (PG3).

Clusters of dye modified VLPs can be formed in a similar manner to those discussed in chapter 4, i.e. by adding PAMAM G3 dendrimers (PG3) to a solution of the VLPs. The electrostatic clustering is charge based and the coupling of the fluorescent dyes is not expected to alter the negatively charged surface at the pH of the clustering (pH 5), therefore no drastic changes in the assembly behaviour are expected. The pH, ionic strength, mass ratios from the procedure, discussed in detail in chapter 4, will be employed for the cluster formation. DLS spectra and TEM images (figure 8 and 9) confirm that these conditions are effective in assembling the dye-coupled VLPs. This suggests that these VLPs can indeed act as modular nano-building blocks, in this case to generate plasmonic materials.

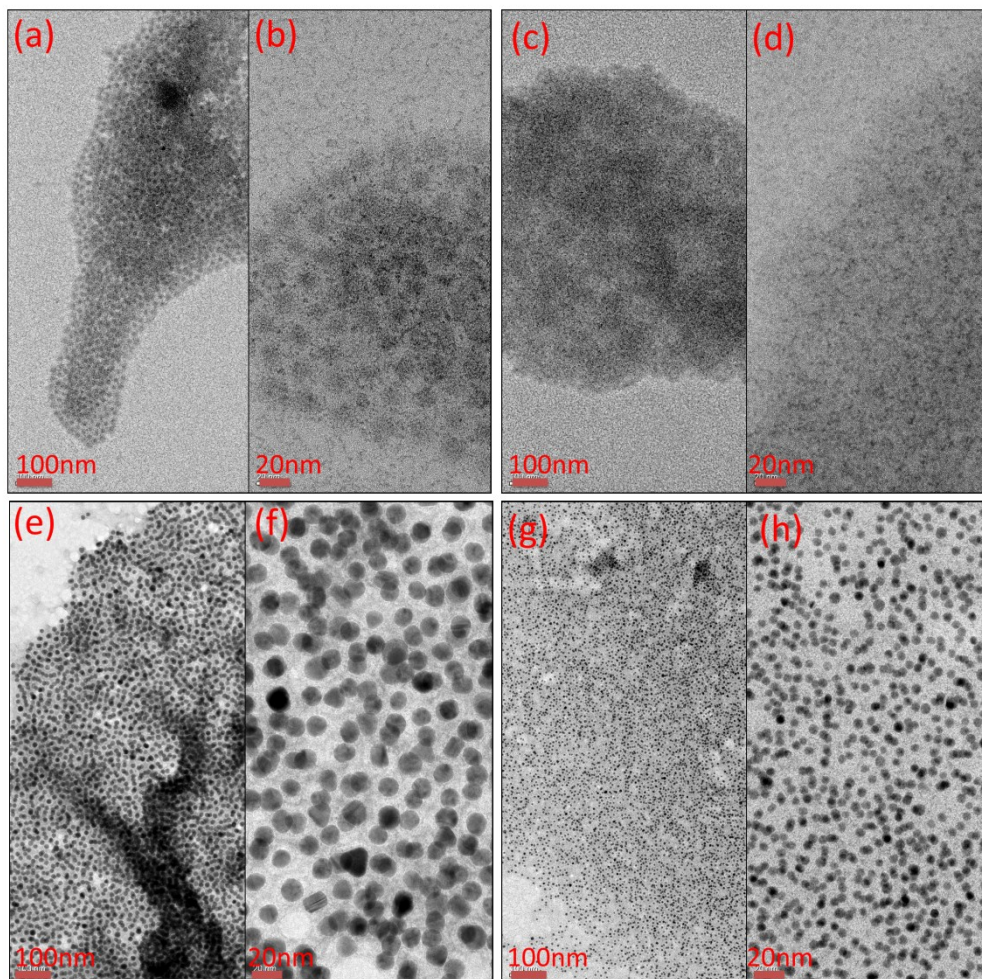


Figure 9: TEM images at two magnifications of VLP clusters formed from Atto390 modified VLPs; (a,b) CCMV with Atto390, (c,d) CPSS with Atto390, (e,f) CA17 with Atto390, (g,h) CA7T with Atto390.

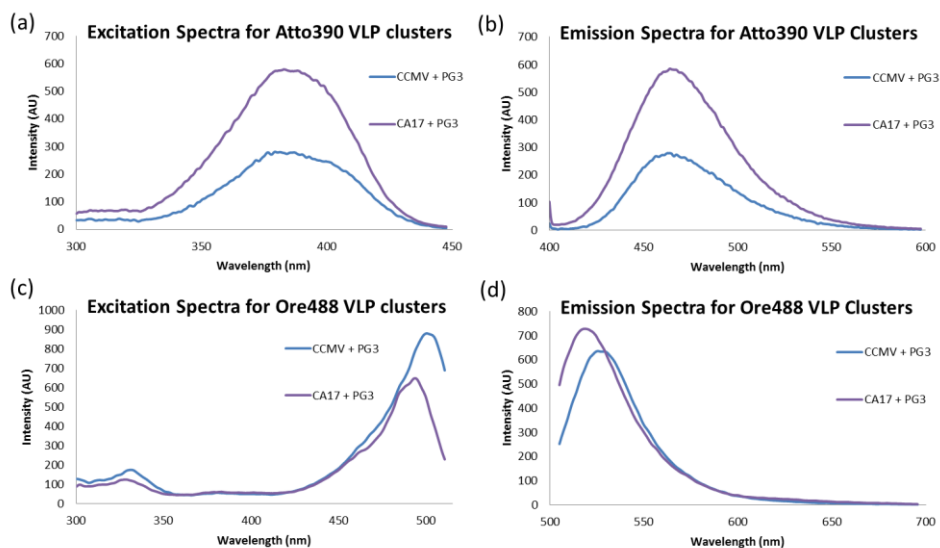


Figure 10: Fluorescence spectra of clustered T=3 sized VLPs with (CA17) and without (CCMV) a gold core; (a) excitation for Atto390 VLPs (measured at $\lambda = 494$ nm), (b) emission for Atto390 VLPs (with dye excited at $\lambda = 390$ nm), (c) excitation for Ore488 VLPs (measured at $\lambda = 544$ nm), (d) emission for Ore488 VLPs (with dye excited at $\lambda = 470$ nm).

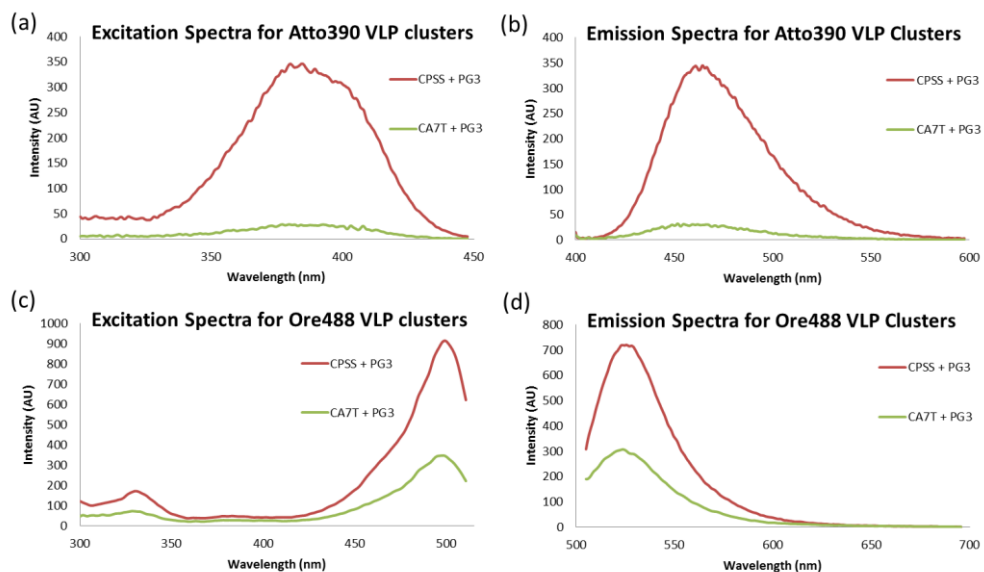


Figure 11: Fluorescence spectra of clustered T=1 sized VLPs with (CA7T) and without (CPSS) a gold core; (a) excitation for Atto390 VLPs (measured at $\lambda = 494$ nm), (b) emission for Atto390 VLPs (with dye excited at $\lambda = 390$ nm), (c)

excitation for Ore488 VLPs (measured at $\lambda = 544$ nm), (d) emission for Ore488 VLPs (with dye excited at $\lambda = 470$ nm).

The relative fluorescence intensity (table 3) for clustered structures seems to decrease slightly for VLPs with an AuNP core and an Atto390 dye and increased for the others. The (slight) increase in the relative fluorescence emission for the non-AuNP containing VLPs is likely a result from an increase in packing density of the fluorophores and subsequent homo-fret arising from it. Assembly of the dye modified AuNP containing VLP into clusters has no further effect upon the Ore488 dye fluorescence intensity beyond the increase seen for the native VLP clusters. The presence of an AuNP core, however, causes a decrease in the Atto390 fluorescence after clustering, especially when compared to the increase seen for the native VLP clusters. The decrease for the AuNP cores can be attributed to further quenching of the absorbance due to the densely packed gold particles in the clustered structure, effectively strengthening the effects seen for the free particles. In this case, the dense packing and overlapping electric field from the gold plasmons would cause a net decrease in the fluorophore activity rather than a further constructive enhancement. This, however, does not explain the difference between the Atto390 and Ore488 AuNP containing VLPs.

T=3 VLPs clustered	Atto390				Ore488		
	τ (ns)	τ_{fast} (ns)	I/I_{CCMV}	I/I_{free}	τ (ns)	I/I_{CCMV}	I/I_{free}
Dye	3.7	N/A	N/A	N/A	3.5	N/A	N/A
CCMV	3.1	N/A	1	1.5	3.0	1	1.3
CA17	4.1	(-)	2.2	0.8	3.9	1.1	1.3

T=1 VLPs clustered	Atto390				Ore488		
	τ (ns)	τ_{fast} (ns)	I/I_{CPSS}	I/I_{free}	τ (ns)	I/I_{CPSS}	I/I_{free}
Dye	3.7	N/A	N/A	N/A	3.5	N/A	N/A
CPSS	3.3	N/A	1	1.1	4.0	1	1.1
CA7T	4.1	0.6	0.1	0.8	3.7	0.42	1.1

Table 3: Overview of the dominant fluorescent lifetimes (τ) and, where present, faster fluorescent lifetime components (τ_{fast}) for Atto390 and Ore488 and both the T=3 and T=1 sized VLP clusters along with intensity increase of the VLPs compared to the CCMV/CPSS cluster intensity (I/I_{CCMV} and I/I_{CPSS}) and the unclustered VLP intensity (I/I_{free}) (decay slope and fit are in appendix B).

Still, the fluorescence lifetime studies on the clusters do not show great differences with the individual particles, indicating that the effect of assembly on the quenching is limited at best. Instead, the decrease in AuNP containing Atto390 VLP fluorescence intensity is more likely due to the dense packing of the gold particles,

as described above.. The Ore488 VLPs are excited at a wavelength where AuNPs absorb less strongly compared to the Atto390 VLPs excitation wavelength, and consequently this effect is limited.

Preliminary studies on more complex systems, where AuNP containing VLPs are used to dope structures formed from native VLPs, suggests even greater enhancements might be possible. We hypothesize that these assemblies combine the enhancement found for AuNP containing VLPs with the enhancement from dense fluorophore packing. Further studies at increasing empty to AuNP containing VLP ratios are needed, as these would allow us to understand the effect of the AuNP core concentration and the relative degree of enhancement. In our concept for these studies, some of the fluorophores in these structures would be at an increased distance from the AuNP core, being on neighbouring empty VLPs. These should show further enhancement due to an effective increase in the rate of emission as predicted by previous studies. [23, 29] Studies on these doped VLP clusters would, however, benefit from a physical modelling of the interacting plasmon fields in these materials and a greater degree of control over the organisation of mixed VLPs in clustered structures.

Conclusion

CCMV based VLPs have been successfully modified with fluorescent dye molecules using NHS-ester labelled dyes. Moreover, both CCMV T=3 and CPSS T=1 VLPs have an equivalent degree of modification per protein, i.e. 2 Atto390 or 0.3 Ore488 dyes per protein, with the gold containing CA17T T=3 and CA7T T=1 VLPs showing a similar trend. Unlike studies by Capehart et al., our dyes were coupled directly to the VLP surface, without a spacer, allowing for a higher degree of modification but less precise control over the fluorophore positioning. The 4.4 fold maximum fluorescence enhancement in our systems is greater than the 2.2 fold enhancement reported by them. This is in agreement with the trend they found for closer positioning of the fluorophore to the VLP capsid, and thus its contained AuNP, enabling a greater enhancement for these relatively small AuNP.[14] Furthermore, our studies allowed for fluorescence measurements in bulk, enabling rapid screening, and could be assembled into clusters to study their potential as plasmonic materials.

Compared to their soft cored equivalents, the T=3 CA17T VLPs enhances the fluorescence of both dyes, likely due to the so-called lightning rod effect, whilst the T=1 CA7T quenches the fluorescence, likely due to an increase in the non-radiative rate of decay. More precise studies on the lifetimes are desirable, however, to fully confirm these explanations, for instance by using single particle techniques.

Furthermore, DLS and TEM data shows that these modified VLPs can be clustered under the same conditions as the non-modified VLPs discussed in chapter 4, whilst retaining their fluorescent enhancement properties. This is a key result, as it suggests that these VLPs can indeed act as modular and programmable nano-building blocks, in this case to generate plasmonic materials. Indeed, preliminary studies indicate that far greater enhancement could be achieved by doping clusters of empty VLPs with AuNP containing VLPs.

VLP-based plasmonic nanostructures, such as those demonstrated here, will be of use as both passive and active components in plasmonic materials to enable precise nanoscale control over optical systems. An important challenge remains in the organisation and structuring of these VLP components, not only in the structural order of the clusters, but also in precise placement of individual components. This challenge can be addressed by using synthetic and genetic site specific modifications to modulate the interaction on and between specific binding sites, either on the VLPs or the cluster inducing macromolecules. If this is achieved, we believe that these materials could be used as part of the photonic equivalent of electronic circuitry for optical signal processing, sub-wavelength resolution optical sensors and other nanoscale optical devices.

Experimental

VLP formation

The formation of the VLPs used in this chapter, is studied and described in detail in chapter 3 and 4.

Dye coupling

First stock solution in DMSO of NHS-ester labelled Oregon Green 488 (5mg in 1000ul) and Atto390 (1mg in 600ul) were made and stored at -20°C until used to couple to VLPs. Subsequently, the VLPs were dialysed to phosphate buffer (100mM PO_4^{2-} , 1mM EDTA, pH 7,5) after which their protein concentration was determined using UV-Vis spectroscopy. A small volume (<5% v/v) of the desired dye in DMSO was then added in a 5:1 molar ratio of dye to protein. In a typical sample 11ul of Atto390 in DMSO is added to 989ul of a CCMV solution for a final concentration of 10 μM of protein and 50 μM of dye. This reaction mixture was mixed on a rollerbank at room temperature for 30 minutes and subsequently at 4°C overnight to allow for the coupling to occur. The resulting samples are purified using spin filtration (30k MWCO, 5krpm, eppendorf 5415 R centrifuge) in which fresh buffer was added at least 4 times to remove unreacted dye.

Clustering procedures

Spin filtration (30k MWCO, 5krpm, eppendorf 5415 R centrifuge) was used to replace the phosphate buffer with a pH 5 acetate buffer (50mM NaCl, 10mM sodium acetate, 1 mM EDTA, 1mM NaN₃). Samples of 500µl were prepared by diluting the protein solutions to a fixed concentration of 5µg/ml of protein for CA17 and 25µg/ml of protein for all other VLPs. For clustered samples 1 to 5µl of a 1mg/ml PAMAM G3 dendrimers solution was added to 495µl of protein solution to achieve a 10:25 mass ratio of dendrimer to protein.

DLS

Dynamic light scattering samples were prepared from 500 µl fresh sample solutions and allowed to equilibrate for 2 minutes on a roller bank after mixing. Each sample was measured five times for 120 seconds using an Anaspec nanotrack wave dynamic light scattering instrument with the best of these five measurements selected.

UV-Vis

UV-Visible samples are prepared from 500 µl or 1000 µl fresh sample solutions. All solutions were measured in a 1cm quartz cuvette in a PerkinElmer Lambda 850 UV/VIS Spectrometer.

Fluorescence (spectroscopy and lifetime imaging)

Fluorescence spectroscopy and lifetime imaging were performed on the same samples. Samples are prepared as described, but subsequently diluted to a uniform protein concentration for all free VLP and VLP cluster solutions.

Fluorescence spectroscopy

Samples were imaged using a Perkin Elmer LS 55 fluorescence spectrometer for fluorescence intensity. For the Atto390 dye the excitation spectra samples were measured at $\lambda = 494$ nm, the emission maximum, whilst the emission spectra were measured whilst the dye was excited at $\lambda = 390$ nm, the excitation maximum. For the Ore488 dye the excitation spectra samples were measured at $\lambda = 544$ nm, an offset of $\Delta\lambda = 26$ nm from the $\lambda = 518$ nm emission maximum, whilst the emission spectra were measured whilst the dye was excited at $\lambda = 470$ nm, an offset of $\Delta\lambda = 24$ nm from the $\lambda = 494$ nm the excitation maximum. These offsets were introduced to prevent overlap between the excitation pulse and the measurement, whilst still allowing significant signal intensity.

Fluorescence lifetime imaging

Samples were imaged using a Fluoromax spectrophotometer for fluorescence lifetime imaging using either a NanoLED-370 LED ($\lambda_{\text{diode}} = 364\text{nm}$, for Atto390 dye) or a NanoLED-460 LED ($\lambda_{\text{diode}} = 462\text{nm}$, for Ore488 dye) for the excitation pulse. The fluorescence lifetime data was fitted using 2nd order or 3rd order exponential decay functions, and has been corrected for particle light scattering.

The fitted lifetimes found in this chapter fall in the $3\text{ ns} < \tau < 5\text{ ns}$ range typical for these dyes. The low fluorescence intensity for some samples resulted in long measurement times, i.e. $>2\text{ hrs.}$, and created measurement artefacts that could reduce the accuracy of the lifetime measurements. Therefore, lifetimes of $\tau > 7$ are ascribed to uncorrelated photons from light leaking in from outside.

TEM

TEM samples were prepared by depositing $5\mu\text{l}$ of a sample solution on a formvar carbon coated copper mesh grid and removing the remaining drop after 5 minutes by blotting it gently with fibre free paper. Subsequently these samples were stained by depositing $5\mu\text{l}$ of a Uranyl acetate (1% w/v in milliQ) staining solution and removing the remaining drop after 30 seconds by blotting it gently with fibre free paper. Samples were imaged using a Philips CM300ST-FEG TEM.

Bibliography

1. Gramotnev, D.K. and S.I. Bozhevolnyi, *Plasmonics beyond the diffraction limit*. Nat Photon, 2010. **4**(2): p. 83-91.
2. Anker, J.N., et al., *Biosensing with plasmonic nanosensors*. Nat Mater, 2008. **7**(6): p. 442-453.
3. Chang, D.E., et al., *A single-photon transistor using nanoscale surface plasmons*. Nat Phys, 2007. **3**(11): p. 807-812.
4. Zhang, R., et al., *Chemical mapping of a single molecule by plasmon-enhanced Raman scattering*. Nature, 2013. **498**(7452): p. 82-86.
5. Schuller, J.A., et al., *Plasmonics for extreme light concentration and manipulation*. Nat Mater, 2010. **9**(3): p. 193-204.
6. Ozbay, E., *Plasmonics: Merging Photonics and Electronics at Nanoscale Dimensions*. Science, 2006. **311**(5758): p. 189-193.
7. Søndergaard, T. and S. Bozhevolnyi, *Slow-plasmon resonant nanostructures: Scattering and field enhancements*. Physical Review B, 2007. **75**(7): p. 073402.
8. Akimov, A.V.M.A.Y.C.L.C.D.E.Z.A.S.H.P.R.P.H.L.M.D., *Generation of single optical plasmons in metallic nanowires coupled to quantum dots*. Nature, 2007. **450**(7168): p. 402-406.

9. Quinten, M., et al., *Electromagnetic energy transport via linear chains of silver nanoparticles*. Optics Letters, 1998. **23**(17): p. 1331-1333.
10. Rycenga, M., et al., *Controlling the Synthesis and Assembly of Silver Nanostructures for Plasmonic Applications*. Chemical Reviews, 2011. **111**(6): p. 3669-3712.
11. Tam, F., et al., *Plasmonic Enhancement of Molecular Fluorescence*. Nano Letters, 2007. **7**(2): p. 496-501.
12. Bardhan, R., et al., *Fluorescence Enhancement by Au Nanostructures: Nanoshells and Nanorods*. ACS Nano, 2009. **3**(3): p. 744-752.
13. Acuna, G.P., et al., *Fluorescence Enhancement at Docking Sites of DNA-Directed Self-Assembled Nanoantennas*. Science, 2012. **338**(6106): p. 506-510.
14. Capehart, S.L., et al., *Controlled Integration of Gold Nanoparticles and Organic Fluorophores Using Synthetically Modified M52 Viral Capsids*. Journal of the American Chemical Society, 2013. **135**(8): p. 3011-3016.
15. Lee, L.A., H.G. Nguyen, and Q. Wang, *Altering the landscape of viruses and bionanoparticles*. Organic & Biomolecular Chemistry, 2011. **9**(18): p. 6189-6195.
16. Wang, Q., et al., *Natural Supramolecular Building Blocks: Wild-Type Cowpea Mosaic Virus*. Chemistry & Biology, 2002. **9**(7): p. 805-811.
17. Minten, I.J., et al., *Controlled Encapsulation of Multiple Proteins in Virus Capsids*. Journal of the American Chemical Society, 2009. **131**(49): p. 17771-17773.
18. Sun, J., et al., *Core-controlled polymorphism in virus-like particles*. Proceedings of the National Academy of Sciences, 2007. **104**(4): p. 1354-1359.
19. Sikkema, F.D., et al., *Monodisperse polymer-virus hybrid nanoparticles*. Organic & Biomolecular Chemistry, 2007. **5**(1): p. 54-57.
20. Kostianinen, M.A., et al., *Electrostatic self-assembly of virus-polymer complexes*. Journal of Materials Chemistry, 2011. **21**(7): p. 2112-2117.
21. Mikkilä, J., et al., *Janus-Dendrimer-Mediated Formation of Crystalline Virus Assemblies*. ACS Macro Letters, 2013. **2**(8): p. 720-724.
22. Lakowicz, J.R., *Radiative Decay Engineering: Biophysical and Biomedical Applications*. Analytical Biochemistry, 2001. **298**(1): p. 1-24.
23. Lakowicz, J., *Plasmonics in Biology and Plasmon-Controlled Fluorescence*. Plasmonics, 2006. **1**(1): p. 5-33.
24. Anger, P., P. Bharadwaj, and L. Novotny, *Enhancement and Quenching of Single-Molecule Fluorescence*. Physical Review Letters, 2006. **96**(11): p. 113002.
25. Dulkeith, E., et al., *Fluorescence Quenching of Dye Molecules near Gold Nanoparticles: Radiative and Nonradiative Effects*. Physical Review Letters, 2002. **89**(20): p. 203002.

26. Dulkeith, E., et al., *Gold Nanoparticles Quench Fluorescence by Phase Induced Radiative Rate Suppression*. *Nano Letters*, 2005. **5**(4): p. 585-589.
27. Schneider, G., et al., *Distance-Dependent Fluorescence Quenching on Gold Nanoparticles Ensheathed with Layer-by-Layer Assembled Polyelectrolytes*. *Nano Letters*, 2006. **6**(3): p. 530-536.
28. Jain, P.K., et al., *Calculated Absorption and Scattering Properties of Gold Nanoparticles of Different Size, Shape, and Composition: Applications in Biological Imaging and Biomedicine*. *The Journal of Physical Chemistry B*, 2006. **110**(14): p. 7238-7248.
29. Lakowicz, J.R., et al., *Release of the self-quenching of fluorescence near silver metallic surfaces*. *Anal Biochem*, 2003. **320**(1): p. 13-20.

Appendix A: Coupling data AuNP VLPS

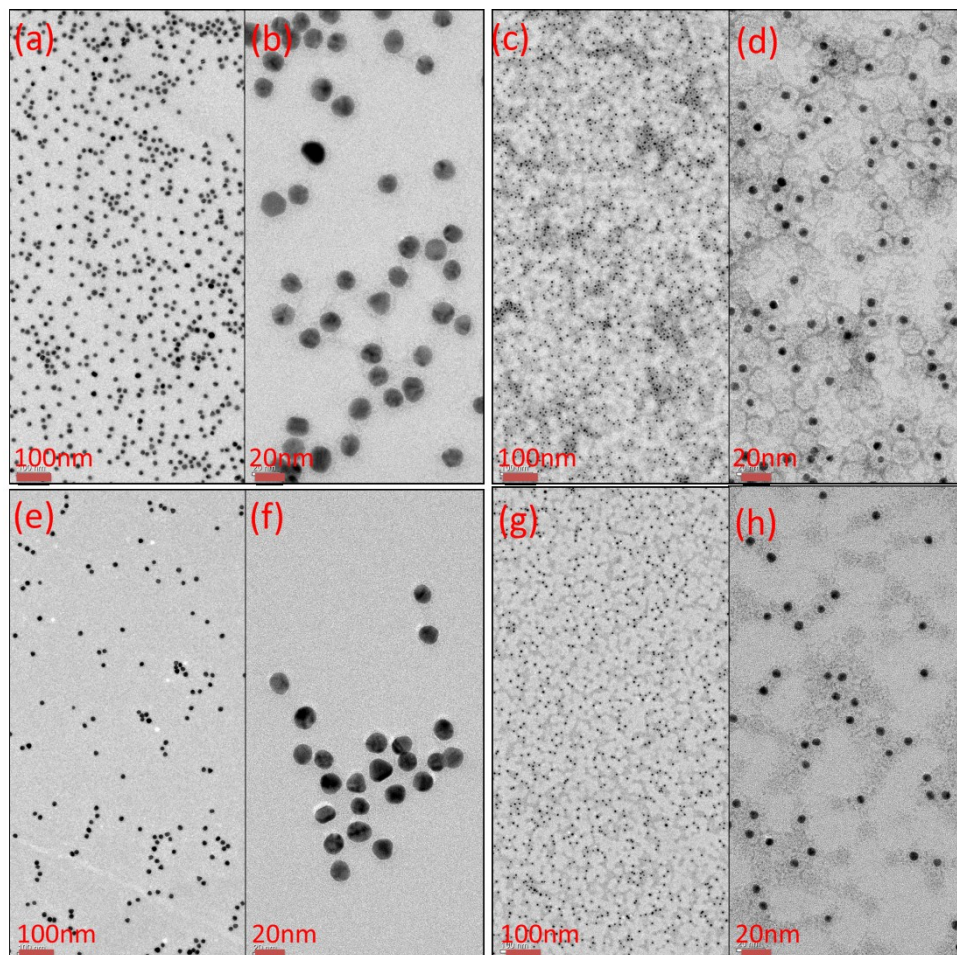


Figure 12: TEM images at two magnifications of (a,b) CA17 after Atto390 coupling, (c,d) CA7T after Atto390 coupling, (e,f) CA17 after Ore488 coupling, (g,h) CA7T after Ore488 coupling.

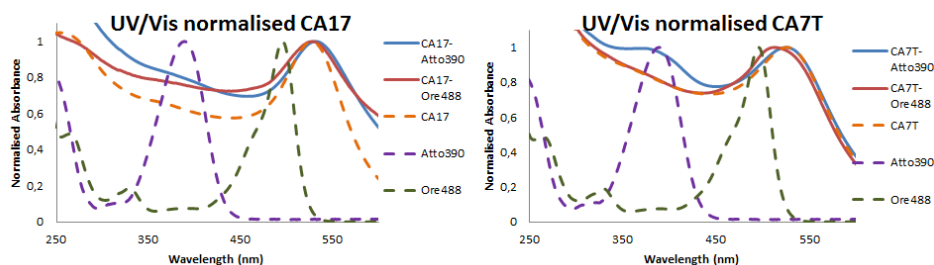


Figure 13: Normalised UV-Visible spectra of VLP and dyes before and after dye coupling and purification; (left) the T=3 sized CA17 VLP and dyes, (right) the T=1 sized CA7T VLP and dyes.

Appendix B: Fluorescence lifetime data

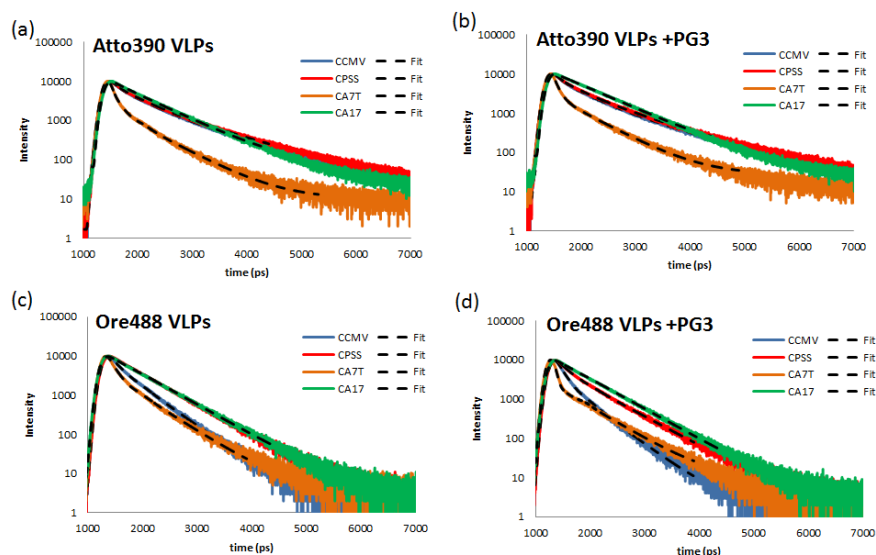


Figure 14: Fluorescence lifetime decay of VLPs with coupled dye. (a) Atto390 VLPs, (b) Atto390 VLPs clustered with PAMAM-G3 dendrimers, (c) Ore488 VLPs, (d) Ore488 VLPs clustered with PAMAM-G3.

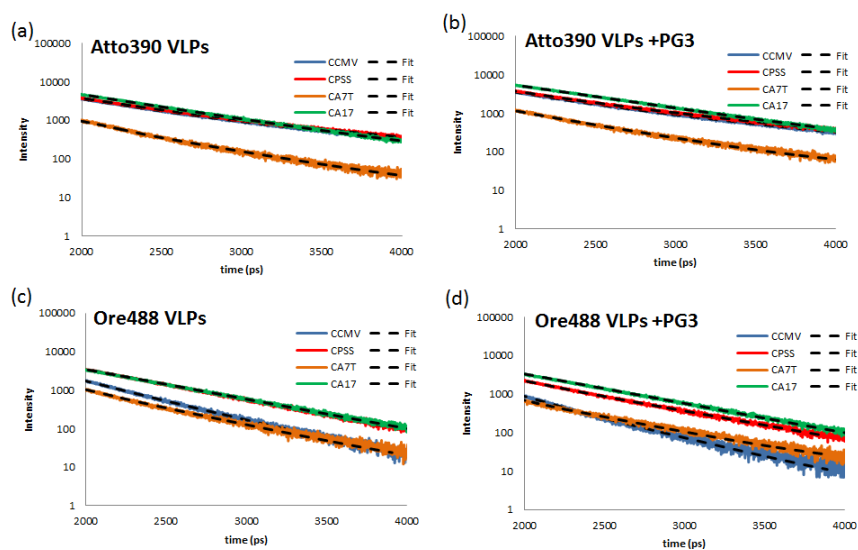


Figure 15: Similar to figure 14, see above, but visualised at the relevant intervals showing the true differences in decay, without measurement artefacts from uncorrelated photons due to light leaking in from outside (resulting in several $\tau > 7$ ns lifetimes) or scattering of excitation light leaking through the monochromator (resulting in a few $\tau < 1.5$ ns lifetimes). Also see the experimental section.

Appendix C: TEM of VLP-Ore488 clusters

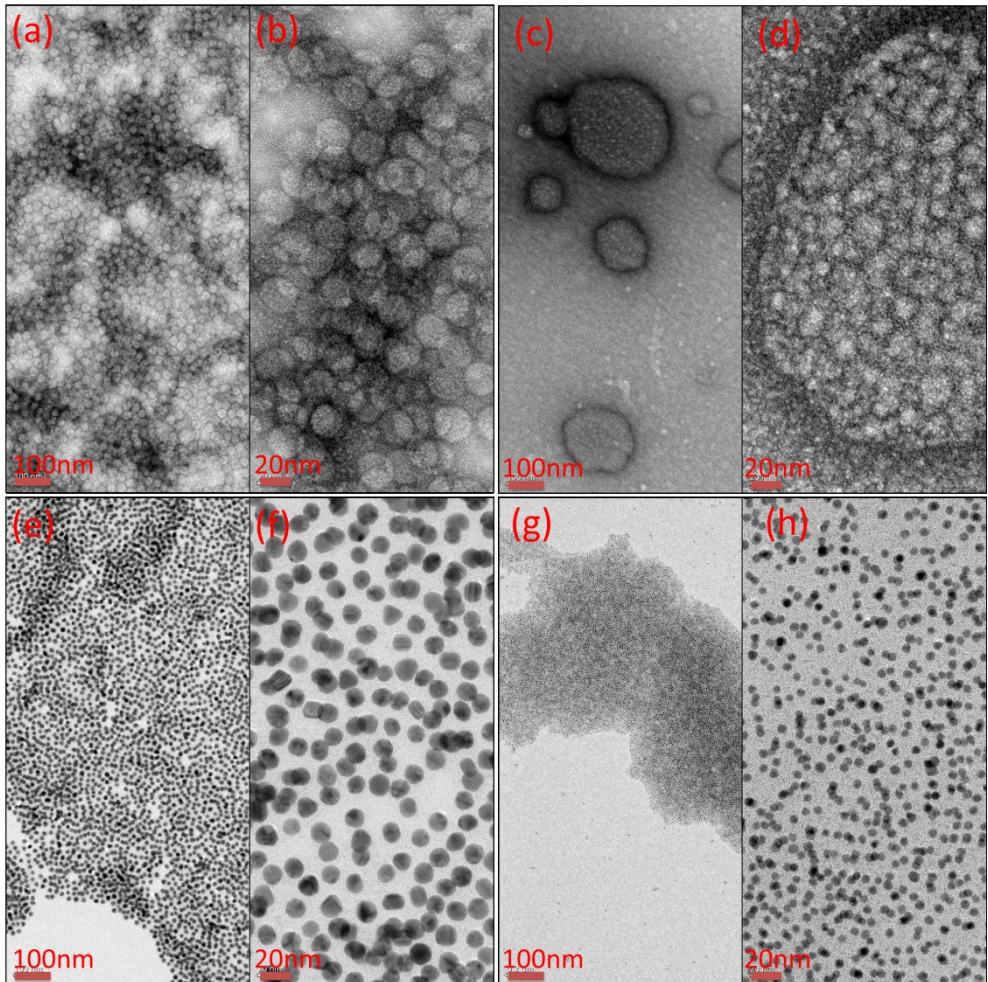


Figure 16: TEM images at two magnifications of VLP clusters formed from Ore488 modified VLPs; (a,b) CCMV with Ore488, (c,d) CPSS with Ore488, (e,f) CA17 with Ore488, (g,h) CA7T with Ore488.

Summary

The bottom up approach in nanotechnology first creates defined components using synthetic chemistry before techniques from supramolecular chemistry are employed to organise these into structured materials. Still, the final nanostructure is limited in the degree of organisation and the size that can be achieved. In **chapter 1** the study, emulation and use of nature's building blocks is presented as an answer to these challenges, as nature excels at self-assembly. Virus-based protein cages form the cornerstone of this work as they offer immense chemical and structural flexibility, whilst retaining a monodispersity and symmetrically organised structure that is unrivalled by any artificial nanoparticle. This allows them, alongside with Virus-Like Particles (VLPs), created by modifying an existing protein cage, to be used as programmable nano building blocks for the formation of complex nano architectures.

A vast amount of work has been done on for the synthesis and design of these virus based nano building blocks. Still, techniques for forming them into structured and functional materials are only just emerging, as detailed in **chapter 2**. The main goal of the work described in this thesis is to investigate how control over the loading and assembly of protein cages can result in functional materials. The well-studied and versatile protein cage of the Cowpea Chlorotic Mottle Virus (CCMV) is used as a basis for these studies. This is addressed by seeking a fast and efficient way to form model VLPs and subsequently use these and other readily synthesised particles in generating clusters of particles and finally work towards a functional system.

Model VLPs were formed by the encapsulation of gold nanoparticles (AuNPs) in CCMV. AuNPs have seen a great deal of research interest as their plasmonic properties make them of interest in plasmonics, sub wavelength optics and sensing applications. These properties are difficult to conserve in clustered systems due to plasmon resonance between nearby particles. By encapsulating them in a protein cage this is prevented. **Chapter3** describes an effective one step method for this encapsulation, without need for prior modification of the particle surface. Furthermore the resulting VLPs are shown to form on a size selective basis following T=1, T=2 and T=3 Caspar Klug symmetry structures at encapsulation efficiencies up to 97%. Additionally, they show good conservation of the plasmon properties, both as individual particles and in a clustered state. We feel that the presented method can be extended to efficiently encapsulate other anionic nanoparticles without the need for surface modification. This will lead to a new

class of virus based nanomaterials, in which individual VLPs will serve as modular building blocks.

Forming these modular nanomaterials of VLPs will require control over their clustering behaviour into higher, defined materials. Electrostatic clustering is known to be driven by a symmetrical arrangement of anionic patches upon the capsid surface. Depending on the size of the VLP, however, the symmetrical arrangement of proteins, and thus charge, changes. **Chapter 4** shows that though the same general principals apply to the electrostatic clustering of T=3 and T=1 CCMV based VLPs, the interaction with linear or branched cationic polymers is radically different. Whilst the larger T=3 VLPs readily forms clusters with either polymer, the T=1 VLP only clusters effectively with the branched polymer. Furthermore, the T=1 VLP shows evidence of trapping the linear polymer in a charged surface groove preventing any clustering until a saturation point is reached. By understanding these differences in clustering between the T=1 and T=3 VLPs, a further step is made towards functional materials though careful control over the desired structure and the resulting properties.

With a variety of cores and clustering materials available VLP based clustering is not limited to using soft macromolecules. Particularly, hard nanoparticles offer a wide range of interesting physical properties that could lead to new material properties. **Chapter 5**, therefore, explores the effect of the cargo on the clustering of different cored VLPs with cationic AuNPs. We found that the dynamics and stoichiometry of binary clusters of CCMV-VLPs and small cationic AuNPs is predominantly determined by the VLP size and structure. For instance, both T=3 sized CCMV and the T=3 sized Prussian blue filled VLP adopt an AB_8^{fcc} crystal structure. The VLP core composition does, however, affect the degree of crystallinity and order found within these clusters, with the native CCMV forming larger crystalline domain sizes than the T=3 sized Prussian blue filled VLP. Similarly, polymer cored T=1 VLPs showed no order, whereas nanoparticle cored T=1 VLP adopt a limited, though unidentifiable, ordered structure. This is attributed to the degree of monodispersity, rigidity and protein cage dynamics allowed by the different cores. These structural similarities between similar T number VLP clusters should allow for the formation of mixed systems, in that way allowing programming of the final material properties.

The ability to cluster AuNP containing VLPs allows us to work towards functional systems using the plasmonic properties of these AuNP, which amongst other things can affect nearby fluorophores. In **Chapter 6** the effect of plasmonic AuNP cores

inside VLPs upon the emission of fluorescent dyes on the protein cage surface is studied. These VLPs showed up to a 4.4 fold enhancement of the fluorescence intensity, which is conserved as a 2.2 fold enhancement after clustering, yet shows no enhancement of the fluorescent lifetime. We believe this is caused by the lightning rod effect of the AuNP, which causes an increase in the local light intensity around the VLP that allows for a strong increase in the rate of excitation, and not the lifetime of the emission, of the surface fluorophores.

To conclude, let us have a look at the title of this thesis: “Protein cage clustering: towards functional materials” Certainly the clustering of VLPs made from protein cages seems promising. From a research perspective clusters of VLPs are shown to be fast and easy to make compared to traditional protein crystallisation techniques. This thesis shows such clustering is dependent on the structure, the size and resulting symmetry of the VLPs. Furthermore, it shows that though the core composition has a significant effect on the VLP size, it only affects the degree and not the type of ordering obtained. And whilst large scale organised structures would require fine-tuning for each sample, the parameters that need to be tuned fall within a limited range. Furthermore, this thesis shows proof that these clusters allow us to alter the physical properties of their environment based on the core composition. Combined this would allow for a wide variety of systems to be designed, from mixed hard nanoparticle core systems to carefully constructed multiple enzymatic pathways inside the same material. So whether we want to go beyond nature and create the next generation of nano-devices and -structures, or want to build a cellular mimic out of protein cages, the basis can be found in the techniques described in this thesis.

Samenvatting

Binnen de 'bottom-up' aanpak in nanotechnologie maakt men eerst goed gedefinieerde componenten door middel van synthetische chemie om deze daarna te organiseren in gestructureerde materialen door gebruik te maken van technieken uit de supramoleculaire chemie. Echter, de uiteindelijke mate van organisatie en grootte van deze nanostructuren die bereikt kan worden is gelimiteerd. In **hoofdstuk 1** wordt het onderzoek naar, nabootsing van en het gebruik van deze natuurlijke bouwstenen gepresenteerd als een oplossing voor deze uitdagingen. De natuur blinkt namelijk uit in zelf-assemblage. Eiwitkooien van virussen vormen de hoeksteen van dit werk, omdat deze structuren een immense chemische en structurele flexibiliteit bezitten, terwijl ze een monodispersiteit en symmetrische organisatie bezitten die met kunstmatige nanodeeltjes niet bereikt kan worden. Hierdoor kunnen ze, net als virus-achtige deeltjes (virus-like particles, VLP) die ontstaan na modificatie van een bestaande eiwitkooi, gebruikt worden als programmeerbare nanobouwstenen om complexe nano-architecturen mee te maken.

Veel onderzoek is gedaan naar het maken en ontwerpen van deze, op virussen gebaseerde, nanobouwstenen. De technieken om met deze bouwstenen gestructureerde en functionele materialen te vormen zijn nog maar net in opkomst, zoals beschreven in **hoofdstuk 2**. Het hoofddoel van het werk beschreven in dit proefschrift is om te onderzoeken hoe controle over de lading en de assemblage van eiwitkooien kan resulteren in functionele materialen. De goed bestudeerde en veelzijdige eiwitkooi van het 'Cowpea Chlorotic Mottle Virus' (CCMV) is gebruikt als basis voor dit onderzoek. Om de hoofdvraag te beantwoorden is eerst gezocht naar een snelle en efficiënte manier om model VLPs te vormen. Vervolgens zijn deze model VLPs en andere gemakkelijk te gesynthetiseerde deeltjes gebruikt om clusters te vormen om uiteindelijk toe te werken naar een functioneel systeem.

Model VLPs zijn gemaakt door goud nanodeeltjes (AuNPs) in CCMV in te sluiten. AuNPs hebben veel onderzoekaandacht ontvangen, omdat hun plasmonische eigenschappen hen erg interessant maken voor plasmonica, 'sub-wavelength' optica en detectie applicaties. Deze eigenschappen zijn moeilijk te behouden in een geclusterd systeem, vanwege de plasmon resonantie tussen nabijgelegen deeltjes. Door deze deeltjes in te sluiten in een eiwitkooi kan dit voorkomen worden. In **hoofdstuk 3** wordt een effectieve één-stapmethode beschreven voor deze

insluiting zonder voorafgaande modificatie van het deeltjesoppervlak. Bovendien wordt aangetoond dat de resulterende VLPs zich vormen naar een select aantal afmetingen, die de Casper-Klug T=1, T=2 en T=3 symmetrie volgen, naar gelang de grootte van het ingesloten AuNP. Deze insluitingsmethode is tot 97% efficiënt. Daarnaast tonen de deeltjes een goed behoud van de plasmon eigenschappen, zowel als individuele deeltjes als in clusters. Wij denken dat de gepresenteerde methode uitgebreid kan worden om efficiënt andere anionische nanodeeltjes in te sluiten, zonder noodzaak voor voorafgaande modificatie van het oppervlak. Dit zal leiden tot een nieuwe klasse van op virussen gebaseerde nanomaterialen, waarin individuele VLPs zullen dienen als modulaire bouwstenen.

Om deze modulaire nanomaterialen uit VLPs te maken is controle vereist over hun clustering in hogere, goed gedefinieerde materialen. Het is bekend dat elektrostatische clustering gedreven wordt door de symmetrische plaatsing van anionische gebieden op het capsid oppervlak. Afhankelijk van de grootte van de VLP kan de symmetrische plaatsing van eiwitten, en dus lading, echter veranderen. In **hoofdstuk 4** wordt beschreven dat dezelfde algemene principes van toepassing zijn op de elektrostatische clustering van T=3 en T=1 CCMV VLPs. Echter, de interactie met lineaire of vertakte cationische polymeren gebruikt in de clustering is voor beide type VLPs heel anders. Terwijl de grotere T=3 VLPs gemakkelijk clusters vormen met beide polymeren, clusteren de T=1 VLPs alleen effectief met de vertakte polymeer. Bovendien lijkt de T=1 VLP de lineaire polymeer te vangen in een geladen groef in het oppervlakte, waardoor geen clustering mogelijk is tot een verzadigingspunt is bereikt. Door deze verschillen in clustering tussen de T=1 en T=3 VLPs te begrijpen is een volgende stap gemaakt in het vormen van functionele materialen middels controle over de gewenste structuur en de resulterende eigenschappen daarvan.

Er is veel variatie aan capsid inhoud en clusteringsmaterialen beschikbaar, en VLP clustering is niet gelimiteerd tot zachte macromoleculen. Met name harde nanodeeltjes bieden een grote variatie aan fysische eigenschappen, die kunnen leiden tot nieuwe materiaaleigenschappen. Daarom wordt in **hoofdstuk 5** het effect van de capsid inhoud op de clustering van VLPs met verschillende kernen met kleine cationische AuNPs verkend. We hebben gevonden dat de dynamiek en de stoichiometrie van de binaire clusters tussen CCMV-VLPs en kleine cationische AuNPs vooral afhankelijk is van de grootte en de structuur van de VLPs. Zo nemen de T=3 CCMV VLP en de T=3 VLP gevuld met Pruisisch blauw een AB_8^{fcc} kristalstructuur aan. De compositie van de VLP kern heeft echter geen effect op de kristalliniteit en de mate van orde die wordt waargenomen in deze clusters,

behalve dat de CCMV VLPs grotere kristallijne domeinen vormen dan de T=3 VLPs gevuld met Pruisisch blauw. Eveneens toont de T=1 VLP met polymeer kern geen orde, terwijl T=1 VLPs met nanodeeltje kern een structuur met zekere ordening aannemen, ook al kan deze niet geïdentificeerd worden. Dit kan verklaard worden door de mate van monodispersiteit, rigiditeit en dynamiek van de eiwitkooi die beïnvloed worden door de verschillende kernen. Deze structurele overeenkomsten tussen clusters van VLPs met hetzelfde T nummer maakt de vorming van gemengde systemen mogelijk en daarmee het programmeren van de uiteindelijke materiaaleigenschappen.

Door VLPs die een AuNP bevatten te kunnen clusteren kan gewerkt worden naar functionele systemen, die gebruik maken van de plasmon eigenschappen van de AuNPs. Deze kunnen onder andere nabijgelegen fluoroforen beïnvloeden. In **hoofdstuk 6** wordt het effect van plasmonische AuNP kernen in VLPs op de emissie van fluorescente kleurstoffen op de eiwitkooi-oppervlakte bestudeerd. Deze VLPs lieten een 4,4-voudige versterking van de fluorescentie-intensiteit zien in vergelijking met VLPs zonder AuNP kern, maar er is geen verbetering van de fluorescentielevensduur waargenomen. Na clustering van deze VLPs wordt de versterking van de intensiteit behouden, hetzij 2,2 keer zo sterk. Wij denken dat dit wordt veroorzaakt door het 'bliksemafleider-effect' van de AuNP, die zorgt voor een toename in de lokale licht intensiteit rondom de VLP. Hierdoor neemt de excitatiesnelheid, maar niet de levensduur van de emissie, van de fluoroforen aan het capsid-oppervlak sterk toe.

Laten we tot slot kijken naar de titel van dit proefschrift 'Eiwitkooi clustering: op weg naar functionele materialen'. De clustering van VLPs gemaakt van eiwitkooien lijkt zeker veelbelovend. Vanuit onderzoeksperspectief zijn clusters van VLPs sneller en makkelijker te maken in vergelijking tot traditionele technieken voor eiwitkristallisatie. Het onderzoek in dit proefschrift heeft laten zien dat zulke clustering afhankelijk is van de structuur, de grootte en de resulterende symmetrie van de VLPs. Bovendien blijkt dat hoewel de kern een significant effect heeft op de VLP grootte, deze kern alleen invloed heeft op de mate en niet het type van de ordening die wordt verkregen. Hoewel het maken van georganiseerde structuren op grotere schaal fine-tuning van elk monster vereist, vallen de parameters hiervoor in een beperkt gebied. Bovendien heeft dit onderzoek ook aangetoond dat deze clusters de fysieke eigenschappen van hun omgeving kunnen veranderen afhankelijk van de kern compositie. Hierdoor kunnen zeer gevarieerde systemen ontworpen worden, van gemengde systemen met verschillende harde nanodeeltjes als kern tot precies geconstrueerde enzymatische paden in hetzelfde materiaal.

Dus, of we de natuur voorbij willen gaan om de volgende generatie aan nano-apparaten en –structuren te maken, of juist een cel willen imiteren met eiwitkooien, de basis hiervoor kan worden gevonden in de in dit proefschrift beschreven technieken.

Acknowledgements/Dankwoord

The final words of this thesis do not have to concern science. They are instead directed at scientists and non-scientists alike that have befriended, supported and aided me in the past four years. Yet, to merely use this as a summation of acknowledgements would be a hollow and inadequate expression of my thanks. Therefore, amongst my words of praise to my mentors, peers, friends and family, I hope to share with you some insights into what drives me and what I have learned these past four years.

Quite a few of you have found me curious, memorable and probably a bit eccentric. For better or worse, I enjoy finding my own path and learning from the experience. Though, to be completely honest, I also value encouragement and a second opinion when I am stuck. This is precisely what drew me to want to work with **Prof. Dr. J.J.L.M. Cornelissen** as my supervisor. **Jeroen**, working with you has certainly not disappointed and I thank you for your positive encouragement and giving me the freedom to develop not only as a scientist, but also as a person.

The idea of personal development is an admirable one. Under its banner people are usually taught that they should all hold true to the very same group standards of being liberal minded, critical individuals. To me this has always seemed quite ironic, but then again I've been taught to be a critical individual. During my research I've had the pleasure to work with many other critical individuals, including most of you. My most prominent collaborations, however, were with **Dr. C Blum**, **Prof. M. Kostiainen** and **Mr. Liljeström**. People whom, beyond this critical mind-set, I can praise for their helpful, realistic and relativistic qualities. **Christian**, **Mauri** and **Ville**, I thank you for the time and effort you have spent helping me with both practical work and in discussions to understand the results.

Fortunately there are no perfectly critical people, many possess a wide variety of qualities that go far beyond this. Perfect people would probably make the world rather boring, at least from my perspective. Instead the world offers flavour and comprises of a lot of interesting people that each come with their own valuable contribution. Again, this holds for many of you, but I have come to especially appreciate this diversity in the academic staff of the SaNS cluster. As such, I admire the genius of **Prof. Dr. Ir. J. Huskens**, the drivenness of **Dr. N. Katsonis**, the insights of **Dr. M. Koay**, the critical questions of **Prof. Dr. Ir. P. Jonkheim**, the realism and wit of **Dr. W. Verboom** and the kindness of **Dr. T. Kudernac**. **Jurriaan**, **Nathalie**, **Melissa**, **Pascal**, **Wim** and **Tibor** I thank you for all your insights, contributions and questions.

Beyond these academic ideals, research is generally a very practical subject with very real problems, some of which I helped create. Equipment breaks down, supplies are out of order and some machines simply should not be handled without a skilled operator. Though I could argue this is inevitable when pushing technology to the limits, I cannot help but be thankful to a very special group of people that have helped me in this. **Regine, Richard, Marcel** and **Bianca** thanks to your efforts my problems, self-inflicted or otherwise, have always been solved. Also, to **Rico** and **Mark**, just beyond the borders of our labs, your expertise and practical skills in electron microscopy have been vital in the visualisation of my work. Some problems, however, are of a non-technical nature, such as finding time to speak to your supervisor, battling the university bureaucracy, or simply ensuring that you have a comfortable bed to sleep during a conference. **Izabel** and **Nicole**, thanks to you these things always went perfectly and without you I would undoubtedly have managed to tear out my hair in frustration at times. I am quite fond of my hair.

Putting the ideals and the practical problems aside, modern science is at times described as a frustrating rat-race full of conflict, anxiety and stress. Probably old science was no different, but perhaps involved more actual rats. Despite having been described by several people as a generally calm and relaxed person, I have certainly experienced my share of frustration, anxiety and stress at times. I wouldn't have wanted to miss one minute of that, for these were challenges I have overcome and have learned from. Still I feel fortunate that I have never felt like I was stuck in a rat-race and I think I owe this to my wonderful colleagues within the BNT group. This leaves me with a lot of people to thank. **Melanie, Rik** and **Anne**, together we formed the foundation of the BNT group and its first virus team. All beginnings are rocky and exciting, but we pulled through and I'm grateful to have been able to work, learn and grow with you. **Inge**, whilst not a true part of BNT, I thank you for helping us to get started as our colleague from Nijmegen. **Rianne, Aijie** and **Rindia**, you have joined us since then and picked up where we left of. Thank you for the time we have had together in the lab and refreshing new ideas on the virus research. I wish you and your new colleague **Stan** the best of luck. New colleagues joined BNT as the group grew. **Oya, Yujie** and **Chengfen** our first post-docs to help us get going. **Sarah** and **Supitchaya**, who broadened the group's topics beyond protein cages and were joined by **He, Supaporn** and briefly **Dasha, Jealemy** and **Vijay** adding their experience and skills during the final year of their PhD programs. Thank you all for expanding the collective wisdom and experience in the group and it was a pleasure to work you with during my time within BNT. **Maarten** and **Benjamin**, you were kind enough to share your insights both on research and on life. And of course, **Piotr**, thank you for sharing the final year of our PhDs in the same group, which is helpful in so many small ways.

The list of colleagues, however, does not stop here. Understanding the importance of an open environment, the BNT group shares its laboratories with the MNF group. This expands the range of scientific possibilities, but more importantly the range of skilled colleagues to work with. **Carmen**, with your efforts to keep the DLS afloat you should claim an extra salary as a technician. I thank you for this and for being an open person with whom it is easy to share a good conversation. **Rajesh**, you are hardworking, quiet and kind, and I treasure those words and times we have shared. Also **Wouter**, sharing an office with you in the final months was an absolute joy. I also thank the many others colleagues that have made my time enjoyable: **Jenny, Emanuela, Rick, Laura, Gülistan, Andrea, Ye, Raquel, Roberto, Shirish, Tushar, Bettina, Tom, Andreas, Janneke, Mark, Jasper, Alejandro, Jens, Wies**, and further including those that have left before me: **Pieter, Sven, Carlo, Kim, Jordi, Mudassir, Raluca, Nicolai, Deniz, Angel, Alberto, Erhan** and **Fransceca**. I wish you all good luck on your research efforts and any of life's other endeavours that you might pursue. And though this is a long list and some have undoubtedly impacted me more than others, it will ensure that I remember your names when I am much older, as I do not wish forget any of you.

Up until this point I've thanked 75 people for their aid and assistance in various ways. I hope that I have done enough to pay this forward to my own students. Certainly, the experience of teaching and coaching them has been rewarding for me and I have learned many things from this. Mostly, that I did by far not know enough and had to scramble to keep up on your diverse topics. **Jessica**, my first student, you were initially unsure about your abilities. You nevertheless succeeded in the complex synthetic task set out for you. I also enjoyed our talks on the more important things in life. **Thomas**, you were challenged outside your field of expertise, but we managed to redesign your project and I'm happy that you rose to that challenge. **Petra**, my most independent student, you will doubtlessly have a bright academic future. I'm proud that the foundations we laid have resulted in a new PhD position for the group. And **Liuyi**, always following instructions to the letter, but in the end learning how to write those instructions yourself. You were a little bit of sunshine in the lab during my final year. To the four of you, I'm grateful for all of your efforts and contributions that helped shape my thoughts, but most importantly I'm grateful for the joy of having been your supervisor.

I tend to believe that all things are connected, on all sorts of levels. Yet to ease our understanding of the world, setting boundaries is entirely within human nature. It helps us make sense of a world which is inherently complex, chaotic and potentially fraught with danger. I am about to cross the boundary leaving science. Not because there are no more scientists to thank or because it has nothing to do with science,

but rather because I need to define a boundary somewhere. A grey area immediately emerges in the form of the faculty council and all related activities. Talking about science, without mentioning the actual science. Quite an accomplishment if you regularly gather a dozen or so academics and students in a professional setting. Still, I feel fortunate to have worked with passionate individuals enabling me to develop my ideas on how science should be organised. **Herman**, thank you for showing me how wit and cleverness can be employed to make a clear point and helping me as a referee during my job interviews. **Ingrid**, I've not stopped by for coffee as often as I might have liked these past months, but I would like to thank you for these moments of calm in the academic storm. **Wouter, Gertjan, Bert, Dimitris, Jeroen, Raimond, Mirjam, Robin, and Tom**, thank you all of our discussions and shared successes. I also thank **Prof. Dr. G. van der Steenhoven**, our former dean, who metaphorically sat on the opposite side of the table. Thank you for your positive approach to all problems, I mean 'challenges', and the open, cooperative spirit you evoked. Lastly, **Herbert, Jörgen** and all others that I have met and worked with in related activities, thank you for these experiences.

A university, however, is broader than the science and education that today form its core. I would argue that its role as a cultural institute is perhaps far more important. Not to train the next generation of leaders, high value workers or entrepreneurs for the knowledge based economy, but rather to unite these and allow them to share ideas and ideals. To facilitate this is easy, all we have to do is give an intelligent person some time to do this in. Some money might help too. The University of Twente fortunately offers plenty of this, provided you look and make time for it and go beyond the professional boundary. As such I dived into the weird world of underwater hockey. Thank you **Fabian** for introducing me. From there I was introduced to improvisational theatre at Pro Deo, where several people urged me to join the Fanaat gaming society and Bellettrie library, of which I held a joint presidency. To top it off 7Realms, a life roleplaying setting, was founded and is due to become an independent organisation around the time of this writing. None of this would have been possible without the many wonderful people I met on the way. There are too many to name, but I'll highlight a few. **Michael, Regine and Mareen**, thank you for teaching me the techniques to improvise on stage. **Tim, Ronald, Bouke and Bruno**, I am happy to have shared time and effort with you on the Fanaat/Bellettrie board. **Frank, Anja, Anne, Rik, Lennart, Wilco, Sjonnie, Elise, Sebas, Vincent** and an increasing number of others, I thank you for the efforts going into 7Realms. **Johannes**, you are a friend found in many of these groups and a skilled artist, thank you for the beautiful cover and animations. On a related note,

but beyond the universities walls, I thank the members of Attila, where I have been able to find enjoyment and relaxation.

Having safely crossed the boundary of the universities walls and coming to a milestone in my life it is perhaps safe to also briefly cross the boundary of time. Reflecting on the past to appreciate those key people that have helped me become whom I am today, my old friends. I cannot find words more adequate than these: **Jeroen, Martijn, Angelique** and **Jack**, thank you for being my friends.

To another friend, but old in a different way. **Rudie**, I thank you for our good discussions, friendship and support. Dear **Rudie**, rest in peace.

For my paranymphs I have chosen an old friend and a new friend, one from outside the university and one from within. The choice is symbolic in nature, binding me to many places, but also more than deserved. **Jack**, you are my oldest friend and an accomplished scientist in your own right. I am grateful to still have you in my life after all this time and many separations by long distances. **Wilco**, I've met you more recently, but there is a strong connection nevertheless. I am grateful to call you my friend and am happy for the daily lunches, weekly games and frequent drinks over the past few years.

On to the final disputable boundary, perhaps a watershed between scientists and non-scientists. This division can perhaps be made by using Clarke's third law, "*Any sufficiently advanced technology is indistinguishable from magic.*" In essence, those of you who could potentially understand my work and those of you that often see most of the other group as wizards locked in an ivory tower. I'm talking of course about my family and loved ones. I'll write this in Dutch, for emotions are strongest in one's native language and I'll need neither my reason nor my wits for this.

Mamma, Pappa, een promotie onderzoek in een lab was een onverwachte stap zo kort na mijn avonturen bij United Netherlands en de Nationale Denktank. Jullie waren dan ook blij verrast toen ik aan dit avontuur begon. Al lang vonden jullie dat ik, met mijn vele vragen, thuis hoorde in de academische wereld. Jullie kennen mij immers beter als ik mezelf ken, maar hebben mij altijd geholpen om zelf een pad te vinden. Daarbij zijn jullie een constante bron van steun, liefde en ruggespraak voor mij. Dankjewel, ik kan me geen betere ouders wensen.

Loes, je bent een geweldige zus en een sterke schouder als het tegen zit. In de afgelopen vier jaar kon ik altijd bij jou terecht voor wat rust, gezelligheid en een lekkere maaltijd. Zeker toen mamma en pappa ver weg woonden was jij een

tweede thuis voor mij. **Maarten**, ook jij bent hier een deel van geworden. Dankjewel, voor alle tijd en warmte die jullie voor me vrij maakten.

Inge, Herbert, onze familie is wellicht klein, maar hij is zeker hecht. Ik voel me altijd welkom bij jullie en weet dat jullie altijd in mij geïnteresseerd zijn en willen weten waar ik mee bezig ben. Dat is belangrijk, want daardoor kan ik bij mezelf toetsen of ik het werkelijk ook zelf snap. Dankjewel, dat ik zo'n geweldige oom en tante heb.

Anne, driemaal is scheepsrecht. Je was er bij op de eerste dag van mijn studie, maar ik zag je niet. Je was er bij op de eerste dag van mijn eerste stage, maar dat was jouw laatste. Je was er bij op de eerste dag van mijn promotie onderzoek, maar dat deden we samen. Nu zijn we samen en ik hou heel veel van je. Bedankt voor alle steun, liefde en vriendschap in de afgelopen maanden en jaren.

I conclude by thanking all of you a final time, wizards and non-wizards alike, for making the past four years useful, memorable and deeply enjoyable.

Martijn

List of Publications

Martijn Verwegen, Ville Liljeström, Mauri Kostianen, Jeroen J.L.M Cornelissen, *“Cargo independent clustering of virus like particles”*, Manuscript in preparation.

Martijn Verwegen, Christian Blum, Jeroen J.L.M Cornelissen, *“Metal enhancement fluorescence in plasmonic virus-like particle clusters”*, Manuscript in preparation.

Martijn Verwegen, Jeroen J.L.M Cornelissen, *“Clustered nanocarriers: the effect of size on the clustering of virus-like particles with soft macromolecules”*, submitted

Martijn Verwegen, Jeroen J.L.M Cornelissen, *“Virus based systems for functional materials”*, submitted

Andrés de la Escosura, **Martijn Verwegen**, Friso D. Sikkema, Marta Comellas-Aragonès, Andrei Kirilyuk, Theo Rasing, Roeland J. M. Nolte and Jeroen J. L. M. Cornelissen, *“Viral capsids as templates for the production of monodisperse Prussian blue nanoparticles”*, Chemical Communications, 2008. **0**(13): p. 1542-1544.

About the Author

Martijn Verwegen was born in Dordrecht, the Netherlands on the 7th of March 1984. He graduated from high school with a bilingual IB-diploma in Muscat, Oman in 2002. That same year he returned to the Netherlands to study Natural Sciences at the Radboud University of Nijmegen. During this time he performed three internships, two involving natural sciences at the departments of Prof. Dr. Theo Rasing and Prof. Dr. Roeland J.M. Nolte and one concerning management under the supervision of Prof. Dr. Ben Dankbaar. Also he held several board positions on student organisations and was part of both the United Netherlands delegation and the National Think Tank. He received a Master of Science degree in 2009.

In 2010 he started as a Ph.D. candidate at the department of Biomolecular NanoTechnology at the University of Twente. Whilst at the University of Twente he was a part of the Faculty Council and founded a live role-play organisation. Professionally, he worked on creating functional biohybrid materials by assembling protein cages under the supervision of Prof. Dr. Jeroen J.L.M. Cornelissen. The results of this research are described in this thesis. As of August 2014 he is working as a policy officer at the Netherlands Organisation for Scientific Research (NWO).

THESES

Part of the thesis

PROTEIN CAGE CLUSTERING: TOWARDS FUNCTIONAL BIOHYBRID MATERIALS

by

Martijn Verwegen



THE BEST THESIS DEFENSE IS A GOOD THESIS OFFENSE.

Image copyright © of Randall Munroe, xkcd.com

- 1) With such a vast library of virus protein cages available, nanotechnology research limits itself to much too few of these and is content to tinker with the genetics rather than look for a better predesigned package. – Chapter 2
- 2) Encapsulation inside a virus capsid is straight forward, but not every material can template different sized, stable virus-like particles as readily as gold nanoparticles, even if it is potentially of proper size and surface charge. – Chapter 3
- 3) Virus-like particles are not an ideal building block for biomedical nanotechnology due to their biocompatibility, but rather due to their modular functionality and ability to form clusters. – Chapters 4 and 5
- 4) Any system based on virus-like particles will suffer from biological complexity in trying to study and control it. – Chapter 6
- 5) Given the costs of maintaining and defending them, scientific patents should not be acquired by universities.
- 6) Arts and culture train and provoke your imagination and should therefore form an integral part of any academics life.
- 7) Due to their increased emphasis on facts, methods and soft skills universities do not train good scientists, but will produce excellent research workers.
- 8) Often, in science, we are stepping on the toes of living giants, not standing on their shoulders.
- 9) “Every so often, you have to unlearn what you thought you already knew, and replace it by something more subtle. This process is what science is all about, and it never stops.” – Terry Pratchett, *The Science of Discworld*, p43
- 10) “The freedom to criticize ideas, any ideas – even if they are sincerely held beliefs – is one of the fundamental freedoms of society.” – Rowan Atkinson